



US Army Corps  
of Engineers

# IMPROVEMENT OF OPERATIONS AND MAINTENANCE TECHNIQUES RESEARCH PROGRAM

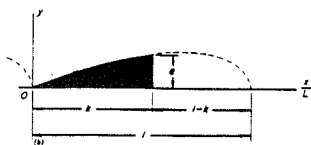
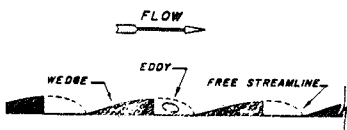
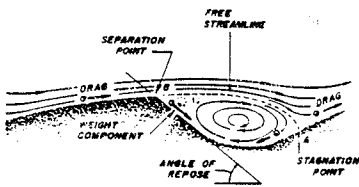
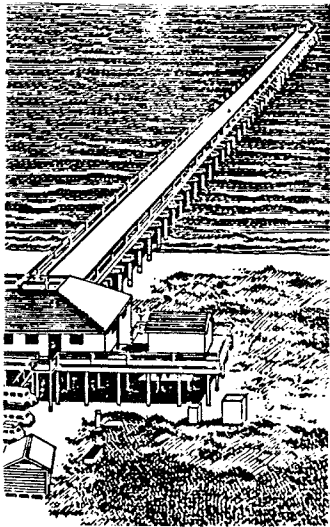
CONTRACT REPORT CERC-91-2

## INFORMAL MONOGRAPH ON RIVERINE SAND DUNES

by

John F. Kennedy, A. Jacob Odgaard

Iowa Institute of Hydraulic Research  
The University of Iowa  
Iowa City, Iowa 52242



October 1991

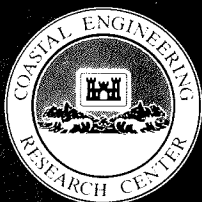
Final Report

Approved For Public Release; Distribution Is Unlimited

Prepared for DEPARTMENT OF THE ARMY  
US Army Corps of Engineers  
Washington, DC 20314-1000

Under Work Unit No. 32386

Monitored by Coastal Engineering Research Center  
US Army Engineer Waterways Experiment Station  
3909 Halls Ferry Road, Vicksburg, Mississippi 39180-6199



Destroy this report when no longer needed. Do not return  
it to the originator.

The findings in this report are not to be construed as an official  
Department of the Army position unless so designated  
by other authorized documents.

The contents of this report are not to be used for  
advertising, publication, or promotional purposes.  
Citation of trade names does not constitute an  
official endorsement or approval of the use of  
such commercial products.

REPORT DOCUMENTATION PAGE			Form Approved OMB No. 0704-0188	
Public reporting burden for this collection of information is estimated to average 1 hour per response, including the time for reviewing instructions, searching existing data sources, gathering and maintaining the data needed, and completing and reviewing the collection of information. Send comments regarding this burden estimate or any other aspect of this collection of information, including suggestions for reducing this burden, to Washington Headquarters Services, Directorate for Information Operations and Reports, 1215 Jefferson Davis Highway, Suite 1204, Arlington, VA 22202-4302, and to the Office of Management and Budget, Paperwork Reduction Project (0704-0188), Washington, DC 20503.				
1. AGENCY USE ONLY (Leave blank)	2. REPORT DATE October 1991	3. REPORT TYPE AND DATES COVERED Final report		
4. TITLE AND SUBTITLE Informal Monograph on Riverine Sand Dunes			5. FUNDING NUMBERS WU 32386	
6. AUTHOR(S) John F. Kennedy A. Jacob Odgaard				
7. PERFORMING ORGANIZATION NAME(S) AND ADDRESS(ES) Iowa Institute of Hydraulic Research University of Iowa Iowa City, IO 52242			8. PERFORMING ORGANIZATION REPORT NUMBER	
9. SPONSORING/MONITORING AGENCY NAME(S) AND ADDRESS(ES) USAE Waterways Experiment Station, Coastal Engineering Research Center, 3909 Halls Ferry Road, Vicksburg, MS 39180-6199			10. SPONSORING/MONITORING AGENCY REPORT NUMBER Contract Report CERC-91-2	
11. SUPPLEMENTARY NOTES Available from National Technical Information Service, 5285 Port Royal Road, Springfield, VA 22161				
12a. DISTRIBUTION/AVAILABILITY STATEMENT  Approved for public release; distribution is unlimited			12b. DISTRIBUTION CODE	
13. ABSTRACT (Maximum 200 words)  This report presents an investigation of riverine sand dunes and includes an extensive literature review on the subject. It was concluded that the principal mechanisms responsible for river bed instability, which results in the production of ripples, dunes, etc., are fairly well understood. However, several of the key constituent processes are not well formulated. Principal among these are the phase shifts that occur between the local sediment discharge, the local near-bed velocity, local bed-profile displacement, and local bed shear stress. The reasons for the current deficiencies in the theoretical models are discussed and are concluded to stem from the difficulties inherent to analysis of nonuniform, turbulent, boundary-layer-type flows. Several existing theories for prediction of dune height were verified. None of the five published predictors evaluated was found to be satisfactory. A new, "inverse" model for prediction of dune height was developed.				
14. SUBJECT TERMS River bed instability Riverine sand dunes			15. NUMBER OF PAGES 199	
			16. PRICE CODE	
17. SECURITY CLASSIFICATION OF REPORT UNCLASSIFIED	18. SECURITY CLASSIFICATION OF THIS PAGE UNCLASSIFIED	19. SECURITY CLASSIFICATION OF ABSTRACT	20. LIMITATION OF ABSTRACT	

## PREFACE

This study was conducted by Messrs. John F. Kennedy and A. Jacob Odgaard at the Iowa Institute of Hydraulic Research (IHR), University of Iowa, under an Intergovernmental Personnel Agreement through the Coastal Engineering Research Center (CERC) of the US Army Engineer Waterways Experiment Station (WES). The study was sponsored by Headquarters, US Army Corps of Engineers (HQUSACE), as part of the Improvement of Operations and Maintenance Techniques (IOMT) Program, under Work Unit 32386, "Mitigating Sand Waves in Navigation Channels." The HQUSACE Technical Monitors were Messrs. John H. Lockhart, Jr.; John G. Housley; James E. Crews; and Robert H. Campbell.

A state-of-the-art study, like the present one, involves a tremendous amount of collecting, sorting, collating, and copying of several types of materials. In these efforts, the authors received invaluable assistance from several of their colleagues. Dr. Anita Spoljaric, IHR, collected much of the literature and assisted materially in the initial evaluation. The word processing and figure mounting were by Meses. Twila Meder and Robyn Wright, respectively. Final editing, copying of figures, and proofreading were handled by Mr. Dan Daly, IHR.

Supervision during this study was provided by Dr. James R. Houston, Chief, CERC; Mr. Charles C. Calhoun, Jr., Assistant Chief, CERC; Mr. Thomas W. Richardson, Chief, Engineering Development Division (EDD); Ms. Joan Pope, Chief, Coastal Structures and Evaluation Branch (CSEB), EDD; Dr. Yen-hsi Chu, Chief, Engineering Application Unit, CSEB; and Mr. W. Jeff Lillycrop, EDD, Principal Investigator. The IOMT Program Manager was Mr. Robert Athow.

Commander and Director of WES during this investigation was COL Larry B. Fulton, EN. Technical Director was Dr. Robert W. Whalin.

# TABLE OF CONTENTS

	<u>Page</u>
ACKNOWLEDGEMENTS .....	i
ABSTRACT.....	iv
I. INTRODUCTION .....	1
II. SUMMARIES OF RESULTS.....	5
A. Introductory Remarks.....	5
B. Analytical Models .....	5
B.1. Exner (1925).....	6
B.2. Anderson (1953) .....	11
B.3. Kennedy (1963).....	16
B.4. Kennedy (1969).....	21
B.5. Hayashi (1970).....	27
B.6. Engelund (1970).....	31
B.7. Gill (1971) .....	37
B.8. Fredsoe (1974) .....	42
B.9. Richards (1980) .....	45
B.10. Fredsoe (1982) .....	51
B.11. Haque and Mahmood (1985) .....	58
C. Empirical Methods .....	64
C.1. Garde and Albertson (1959) .....	65
C.2. Yalin (1964).....	69
C.3. Ranga Raju and Soni (1976).....	76
C.4. Yalin and Karahan (1979).....	82
C.5. Jaeggi (1984) .....	87
C.6. Ikeda (1984) .....	91
C.7. van Rijn (1984).....	95
C.8. Menduni and Paris (1986).....	101
D. Statistical Models.....	108
D.1. Nordin and Algert (1966) .....	109
D.2. Hino (1968).....	118
D.3. Annambhotla, Sayre and Livesey (1972).....	123
D.4. Jain and Kennedy (1974).....	134
III. CURRENT STATUS AND PROSPECTS .....	145
A. Introduction .....	145
B. What is Known.....	145
C. Why is the "Dune Problem" so Intractable?.....	160
IV. A NEW THEORY FOR DUNE HEIGHTS .....	163

V. VERIFICATION.....	169
VI. DUNE-CONTROL METHODS.....	179
VII. SUMMARY AND CONCLUSIONS.....	184
REFERENCES.....	185

CONVERSION FACTORS, NON-SI TO SI (METRIC)  
UNITS OF MEASUREMENT

Non-SI units of measurement used in this report can be converted to SI (metric) units as follows:

Multiply	By	To Obtain
cubic feet	0.02831685	cubic metres
Fahrenheit degrees	5/9	Celsius degrees or kelvins*
feet	0.3048	metres
square feet	0.092290304	square metres

---

\* To obtain Celsius (C) temperature readings from Fahrenheit (F) readings, use the following formula:  $C = (5/9) (F - 32)$ . To obtain kelvin (K) readings, use:  $K = (5/9) (F - 32) + 273.15$ .

# AN INFORMAL MONOGRAPH ON RIVERINE SAND DUNES

## I. INTRODUCTION

The formation and behavior of sediment waves produced by moving fluids (principally water and air) are, in equal measure, intellectually intriguing; of great engineering importance; and aesthetically engaging. Because of the central role they play in river hydraulics, fluvial ripples and dunes have received extensive analytical attention from engineers for at least the past two centuries (e.g., Sainjon's 1871 publication, cited by Leliavsky (1955); and Du Buat's 1786 work, cited by Graf (1971)); and even more intensive descriptive study for even longer from geologists (formerly, before this age of specialization, known as natural philosophers). A comprehensive review and assessment of the resulting body of literature would be far beyond the scope of this investigation. Indeed, such an effort would be a scholarly enterprise requiring many years--perhaps a whole career--of effort by one versed in subjects ranging from descriptive geomorphology to mathematical theory of autocorrelation analysis. The review reported here was limited to the analytical aspects of riverine bed forms, principally large dunes and bars--those of sufficient size to interfere with navigation and other uses of rivers. Herein these are referred to collectively by the geological term "megadunes." Attention is focused on the mechanics of megadune formation, and the geometrical and kinematical characteristics of the resulting bed forms.

The modern, and far more successful, era of bed-form analysis was initiated, without question, by the work of Exner (1925), which brought (unknowingly) small-

perturbation stability theory to bear on the problem. A second rebirth of the subject was brought about by Nordin and Algert's (1966) application of time-series analysis (also referred to as autocorrelation analysis, or spectral analysis) to the description and analysis of fully developed bed forms. Accordingly, this study was limited to Exner's (principally because of its historical importance) and subsequent developments; i.e., to the period since 1925.

The principal objective of the study was to ascertain if it is now possible to make reliable predictions of the conditions (combination of flow, fluid, and sediment properties) under which megadunes will form; and of the lengths and heights of the resulting bed forms. By way of preview, the answers turn out, unfortunately, to fall somewhere between "no" and "very approximately."

Chapter II of this report summarizes and critiques the principal publications on the subject, divided into three categories: analytical (principally stability-theory) models; empirical relations resulting from dimensional and other types of analysis of field and laboratory data; and statistical (principally time-series or spectral) models. Chapter III is given over to a discussion of the current status of the problem, and summarizes what is known and reviews the major stumbling blocks to further progress. In Chapter IV a new equation, based on a somewhat unconventional theory, for dune height is developed. Verification of five of the leading empirical dune-height relations is presented in Chapter V. Chapter VI recommends a new approach to dune management, and the summary and conclusions are presented in Chapter VII.

The following considerations, which are somewhat philosophical in nature, may be helpful to the understanding of the analyses reviewed below, and to appreciation of the difficulties encountered in analysis of sedimentary bed forms. First, it should be borne in

mind that bed forms are the result of an instability that is inherent in the flow, or more precisely stated, in the interaction of the flow with the bed. There appear to be at least two types of instability. The first, which occurs at relatively low Froude numbers, is an instability that originates at the flow-bed interface, and is present also in the case of very deep flows and flows without free surfaces (e.g., sediment-transporting flows in closed conduits). It produces ripples, dunes, and bars.\* The second principal type of instability results from an interaction between standing waves on the water surface and the bed, and produces antidunes. The latter type of instability will not be considered further herein.

The first instability--the one that produces ripples, dunes and bars--is, in certain limited respects, similar to that which produces turbulence in fluid flows. Each occurs only over a limited range of conditions. For other conditions--sufficiently low or high sediment-transport rates for bed forms; sufficiently low Reynolds number for turbulence--the flows are stable, resulting in a flat sediment bed and laminar flow, respectively. Both turbulence and bed forms can be prevented for flows in the ranges of instability, provided almost heroic measures are taken to prevent the flow and/or bed surface from becoming even slightly disturbed. Any disturbance rapidly amplifies, and equilibrium turbulence or bed forms soon emerge. Bed forms and turbulence both are comprised of a range of frequencies, and there is flux of wave content among the components of different frequencies. In the case of turbulence, the flux is from the lower frequencies (big eddies), at which the turbulence is generated, to the higher frequencies, where the turbulence energy is dissipated. Bed forms, on the other hand, are generated at the higher frequencies (shorter wavelengths), which merge (due to the frequency dependence of celerity) to form waves of lower frequency which are dissipated by the flow (Jain and Kennedy 1974). Both bed forms and turbulence in their fully developed state are characterized by equilibrium

---

\* The nomenclature utilized herein is that adopted by the ASCE Task Committee on Bed Forms in Alluvial Channels (1966).

distributions of frequencies. For turbulence, the equilibrium spectral content varies as  $f^{5/3}$  ( $f$  = frequency), over the equilibrium range of the well known Kolmogoroff spectrum. Equilibrium-range bed-form spectra vary as  $f^{-3}$  (Jain and Kennedy 1974; see also papers cited therein for further description of frequency content of bed forms).

Finally, and perhaps most important, is the fact that both turbulence and bed forms are an inherent characteristic or property of most flows of engineering interest in their respective fields. Either can be suppressed, but only over short distances or times, and only by extraordinary measures (e.g., turbulence suppression by flow constrictions like those found upstream of wind-tunnel throats). Both have decidedly good effects, and without them Earth would be a far different place. Without turbulence, it could not, for example, support life as we know it. Without bed forms, river stages would vary much more widely with rising and falling discharge, thereby exacerbating flooding and navigation problems.

Both turbulence and bed forms present engineering with formidable problems. Because the underlying instabilities cannot be avoided, both turbulence and bed forms, and the untoward effects they produce, must be allowed for and managed to the extent possible.

## II. SUMMARIES OF RESULTS

A. Introductory Remarks. This review presents the significant results of the principal studies in summary form. The studies are divided into three categories according to the approach followed: analytical, empirical, or statistical. The studies are presented in chronological order in each category. Each summary utilizes the mathematical symbols and, as appropriate, some of the sketches appearing in the source reference. The source-reference figure numbers and figure captions are retained.

B. Analytical Models. Eleven studies of this type were reviewed, starting with the classical study of Exner (1925).

B.1. Exner (1925) (source reference: Leliavsky (1955)).

### Basis of theory

1. "Erosion" equation (sediment-continuity and sediment-transport relations).

$$\frac{\partial \eta}{\partial t} = \varepsilon \frac{\partial v}{\partial x} \quad (1)$$

2. Fluid continuity.

$$b(z-\eta) v = Q = \text{const.} \quad (2)$$

3. Fluid momentum

$$\frac{\partial v}{\partial t} + v \frac{\partial v}{\partial x} + kv - \gamma + \frac{1}{\rho} \frac{\partial p}{\partial x} = 0 \quad (3)$$

### Principal results and observations

1. Combining (1) and (2) yields

$$\frac{\partial \eta}{\partial t} = - \frac{M}{(z-\eta)^2} \frac{\partial \eta}{\partial x} \quad (4)$$

after neglecting  $\frac{\partial z}{\partial x}$ . General solution of (4) is

$$z - \eta = f\left[\frac{Mt}{(z-\eta)^2} - x\right] \quad (5)$$

For initial profile  $\eta_0$  at  $t = 0$

$$\eta_0 = A_0 + A_1 \cos \alpha x \quad (6)$$

bed profile at time  $t$  is

$$\eta = A_0 + A_1 \cos \alpha\left[x - \frac{Mt}{(z-\eta)^2}\right] \quad (7)$$

These profiles are shown for different  $t$  in Fig. B.1.2. Their celerity is

$$c = \frac{M}{(z-\eta)^2} \quad (8)$$

and their amplitude remains constant.

2. Including effects of fluid dynamics, by combining (3) with (1) and (2) yields, after linearization,

$$\frac{\partial^2 \eta}{\partial t^2} - \eta \frac{\partial^2 \eta}{\partial x \partial t} + k \frac{\partial \eta}{\partial t} - E \frac{\partial^2 \eta}{\partial x^2} = 0 \quad (9)$$

For  $\eta_0$  given by (6), bed profile at any  $t$  is

$$\eta = A_0 + A_1 e^{-\left(\frac{k}{2} - j\right)t} \cos \alpha\left[x - \frac{N}{2j} \left(\frac{k}{2} - j\right)t\right] \quad (10)$$

If friction is neglected ( $k = 0$ ) in (10)

$$\eta = A_0 + A_1 \cos \alpha[x - (\sqrt{E + N^2/4} t)]. \quad (11)$$

"Velocity of the bank movement" given by (10) is

$$c = \frac{N}{2j} \left( \frac{k}{2} - j \right) \quad (12)$$

$c$  increases with  $k$  (i.e., with decreasing wavelength,  $\lambda$ ).

3. If friction is included, wave amplitude decreases as waves move downstream. For zero friction, amplitude remains constant but waves distort as they move (see, e.g., figure B.1.2).
4. Because formulation is quasi one-dimensional, analysis is limited to very long bed forms (i.e., dunes and bars; not ripples).
5. No relations for wavelength or height of bed forms result from this analysis.
6. Analysis is noteworthy as first of stability type analyses, and for laying groundwork for most future analyses of this genre.
7. Exner extended analysis to include effects of variation of channel width.

Figures

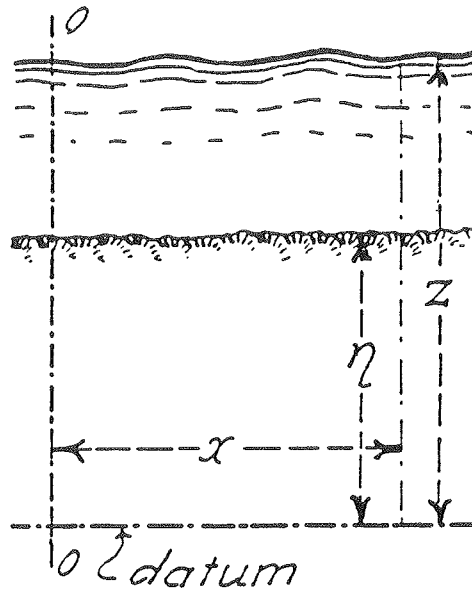


FIG. 12. Key-diagram for Professor Exner's notation.

Figure B.1.1.

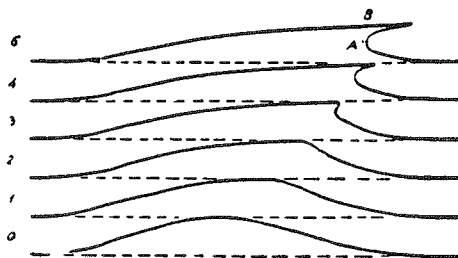


FIG. 13. Professor Exner's mathematically derived dune profile.

Figure B.1.2. Profiles at different times given by (9) and (10).

## Notation

Some notation is defined in the figures.

$A_0, A_1$	=	defined in (6)
$b$	=	channel width
$E$	=	$\epsilon g$
$f$	=	any function
$g$	=	gravity acceleration
$j$	=	function of $\alpha$ and $k$ ; $0 < \frac{k}{2} - j < k/2$ , depending on $\lambda$ .
$k$	=	coefficient in linearized friction term
$M$	=	$\frac{\epsilon Q}{b}$
$N$	=	$gQ/bv_m^2 - v_m$
$p$	=	pressure
$Q$	=	discharge
$t$	=	time
$v$	=	local mean (depth-averaged) velocity
$v_m$	=	average velocity over whole flow
$\alpha$	=	$2\pi/\lambda$
$\gamma$	=	component of fluid weight along channel
$\epsilon$	=	"erosion coefficient"
$\lambda$	=	wavelength
$\rho$	=	fluid density

B.2. Anderson (1953).

Basis of theory

1. Sediment continuity.

$$\frac{\partial Q'}{\partial x} + \frac{\partial \eta}{\partial t} = 0 \quad (1)$$

2. Sediment-transport relation.

$$Q' = \gamma k u(x,0) \quad (2)$$

3. Potential-flow description of stationary water-surface waves of sinusoidal form on flow over a sinusoidal bed (see Fig. B.2.1)

4. Karman's logarithmic velocity distribution is used to estimate  $u$  near the bed, which is required to obtain  $Q'$  from (2):

$$u = \frac{B\sqrt{g}}{C} U \quad (3)$$

Principal results and observations

1. Bed profile is given by

$$\eta = \frac{2a}{\cosh mh} \sin \beta t \cos (mx - \beta t) \quad (4)$$

where

$$c = \frac{\beta}{m} = \frac{\gamma k U m \cosh mh}{2 \sinh mh} \quad (5)$$

2. Wavelength relation is obtained by equating amplitude given by (4) with  $\sin \beta t = 1$  to that for equilibrium flow over a sinusoidal bed:

$$mh(\tanh mh - \frac{2}{\sinh 2mh}) = \frac{gh}{U^2} = \frac{1}{Fr^2} \quad (6)$$

Verification of (4) is presented in Fig. B.2.2.

3. Bed-form celerity is obtained by substituting (3) into (2), and then the resulting expression for  $\gamma k$  into (5):

$$c = \frac{\beta}{m} = \frac{C_m \coth mh}{2\gamma_g B \sqrt{g}} G \quad (7)$$

4. Observations:

- (a) Anderson did not allow for movement of bed forms in formulation of the velocity potential. His formulation actually is for moving bed waves passing under stationary water waves. This gives rise to  $\sin \beta t$  term in (4).
- (b) Wavelength relation is obtained by equating maximum amplitude reached by bed form migrating under stationary surface waves to bed amplitude which produces stationary surface waves of fixed amplitude

- a. Setting  $\sin \beta t = 1$  in (4) is not warranted, and good agreement shown in Fig. B.2.2. is considered almost fortuitous.
- (c) Form of celerity relation is generally correct, with  $c$  increasing with decreasing  $\lambda$  and increasing  $G$ .

Figures

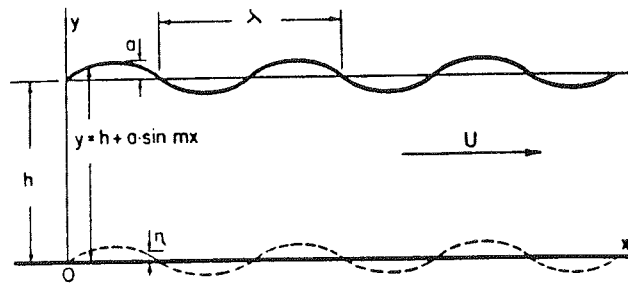


Fig. 4 - Definition Sketch for Evaluating Length of Sediment Waves

Figure B.2.1.

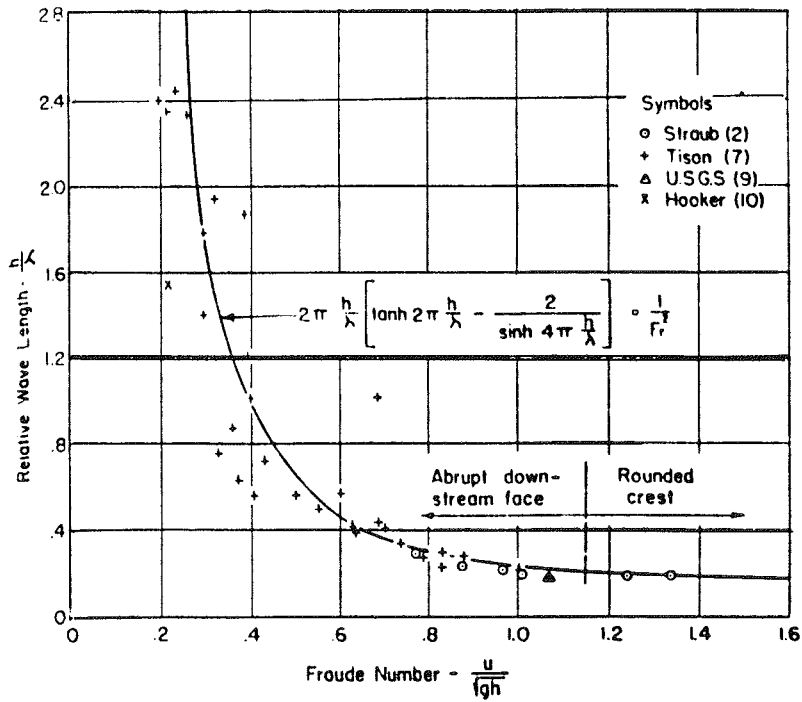


Fig. 5 - Relative Wave Length as a Function of Froude Number

Figure B.2.2

## Notation

Some notation is defined in the figures.

B	=	$8.5 + 5.75 \log y/d_g$
c	=	bed-form celerity
C	=	Chezy coefficient
$d_g$	=	sand size
$F_r$	=	Froude number
G	=	total volumetric sediment discharge per unit width
m	=	$2\pi/\lambda$
$Q'$	=	volumetric discharge, per unit width, of sediment participating in bed-form migration
t	=	time
$u(x,y)$	=	horizontal velocity at (x,y)
U	=	mean velocity
$\beta$	=	cm = temporal frequency of bed forms
$\gamma_g$	=	bulk specific weight of bed sediment
$\gamma_k$	=	constant, equivalent to Exner's "erosion coefficient"
$\lambda$	=	wavelength

### B.3. Kennedy (1963)

#### Basis of theory

1. Potential-flow formulation of free-surface flow over a sinusoidal bed moving downstream with celerity  $U_b$  (see Fig. B.3.1.).

2. Sediment continuity

$$\frac{\partial G}{\partial x} + B \frac{\partial \eta}{\partial t} = 0 \quad (1)$$

3. Power-law sediment transport relation, with phase shift  $\delta$

$$G(x,t) = m \left[ \frac{\partial \phi}{\partial x} (x-\delta, -d,t) \right]^n \quad (2)$$

4. Assumption that observed bed forms are those with wavelength that produces fastest amplitude growth; i.e., those for which

$$\frac{\partial^2 a}{\partial t \partial k} = 0 \quad (3)$$

#### Principal result and observations

1. Wavelength relation is (see Fig. B.3.2)

$$F^2 = \frac{U^2}{gd} = \frac{1 + kd \tanh kd + k\delta \cot k\delta}{(kd)^2 + (2 + k\delta \cot k\delta) kd \tanh kd} \quad (4)$$

2. Bed-form celerity for wavelength given by (4) is

$$U_b = \frac{n\bar{G}k}{2B} \left[ \frac{\sinh 2kd + 2kd}{\sinh^2 kd - jkd \cot jkd - 1} \right] \cos jkd \quad (5)$$

3. Analysis yields mathematical basis for classification of bed forms (see Fig. B.3.3).

4. Observations:

- (a) Phase shift  $\delta$  between local sediment discharge and local near-bed velocity is of central importance to the theory. Such a phase shift unquestionably exists, but it has not been well formulated. In actuality, this phase shift includes: phase shift between local bed elevation and local near-bed velocity; phase shift between local bed elevation and local bed shear stress; "adjustment distance" of local sediment-transport rate to local flow conditions; and gravitational effect of local bed slope on local sediment discharge.
- (b) This is a linearized (small wave amplitude) theory, and therefore is likely of limited value in analyzing fully developed bed forms.

Figures

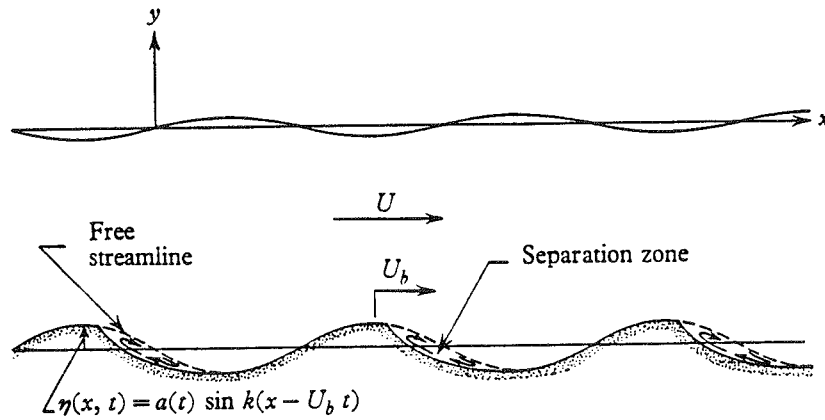


FIGURE 5. Free-surface flow over a dune bed, showing the separation in the lee of each dune. The lowest streamline of the flow is assumed to be a sinusoid.

Figure B.3.1.

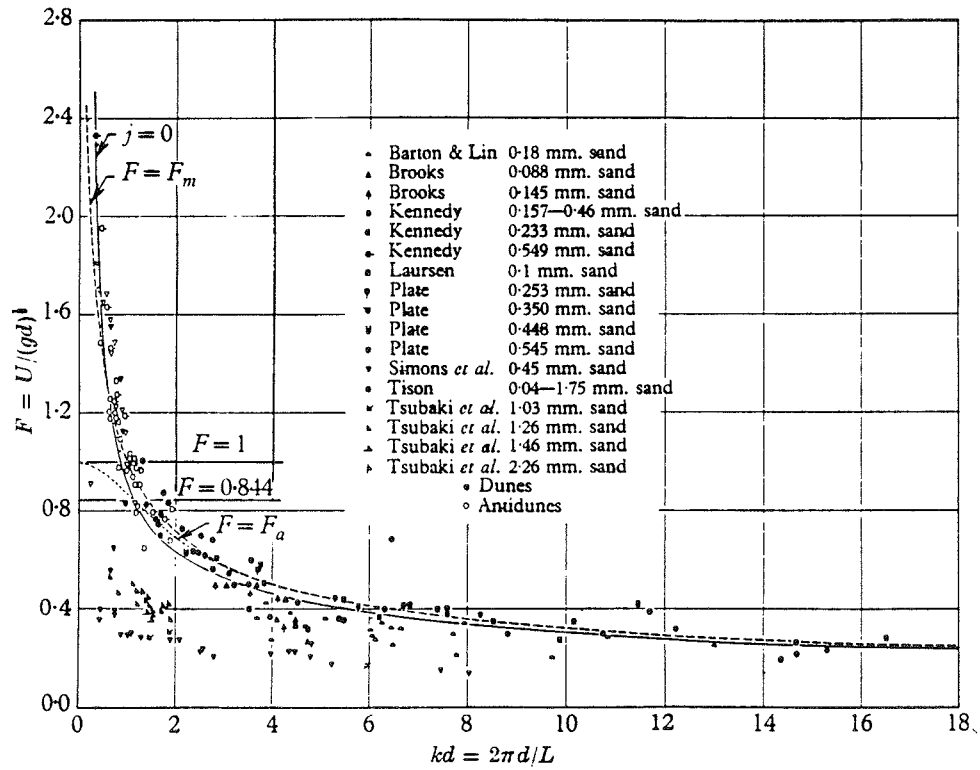


FIGURE 9. Comparison of predicted and observed regions for formation of different bed configurations.

Figure B.3.2.

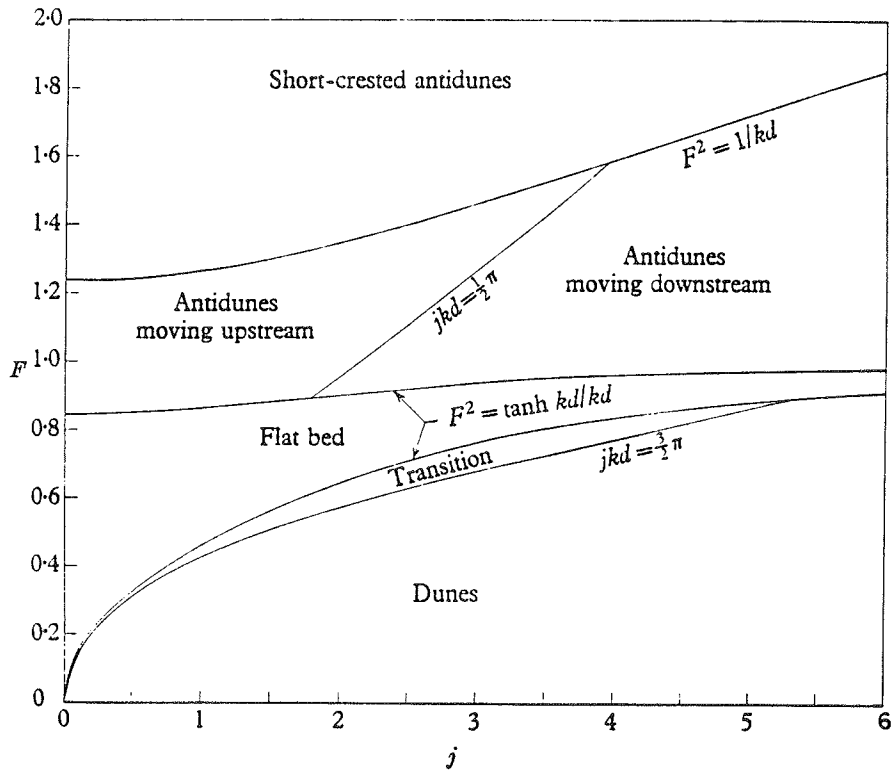


FIGURE 8. Conditions for occurrence of different bed configurations.

Figure B.3.3.

## Notation

Some notation is defined in the figures.

$a$	=	bed-form amplitude
$B$	=	bulk specific weight of bed sediment
$d$	=	mean flow depth
$F$	=	Froude number
$G$	=	sediment discharge per unit width, on a weight basis
$\bar{G}$	=	average (along channel) value of $G$
$j$	=	$\delta/d$
$k$	=	$2\pi/L$
$L$	=	wavelength
$n,m$	=	constants in sediment-discharge relation
$t$	=	time
$U_b$	=	bed-form celerity
$x,y$	=	space coordinates
$\delta$	=	phase shift between local sediment discharge and local near-bed velocity
$\eta(x,t)$	=	bed elevation
$\phi$	=	velocity potential

#### B.4. Kennedy (1969)

This review article presented further development and interpretation of Kennedy's (1963) theoretical model. The principal elements of Kennedy's theory are depicted in Fig. B.4.1. Corrections to the theory made by Reynolds (1965) were included, and the resulting revisions to the predicted conditions for occurrence of different bed forms were made. The principal new development, outlined below, was a predictor for heights of bed forms.

##### Basis of theory

1. Modification of Kennedy's 1963 theory gives bed-form celerity as

$$U_b = (\bar{T}_b/\beta)nk \frac{U}{U - U_c} \frac{1 - F^2kd \tanh kd}{\tanh kd - F^2kd} \quad (1)$$

2. Average sediment discharge in bed-form migration is

$$\bar{T}_b = (U_b/L)a_0 \int_0^L (1 + \sin kx)dx = U_b a_0 \quad (2)$$

##### Principal results and observations

1. Revised diagram for occurrence of different bed forms, given in Fig. B.4.2.
2. Limiting wavelength relations were modified in accordance with Reynolds' (1965) findings, with results shown in Fig. B.4.3. Kennedy's basic wavelength relation ((4) of Section B.3) remained unchanged.

3. (1) and (2) yield the following relation for ripple steepness

$$\frac{2a_0}{L} = \frac{\beta}{n\pi} \frac{U - U_c}{U} \frac{\tanh kd - F^2 kd}{1 - F^2 kd \tanh kd} \quad (3)$$

Good agreement was obtained between the bed-wave-steepness relation and flume data for flows over coarse beds (see Table B.4.1).

Figures and Tables

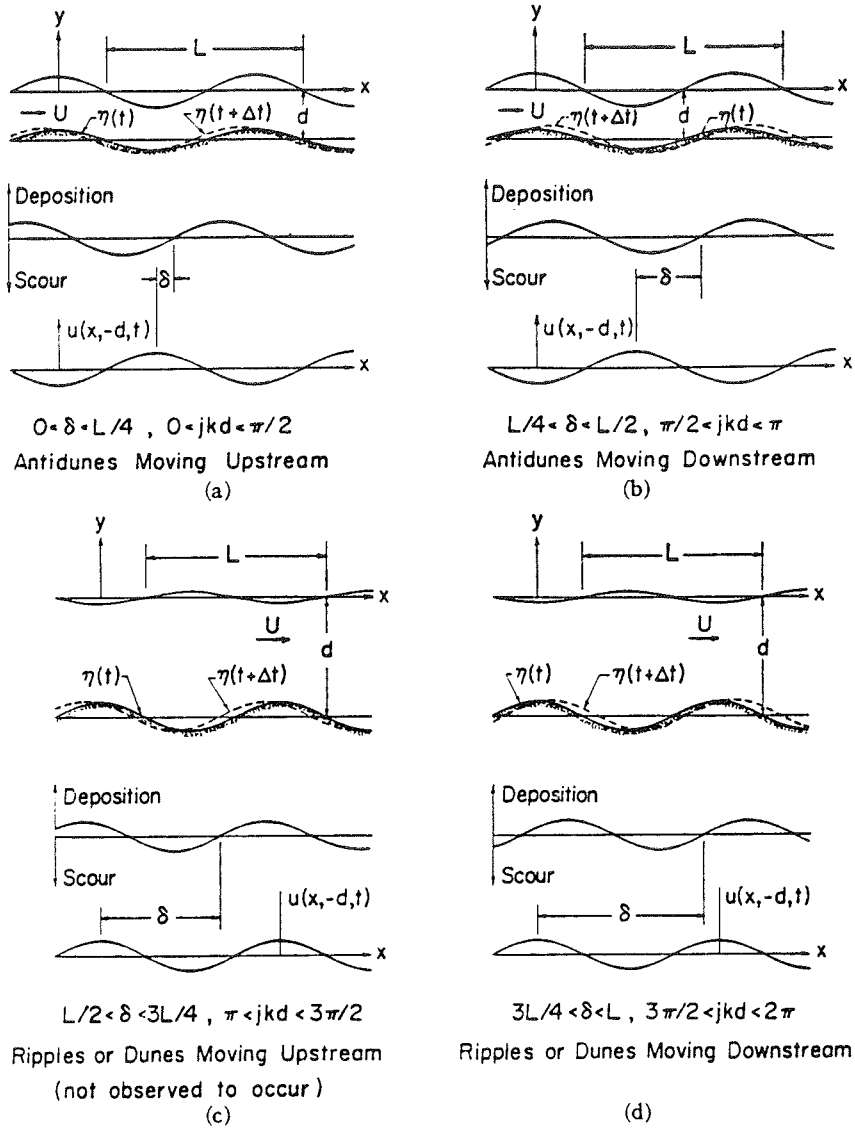


FIG. 2. Mechanisms of instability for principal bed forms predicted by the potential-flow stability analysis ( $u = \phi_x$ , the  $x$  component of the velocity).

Figure B.4.1. Graphical depiction of key elements of Kennedy's (1963) theory.

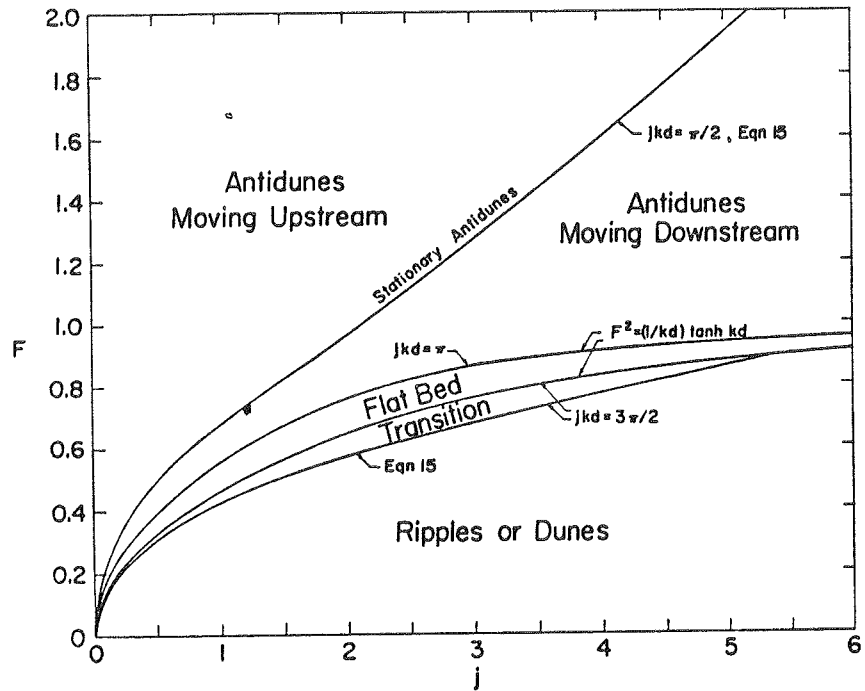


FIG. 4. Conditions for occurrence of various bed forms.

Figure B.4.2.

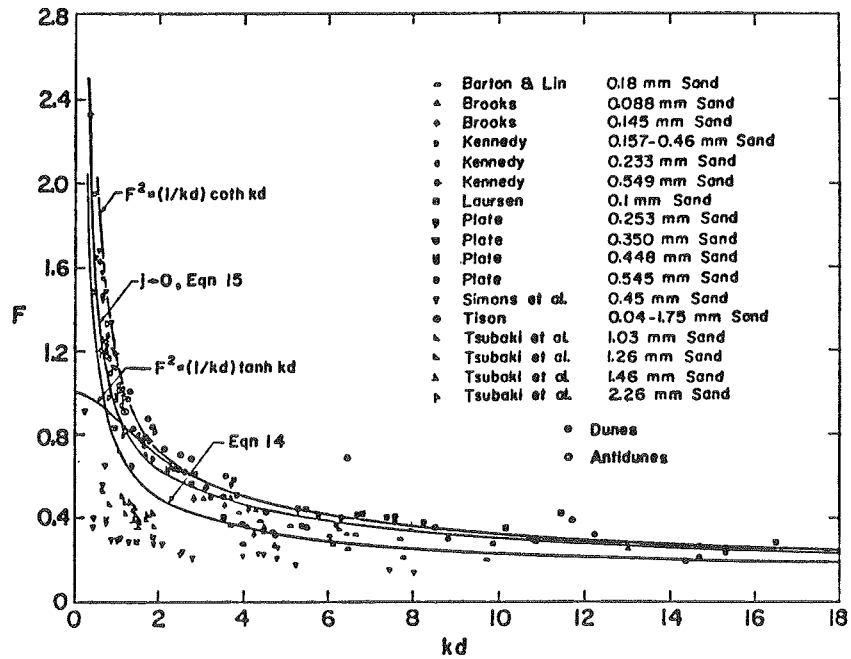


FIG. 5. Comparison of predicted and observed ranges of  $kd$ .

Figure B.4.3.

TABLE II  
COMPARISON OF COMPUTED AND MEASURED<sup>a</sup> VALUES OF  $U_b$  AND  $2a_b$ <sup>b\*</sup>

Run No.	$U$ ft/sec	$L$ ft	$d$ ft	$\bar{T}_b \times 10^3$ ft <sup>2</sup> /sec	$U_b$ (Equation 19) ft/min	$U_b$ (meas.) ft/min	$2a_b$ (Equation 20) ft	$2a_b$ (meas.) ft
18	1.66	2.11	1.01	0.022	0.04	0.06	0.06	0.04
28	1.75	3.7	1.04	0.032	0.03	0.07	0.12	0.05
15	1.93	2.6	1.05	0.077	0.09	0.14	0.11	0.09
14	1.60	2.8	0.58	0.036	0.07	0.07	0.06	0.03
34	1.64	2.9	0.54	0.040	0.08	0.12	0.06	0.02
16	2.03	3.6	1.04	0.168	0.13	0.13	0.15	0.16
35	1.80	2.9	0.53	0.120	0.19	0.20	0.08	0.06
17	2.10	3.5	1.00	0.241	0.19	0.18	0.16	0.18
33	1.83	3.3	0.56	0.161	0.22	0.18	0.09	0.08
5	2.21	5.2	0.93	0.29	0.17	0.17	0.20	0.28
10	1.88	3.9	0.46	0.23	0.31	0.24	0.08	0.12
37	2.54	6.6	1.11	0.60	0.25	0.27	0.28	0.34
36	2.04	3.5	0.55	0.32	0.37	0.32	0.10	0.13
6	2.68	5.8	1.04	0.44	0.70	0.45	0.27	0.31
7	2.14	4.5	0.59	0.37	0.35	0.44	0.12	0.19
38	2.78	6.3	1.02	1.20	0.52	0.58	0.27	0.30
11	3.02	7.4	0.92	0.98	0.46	0.60	0.25	0.32
8	2.46	5.9	0.57	1.03	0.92	0.59	0.14	0.17
12	3.12	4.8	0.89	2.16	1.16	1.16	0.22	0.23

<sup>a</sup> (3) pp. 68-9.

<sup>b</sup>  $n=2.64$ ,  $U_c=1.30$  ft/sec,  $\beta=1$ , mean sand size = 0.93 mm.

Table B.4.1

\* A table of factors for converting non-SI units of measurement to SI (metric) units is presented on page iv.

## Notation

Most of the notation in this paper is the same as in Kennedy's 1963 paper (see B.3). New notation is as follows:

$a_0$	=	equilibrium amplitude of bed forms
$\bar{T}_b$	=	average sediment discharge in migration of the bed forms
$U_c$	=	critical velocity for initiation of sediment motion
$\beta$	=	ratio of bed-load discharge to suspended-load discharge

## B.5. Hayashi (1970)

### Basis of theory

1. Hayashi modified Kennedy's (1963) theory by adopting a slightly different transport relation, which takes account of the effects of bed slope on sediment discharge:

$$T(x,t) = m \left[ 1 + \alpha \frac{\partial \eta(x - \delta, t)}{\partial x} \right] \left[ \phi_x(x - \delta, \underbrace{-d, t}) \right]^4 \quad (1)$$

### Principal results and observations

1. Modified criteria for the conditions of occurrence of different bed forms were obtained (Fig. B.5.1).
2. Agreement of theoretical and observed conditions for occurrence of different bed forms is quite satisfactory (Fig. B.5.2).
3. No new relations for heights or wavelengths of bed forms were developed.
4. Hayashi recommended  $1.5 < C < 3$ .  $C = 2$  appears to yield quite good results.
5. This paper points up the importance of local bed slope along the bed forms on their formation and behavior.

Figures

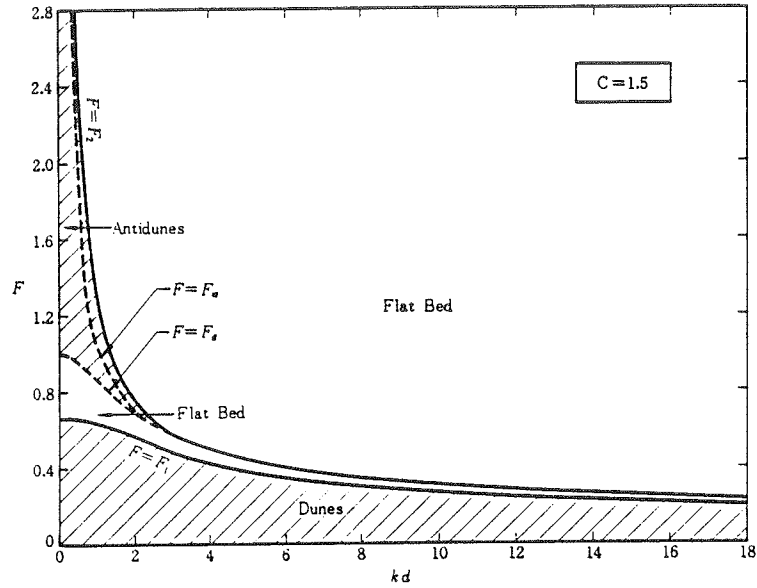


FIG. 4.—REGIONS OF OCCURRENCE OF SAND WAVES FOR CASE  $C = 1.5$

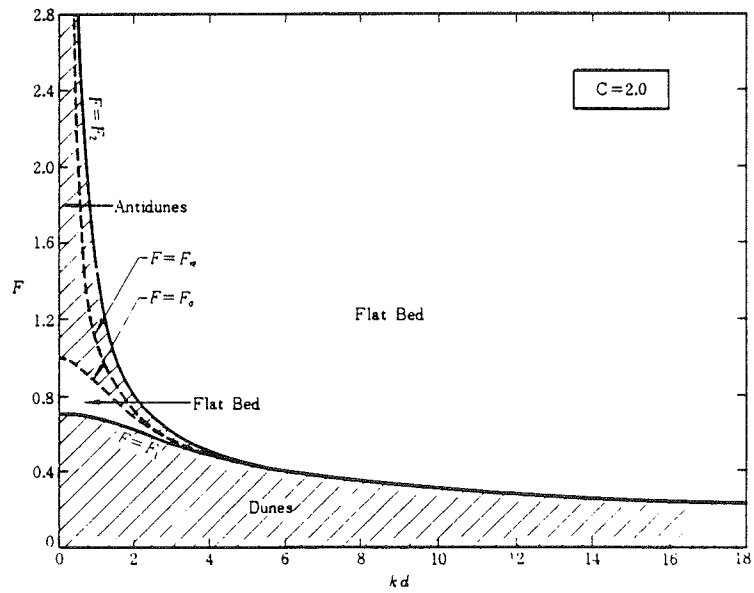


FIG. 5.—REGIONS OF OCCURRENCE OF SAND WAVES FOR CASE  $C = 2.0$

Figure B.5.1.

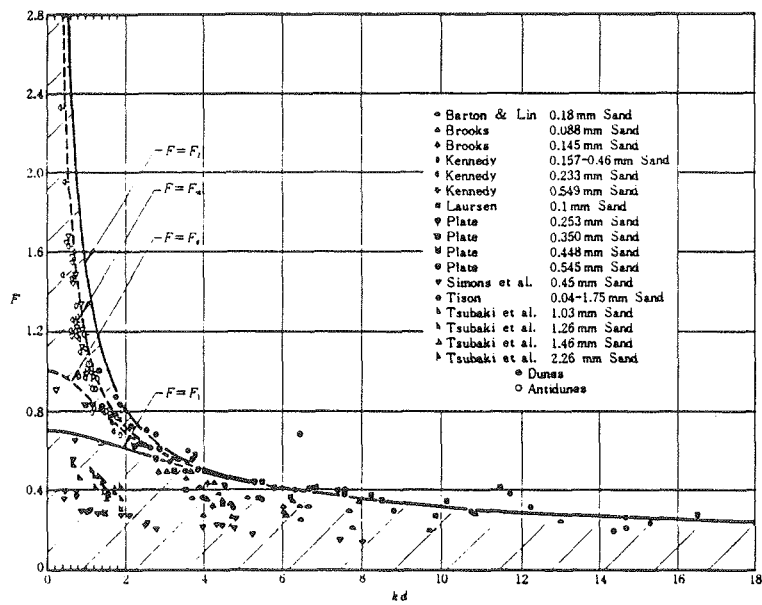


FIG. 8.—COMPARISON OF PREDICTED REGIONS OF OCCURRENCE OF SAND WAVES FOR CASE  $C = 2.0$  WITH EXPERIMENTAL RESULTS SUMMARIZED BY KENNEDY (2)

Figure B.5.2.

## Notation

Most of the notation in this paper is the same as in Kennedy's 1963 paper (see

B.3). New notation is as follows:

$$C = \alpha/[2g\delta/U^2]$$

$$F = \text{Froude number}$$

$$F_1 = \text{maximum. } F \text{ for formation of dunes}$$

$$F_2 = \text{maximum. } F \text{ for formation of antidunes}$$

$$F_a = \text{minimum. } F \text{ for function of antidunes; } F_a^2 = \frac{\tanh kd}{kd}$$

$$F_m = F_2 \text{ for } C = 0; F_m^2 = \frac{\coth kd}{kd}$$

$$T(x,t) = \text{local sediment discharge}$$

$$\text{Note: } (F_2^2, F_1^2) = \frac{1}{4kd \tanh kd} [C + 2 \pm \sqrt{(C+2)^2 - 8 C \tanh^2 kd}]$$

$$\alpha = \text{dimensionless coefficient}$$

## B.6. Engelund (1970)

### Basis of theory

1. Vorticity transport equation. A stream function is used to specify the motion. (Hence, a 2-D analysis).
2. Continuity equations for suspended load and total load.
3. Transport formulas for bed load and suspended load discharges.
4. Assumption that eddy viscosity is uniform over depth and there is a "slip velocity" at the bed between the flow and the bed.
5. Perturbation stability analysis. A sinusoidal perturbation is introduced in bed level and water surface.
6. Boundary conditions: (a) vanishing vertical fluxes at bed and water surface; (b) no shear stress at water surface; (c) appropriate description of bed shear stress in terms of slip velocity; and (d) relation between bed shear stress and sediment concentration at the bed.

### Principal results and observations

1. When bed load discharge is neglected, bed instability is predicted for a range of Froude numbers around and above unity (antidunes). Upper limit is given by

$$F^2 = \coth(kD)kD \quad (1)$$

(same as predicted by Reynolds 1965), and lower limit is given by

$$F^2 = \tanh(kD)/kD \quad (2)$$

(see Fig. B.6.1).

2. When bed load discharge is included, bed instability is predicted in the lower range of Froude numbers as well (dunes) (see Fig. B.6.2).
3. Complete solution is seen in Figure B.6.3.
4. No prediction of dune height is given.

Figures

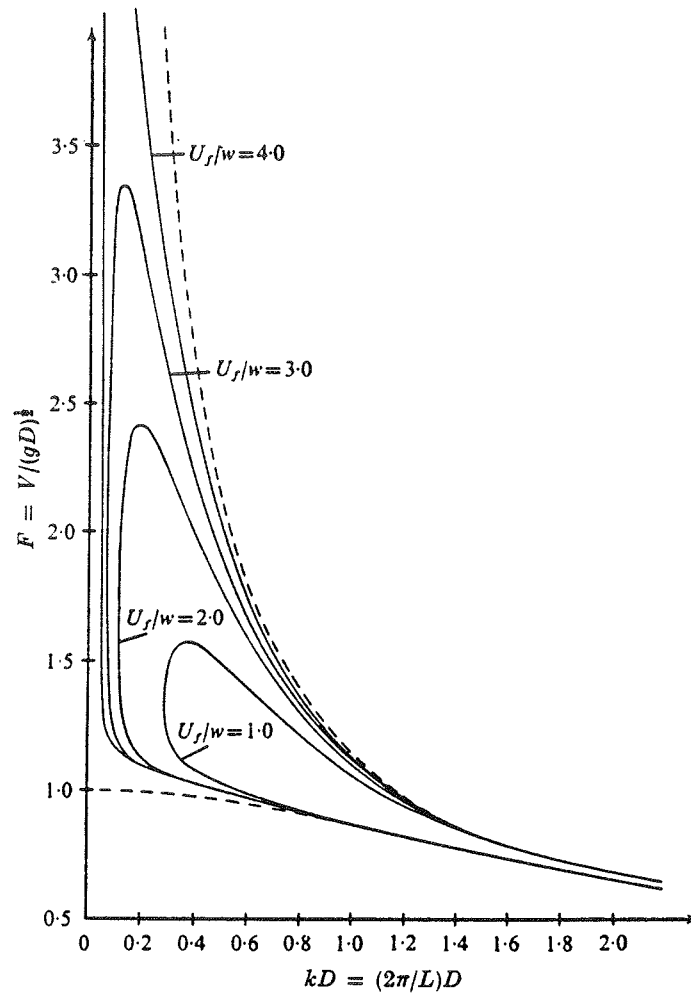


FIGURE 5. Stability diagram for the case of negligible bed load, corresponding to  $V/U_f = 17$ .

Figure B.6.1.

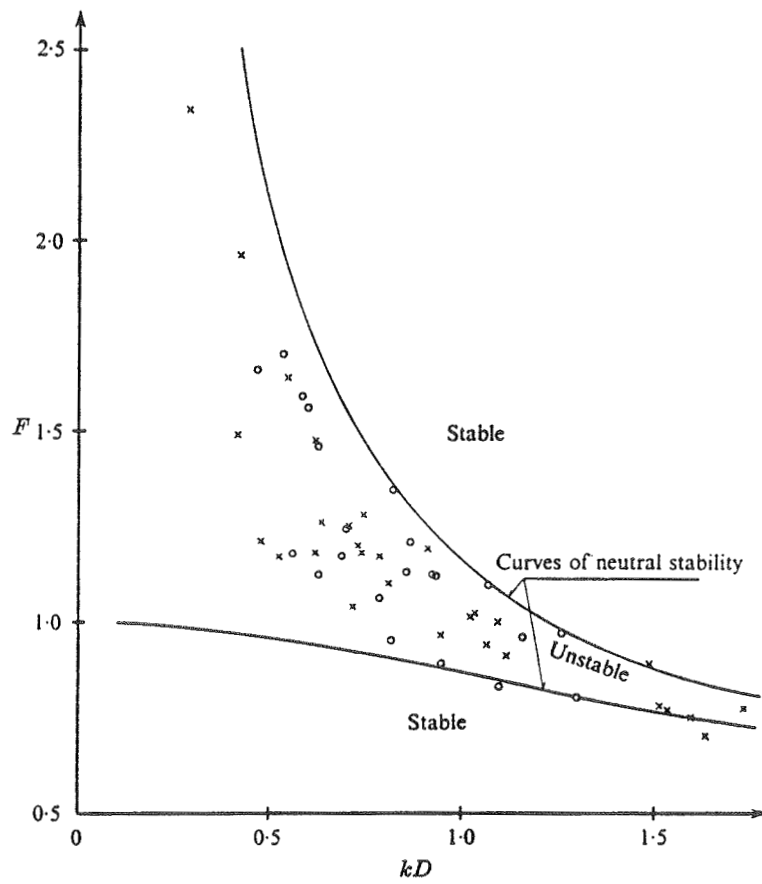


FIGURE 6. Asymptotic stability boundaries. Experiments by Guy, Simons & Richardson (1966): O,  $d = 0.19-0.47$  mm; and by Kennedy (1961): x,  $d = 0.23-0.55$  mm.

Figure B.6.2.

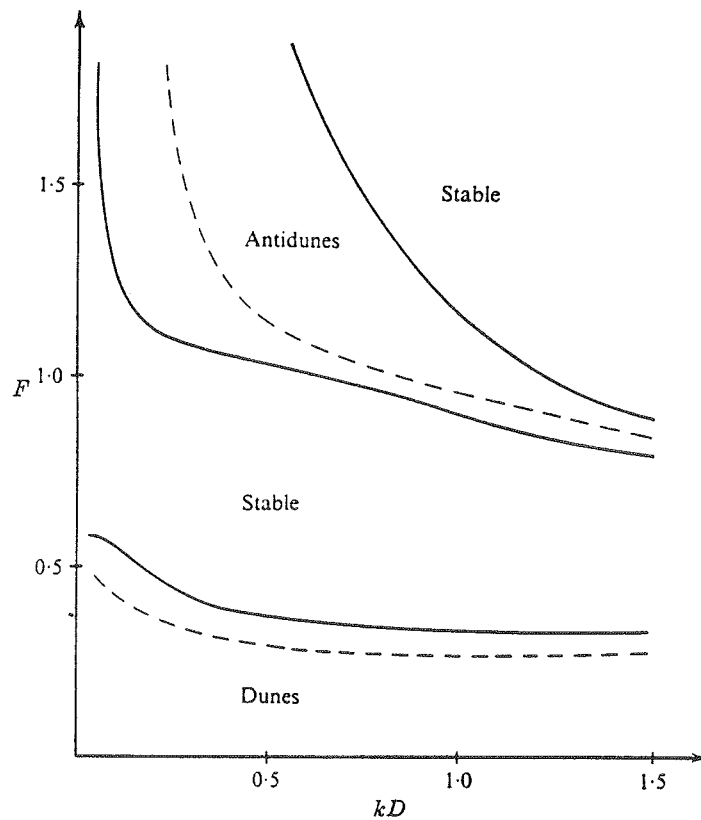


FIGURE 10. Stability diagram for the complete solution. The parameters are  $V/U_f = 21$  and  $U_f/(wF) = 1$ .

B.6.3.

## Notation

$d$	=	grain size
$D$	=	flow depth
$F$	=	Froude number
$k$	=	wave number
$U_f$	=	friction velocity
$V$	=	mean velocity
$w$	=	fall velocity

## B.7. Gill (1971)

### Basis of theory

#### 1. Sediment continuity

$$\frac{\partial z}{\partial t} + \frac{\partial q_s}{\partial v} \frac{\partial v}{\partial x} = 0 \quad (1)$$

#### 2. Flow continuity

$$q = v(h - z) \quad (2)$$

#### 3. Sediment-transport relation

$$q_s = Cq_{so} \left( \frac{\tau}{\tau_c} - 1 \right)^n \quad (3)$$

#### 4. Friction relation

$$\tau = f \frac{\gamma v^2}{2g} \quad (4)$$

#### 5. Momentum equation

$$v \frac{\partial v}{\partial x} + g \frac{\partial h}{\partial x} + \frac{g v^2}{C_o^2 (h-z)} = 0 \quad (5)$$

## Principal results and observations

1. For the case of zero friction ( $f = 0$ ;  $C_0 \rightarrow \infty$ ), the bed-form celerity is

$$v_b = \frac{2nq_s}{d(1 - F^2)} \frac{1}{\left(1 - \frac{\tau_c}{\tau}\right)} \quad (6)$$

and the bed-form height (see Fig. B.7.1) is given by

$$\Delta = \frac{d(1 - F^2)}{2\alpha n} \left(1 - \frac{\tau_c}{\tau}\right) \quad (7)$$

2. The corresponding results if friction is included are

$$v_b = \frac{2nq_s}{d(1-F^2)\left(1-\frac{\tau_c}{\tau}\right)} \left[1 + \frac{1}{2} \frac{v}{f} \frac{\partial f}{\partial v}\right] \quad (8)$$

and

$$\Delta = \frac{d(1 - F^2)}{2n\alpha} \frac{\left(1 - \frac{\tau_c}{\tau}\right)}{\left(1 + \frac{1}{2} \frac{v}{f} \frac{\partial f}{\partial v}\right)} \quad (9)$$

3. General expression, without specification of a sediment-transport relation, for  $v_b$  is

$$v_b = \frac{v}{d(1 - F^2)} \frac{\partial q_s}{\partial v} \quad (10)$$

The relation was earlier obtained by Reynolds (1965) and Gradowczyk (1968).

4. If dynamic effects are neglected ( $F = 0$ ), (7) yields, for  $n = 3$ ,

$$\frac{\Delta}{d} = \frac{1}{6\alpha} \left( 1 - \frac{\tau_c}{\tau} \right) \quad (11)$$

which is identical (except for  $\alpha$ ) to Yalin's (1964; see Section C.2) Eq. 13.

5. Gill presented no verification of his results.

Figures

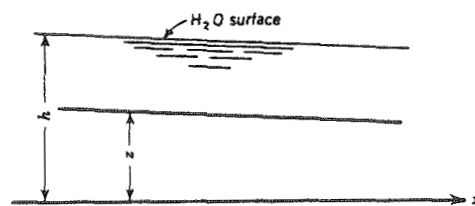


FIG. 1.—DEFINITION SKETCH OF OPEN CHANNEL WATER FLOW

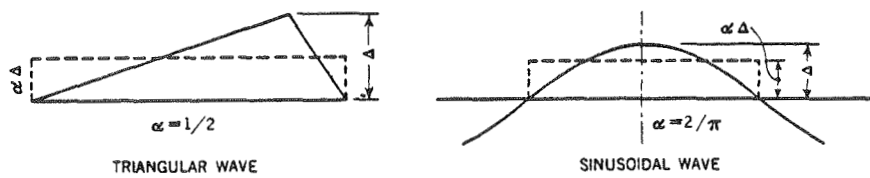


FIG. 2.—DEFINITION SKETCH OF TRIANGULAR AND SINUSOIDAL BED WAVES

Figure B.7.1.

## Notation

Some notation is defined in the figure.

C	=	coefficient in (3)
C <sub>o</sub>	=	Chezy coefficient
D	=	particle diameter
f	=	Darcy-Weisbach friction factor
F	=	Froude number
g	=	gravity acceleration
n	=	exponent in (3)
q	=	water discharge per unit width
q <sub>s</sub>	=	sediment discharge per unit width
q <sub>so</sub>	=	$\sqrt{g(S_s - 1) D^3}$
S <sub>s</sub>	=	specific gravity
t	=	time
v	=	mean velocity
v <sub>b</sub>	=	celerity of bed forms
$\alpha$	=	dune-shape factor ( $\alpha = \frac{1}{2}$ for triangular; $\alpha = \frac{2}{\pi}$ for sinusoidal)
$\gamma$	=	specific weight of fluid
$\tau$	=	bed shear stress
$\tau_c$	=	critical bed shear stress for initiation of motion

B.8. Fredsoe (1974).

Basis of theory

1. Same as that of Engelund (1970)
2. Influence of gravity on bedload transport is accounted for in transport relation:

$$\Phi_b = 8(\theta + \mu I - 0.47) \quad (1)$$

Principal results and observations

1. Stability criteria are somewhat different from those obtained by Engelund. (see Fig. B.8.1).
2. By investigating growth of dunes using second-order-approximation, theory explains asymmetry of dune shape (steepening of the downstream faces).
3. No relation for dune height is derived.

Figure

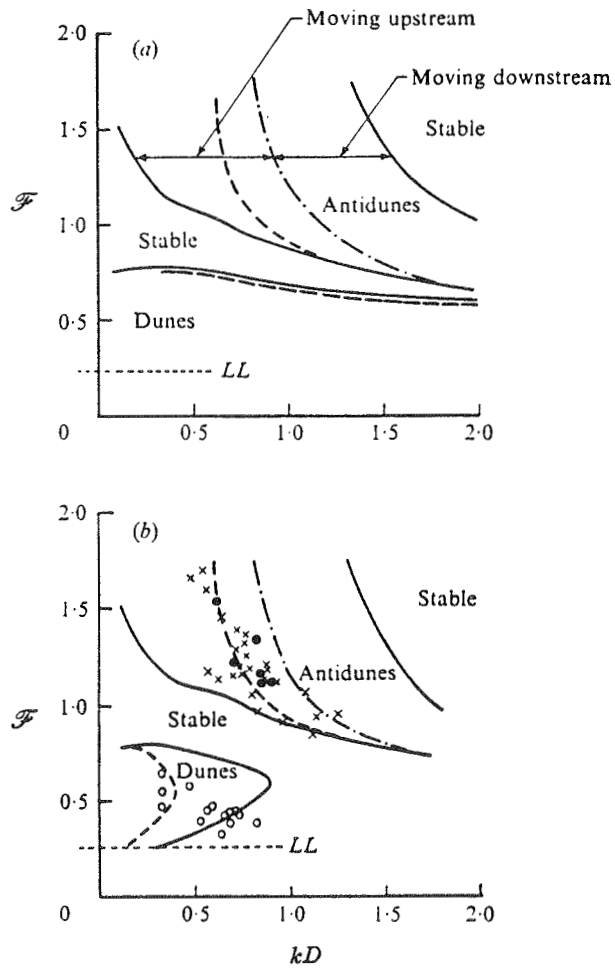


FIGURE 2. Stability diagrams.  $V/U_{*0} = 20$ . (a)  $\mu = 0$ . (b)  $\mu = 0.1$ . Experiments by Guy *et al.* (1966): x, antidunes; ●, standing waves; ○, dunes; LL, lower limit to sediment transport.

Figure B.8.1.

## Notation

$d$	=	particle diameter
$D$	=	depth
$F$	=	Froude number
$g$	=	gravity constant
$I$	=	local bed slope
$k$	=	wave number
$q_b$	=	bed-load discharge
$s$	=	specific gravity of sediment
$u$	=	coefficient ( $\approx 0.1$ )
$\theta$	=	$\frac{\tau}{g(s-1)d}$
$\Phi_b$	=	$\frac{q_b}{[(s-1)gd^3]^{1/2}}$
$\tau$	=	bed shear stress

Basis of theory

1. Equations of motion

$$U \frac{\partial U}{\partial x} + W \frac{\partial U}{\partial z} = - \frac{\partial p}{\partial x} + \frac{\partial}{\partial x} \tau_{xz} + \frac{\partial}{\partial z} \tau_{xz} + g \sin \alpha \quad (1)$$

$$U \frac{\partial W}{\partial x} + W \frac{\partial W}{\partial z} = - \frac{\partial p}{\partial z} + \frac{\partial}{\partial x} \tau_{xz} + \frac{\partial}{\partial z} \tau_{zz}, \quad (2)$$

2. Fluid continuity

$$\frac{\partial U}{\partial x} + \frac{\partial W}{\partial z} = 0 \quad (3)$$

3. Transformed coordinate system

$$x^* = x, z^* = z - h_0 \exp(ikx) F(z^*) \quad (4)$$

where

$$F(z^*) = \frac{\sinh k(D-z^*)}{\sinh kD} \quad (5)$$

4. Closure relations expressing turbulent stresses in terms of turbulent kinetic energy and its dissipation rate (equations not included here).

5. Sediment-transport relation

$$q_b = C(\tau_o)^m \quad (6)$$

6. Sediment-continuity relation

$$\frac{\partial q_b}{\partial x} = - (1-n) \frac{\partial h}{\partial t} \quad (7)$$

7. Perturbed bed-load discharge taken to be

$$q_b^s \sim u_*^2 \left( \tau - \beta \frac{\partial h}{\partial x} \right) \quad (8)$$

8. Linearization of equations to first order in bed forms steepness  $h_o k$ .

9. Examination of maxima of bed-shear-stress variation along  $x$ , and thus also of  $q_b$  (through (6)), to find wavelength that has fastest growth rate.

### Principal results and observations

1. Finds two maxima in bed shear stress. Argues that one corresponds to ripples, the other to dunes.
2. For ripples

$$0.07 < \frac{2\pi z_o}{\lambda} < 0.16 \quad (9)$$

for  $1.4 < \beta < 2.9$ .  $L$  is independent of depth. Bed is always stable for  $\beta > 2.9$ .

3. Stability limits and dominant wavelength for dunes given in Fig. B.9.2.
4. From examination of roughness length  $z_0$  for flow over moving beds, concludes

$$203d < \lambda_r < 4,050 d \quad (10)$$

for ripples.

5. Theoretical prediction of dune wavelength (see, e.g., Fig. B.9.2) are consistent with results of flume experiments cited by Allen (1970)

$$\lambda_d = 2\pi D \quad (11)$$

and Allen's (1970) empirical relation

$$\lambda_d = 1.16 D^{1.55} \quad (\lambda_d, D \text{ in m}) \quad (12)$$

(see Fig. B.9.3).

Figures

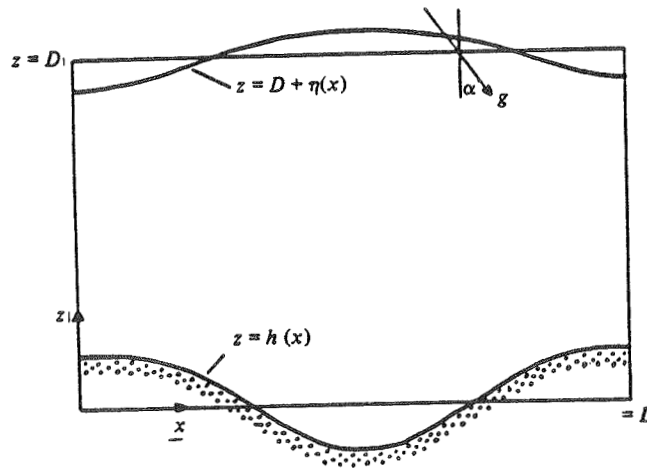


FIGURE 1. Definition sketch of flow region.

Figure B.9.1.

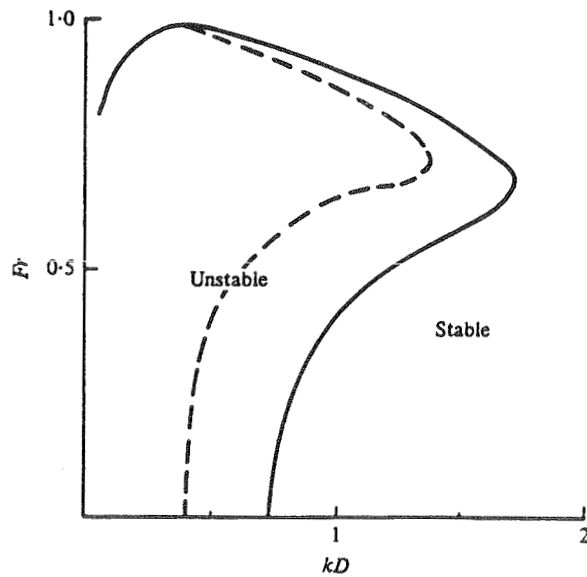


FIGURE 10. Stability limits to the formation of dunes;  $D/z_0 = 3 \times 10^3$ ,  $\beta = 2.8$ .  
The dashed curve corresponds to the fastest-growing wavenumber.

Figure B.9.2.

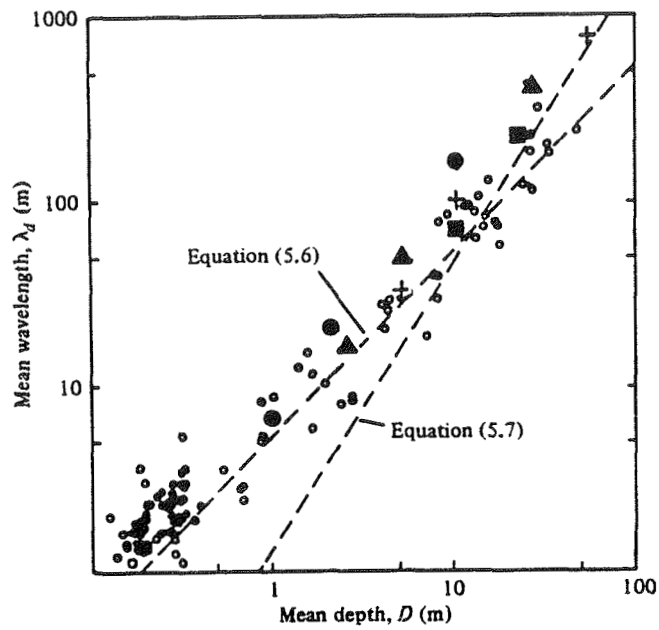


FIGURE 11. Comparison of observations of the group mean wavelength of dunes from flume, river and marine environments (taken from Jackson 1976) with the model's results:  $\circ$ , observations;  $\bullet$ ,  $z_0 = 0.1$  cm;  $\blacktriangle$ ,  $z_0 = 0.25$  cm;  $+$ ,  $z_0 = 0.5$  cm;  $\blacksquare$ ,  $z_0 = 1.0$  cm.

Figure B.9.3. Equation (5.6) is (11); Equation 5.7 is (12).

## Notation

Some notation is defined in the figures.

$C$	=	coefficient
$d$	=	bed-particle diameter
$g$	=	gravity acceleration
$k$	=	$2\pi/L$
$L$	=	$\lambda$ = wavelength
$m$	=	exponent
$n$	=	porosity of bed material
$q_b$	=	bed-load discharge
$q_b^s$	=	perturbed (by bed waves) bed-load discharge
$u_*$	=	bed shear velocity
$U, W$	=	mean velocity in x,z direction
$x^*, z^*$	=	curvilinear coordinate system such that $z^* = \text{const}$ are (approximately) streamlines
$z_0$	=	roughness length
$\beta$	=	coefficient defined by (8)
$\lambda_{r,d}$	=	wavelength of ripples, dunes
$\tau_{xy}$ , etc.	=	stress (usual subscript notation)
$\tau_0$	=	bed shear stress

## B.10. Fredsoe (1982)

This analysis will be described in greater detail because of its particular relevance to the present project.

### Basis of theory

#### 1. Sediment continuity

$$\frac{\partial q}{\partial x} = - (1-n) \frac{\partial h}{\partial t} \quad (1)$$

Integration of (1) yields for bed forms migrating without change of form

$$q = q_0 + a(1-n)h \quad (2)$$

#### 2. If all material is transported as bed load ( $q_0 = 0$ ), bed-form celerity is

$$a = \frac{q_{top}}{(1-n)H} \quad (3)$$

#### 3. From (2) and (3),

$$\frac{h}{H} = \frac{q}{q_{top}} \quad (4)$$

#### 4. Sediment-transport relation

$$\Phi_b = \Phi_b(\theta^*) \quad (5)$$

where

$$\Phi_b = \frac{q_b}{\sqrt{(s-1)gd^3}}, \theta^* = \frac{\tau^*}{\rho(s-1)d} \quad (6)$$

To account for local effects of bed slope, Fredsoe adopts

$$\theta_G^* = \theta^* - \mu \frac{\partial h}{\partial x}; \mu \approx 0.1 \quad (7)$$

Then (4) becomes

$$\frac{h}{H} = \frac{\Phi_n(\theta_G^*)}{\Phi_b(\theta_G^*, \text{top})} \quad (8)$$

5. Distribution of shear stress along upstream face of dune (inferred from experimental results)

$$\frac{\theta^*}{\theta_{\text{top}}^*} = \frac{\left(1 - \frac{H}{2D}\right)^2}{\left(1 + \frac{H}{2D} - \frac{h}{D}\right)^2} f\left(\frac{x}{H}\right) \quad (9)$$

where  $f\left(\frac{x}{h}\right)$  is obtained from experimental data on the distribution of boundary shear downstream from a rearward facing step on a rigid bed.

6. Adopt Meyer-Peter formula to get form of (5):

$$\Phi = 8\left(\theta_G^* - \theta_c\right)^{3/2} \quad (10)$$

Then (5), (6), (7) and (8) yield a differential equation for h

$$\frac{\partial h}{\partial x} + \left( \frac{\theta_{\text{top}}^* - \theta_c}{\mu} \right) \left( \frac{h}{H} \right)^{2/3} = \frac{\theta^* - \theta_c}{\mu} \quad (11)$$

where  $\theta^*$  is given by (9).

### Principal results and conclusions

1. Shape of bed forms is obtained by integrating (11) numerically, with upstream boundary condition  $\theta = \theta_c$  at  $h = 0$ . At bed-form crest,  $\theta^* = \theta_{\text{top}}^*$  on right side of (11). Downstream face of bed form is taken to be at angle of repose of bed material. Bed stress is obtained from

$$\frac{V}{U_f} = 6 + 2.5 \ln \frac{D'}{k} \quad (12)$$

Typical shapes of bed forms are shown in Fig. B.10.2; bed-form steepness is shown in Fig. B.10.3.

2. Bed-form height is calculated by introducing a disturbance at the crest and examining conditions under which it is stable. Result is

$$\frac{H}{D} = \frac{\Phi_b}{\left(1 - \frac{H}{2D}\right) 2\theta \left( \frac{d\Phi_b}{d\theta} + \frac{d\Phi_s}{d\theta} \right)} \quad (13)$$

Theoretical dune-height variation with  $\theta'$  and  $d$  is shown in Fig. B.10.4.

3. Wavelength relation is given by

$$L = \frac{[16Hq_b + (16H + \delta)q_s]}{(q_b + q_s)} \quad (14)$$

Friction relation is obtained by applying Carnot's relation, as used by Engelund, and the theoretical relation for  $h/H$ , (4). Result is

$$\theta = \theta' + \theta'' = \theta' \left[ 1 + \frac{1}{2} \frac{H}{D} \frac{H}{L} \left( \frac{V}{U_f} \right)^2 \right] \quad (15)$$

4. Combining friction and wavelength relations, (14) and (15), gives bed-form steepness as shown in Fig. B.10.5.

Figures

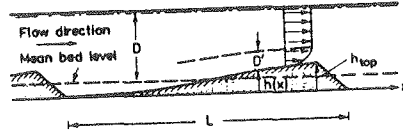


FIG. 1.—Definition Sketch of Migrating Dunes

Figure B.10.1.

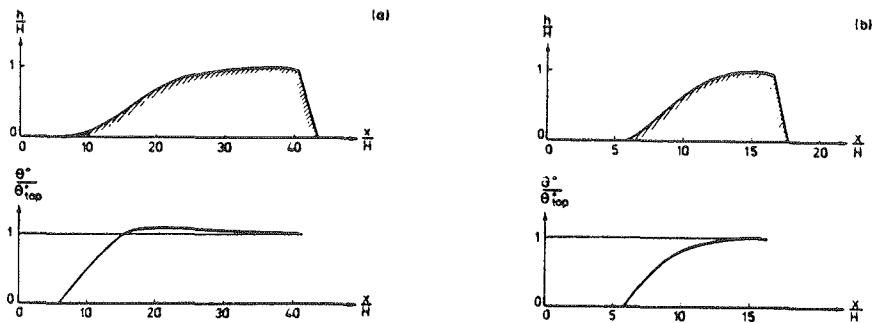


FIG. 5.—Examples on Calculated Dune Profiles and Variation in Bed Shear along These Profiles: (a)  $\theta_{top}^* = 0.057, H/D = 0.04, \theta_c = 0.05$ ; (b)  $\theta_{top}^* = 0.30, H/D = 0.27, \theta_c = 0.05$

Figure B.10.2.

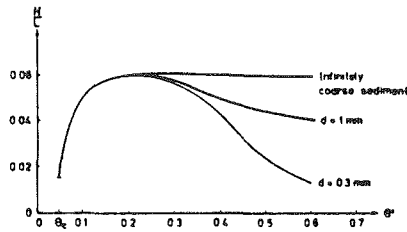


FIG. 6.—Variation in Length-Height Ratio with Bed Shear Stress for Different Grain Sizes

Figure B.10.3.

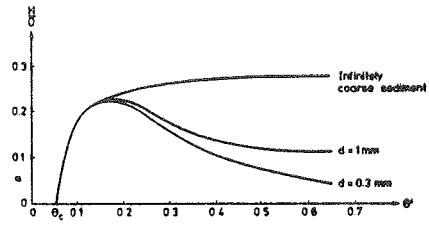


FIG. 8.—Variation in Dune Height—Water Depth Ratio with Bed Shear Stress for Different Grain Sizes

Figure B.10.4.

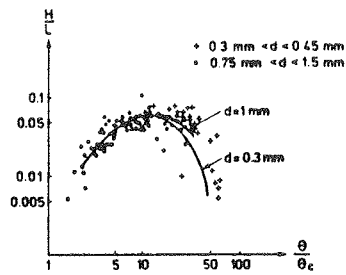


FIG. 10.—Variation in Length-Height Ratio with Total Bed Shear Stress for Different Grain Sizes (21)

Figure B.10.5.

## Notation

The author's full notation list is reproduced here.

$a$	=	migration velocity of dunes;
$a_k$	=	Fourier-coefficient for perturbation of bed;
$c_f$	=	drag coefficient;
$c_{f0}$	=	maximum drag coefficient;
$d$	=	mean grain diameter;
$D$	=	water depth;
$D'$	=	mean boundary layer thickness along dune;
$F$	=	Froude number;
$g$	=	acceleration of gravity;
$h$	=	local dune height;
$\bar{h}$	=	perturbation of dune;
$H$	=	maximum dune height;
$H_s$	=	height of upstream step;
$k$	=	bed roughness;
$k_n$	=	wavenumber of bed perturbation;
$L$	=	dune length;
$n$	=	porosity;
$q_b$	=	bed load sediment transport;
$q_s$	=	suspended sediment transport;
$q_0$	=	constant;
$q_t$	=	total sediment transport;
$q_{top}$	=	sediment transport at dune top;
$\dot{q}$	=	change in sediment transport, due to perturbation of dune;
$s$	=	relative density of sand grains;
$t$	=	time;
$U_b$	=	near bed flow velocity;
$U'_f$	=	effective shear velocity;
$w$	=	fall velocity of suspended sediment;
$x$	=	coordinate in flow direction;
$\gamma$	=	constant, defined in Eq. 21;
$\delta$	=	phase lag;
$\delta^*$	=	displacement thickness;
$\delta_0$	=	upstream boundary layer thickness;
$\epsilon$	=	eddy viscosity;
$\eta$	=	water surface undulations;
$\theta'$	=	effective dimensionless shear stress;
$\theta''$	=	dimensionless shear stress due to form drag;
$\theta_c$	=	critical dimensionless shear stress;
$\theta^*$	=	local dimensionless shear stress;
$\theta^*_{top}$	=	dimensionless shear stress at top;
$\theta^*_{max}$	=	maximum dimensionless shear stress;
$\theta^*_G$	=	local dimensionless shear stress including effect of gravity;
$i$	=	imaginary unit;
$\mu$	=	constant, defined in Eq. 7;
$\rho$	=	density of water;
$\Phi$	=	dimensionless sediment transport;
$\Phi_b$	=	dimensionless bed load transport;
$\Phi_s$	=	dimensionless suspended sediment transport; and
$\tau^*$	=	bed shear stress.

## B.11. Haque and Mahmood (1985).

This paper is the culmination of a series of publications (cited in the paper) by these authors on the subject of ripple and dune geometry. The first of these publications was Haque's (1970) M.S. thesis, under Mahmood, submitted to Colorado State University.

### Basis of theory

1. The flow is treated in two parts (see Fig. B.11.1): an attached-flow zone along the upstream slopes of the bed forms; and a downstream wake-flow zone in which the free streamline is calculated in the basis of potential-flow theory.
2. Admissible bed-form shapes obtained by analyzing the potential flow over an infinite train of bed forms (Fig. B.11.2), to find profile meeting two requirements:
  - (a) There is a standing eddy downstream from each bed form.
  - (b) The velocity gradient along the bed-form profile is continuous at the separation point.
3. Sediment continuity

$$\frac{\partial q}{\partial x} = - \frac{\partial y}{\partial t} \quad (1)$$

4. Sediment-transport relation

$$\left(\frac{u}{u_c}\right) = \left(\frac{y}{a}\right)^m \quad (2)$$

5. Equations and boundary conditions of potential flow.
6. Case of finite depth and rotational inviscid flow is handled using finite-element techniques.

### Principal results and observations

1. Mathematical relation obtained for upstream faces of bed forms is shown in Fig. B.11.3, along with bed-profile data from ACOP Canals (in Pakistan). Results imply homologous shape of all ripple and dune profiles.
2. Upstream face of bed forms is about two-thirds of their total length.
3. For case of infinite depth, bed-form steepness is given by

$$\frac{a}{L} = \frac{0.2463}{m} \quad (3)$$

4. Finite-element analysis yields results shown in Figs. B.11.3, B.11.4, and B.11.5 for steepness and relative depth of bed forms. Optimization is obtained by minimizing differences between values of left-hand and right-hand sides of (2).

Figures

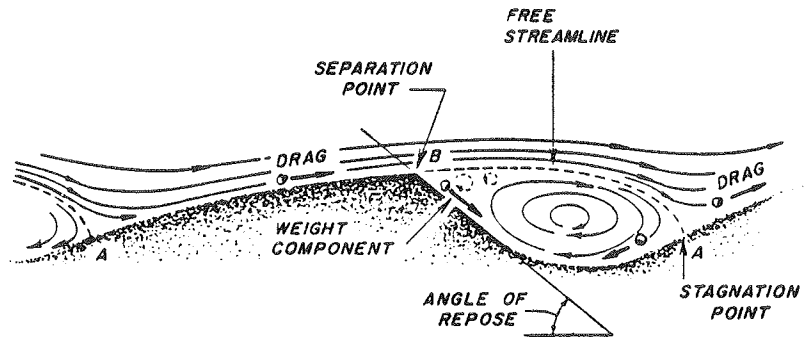


FIG. 1.—Schematic Sketch for Ripple or Dune

Figure B.11.1.

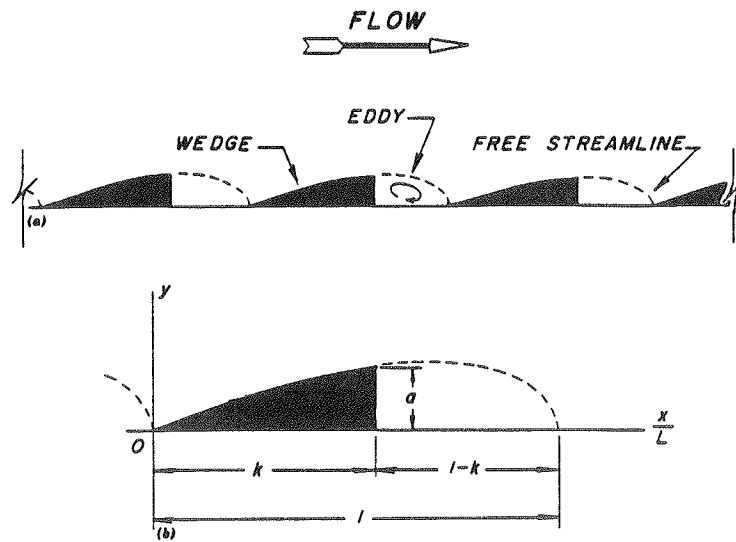


FIG. 3.—(a) Infinite Sequence of Alternating Wedges and Eddies; and (b) Definition Sketch for Bedform Shape Functions

Figure B.11.2.

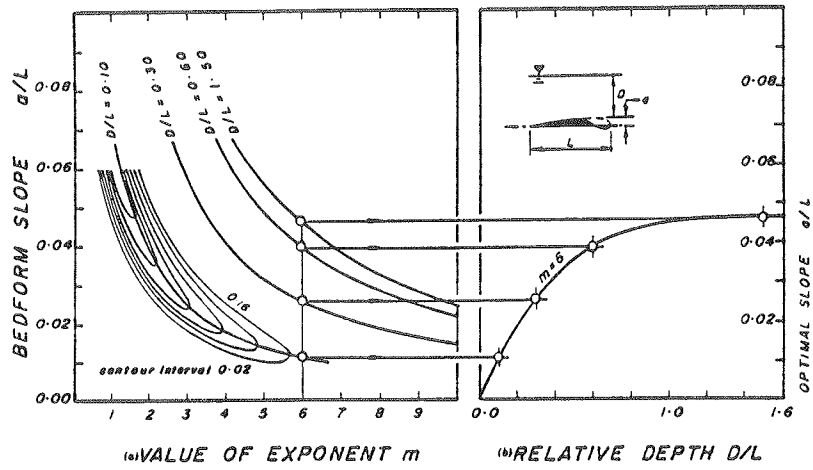


FIG. 9.—Effect of Flow Depth on Optimal Bedform Steepness

Figure B.11.3.

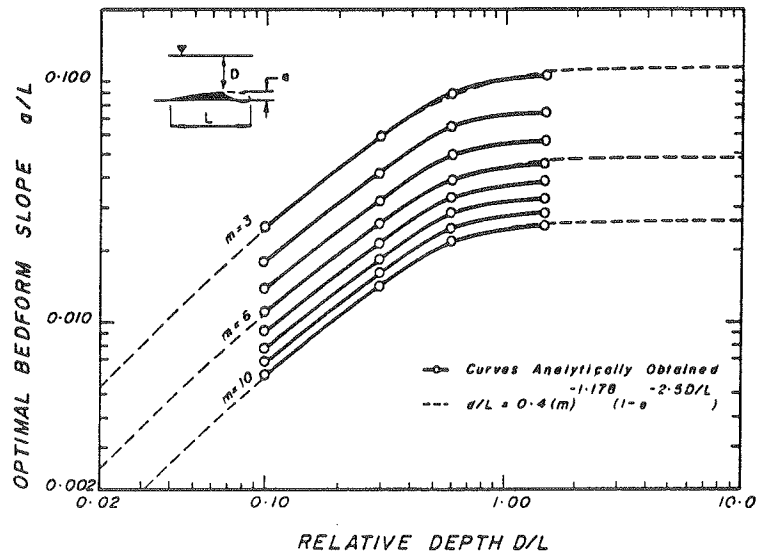


FIG. 10.—Relationship between Optimal Bedform Steepness and Relative Depth for Different Values of  $m$

Figure B.11.4.

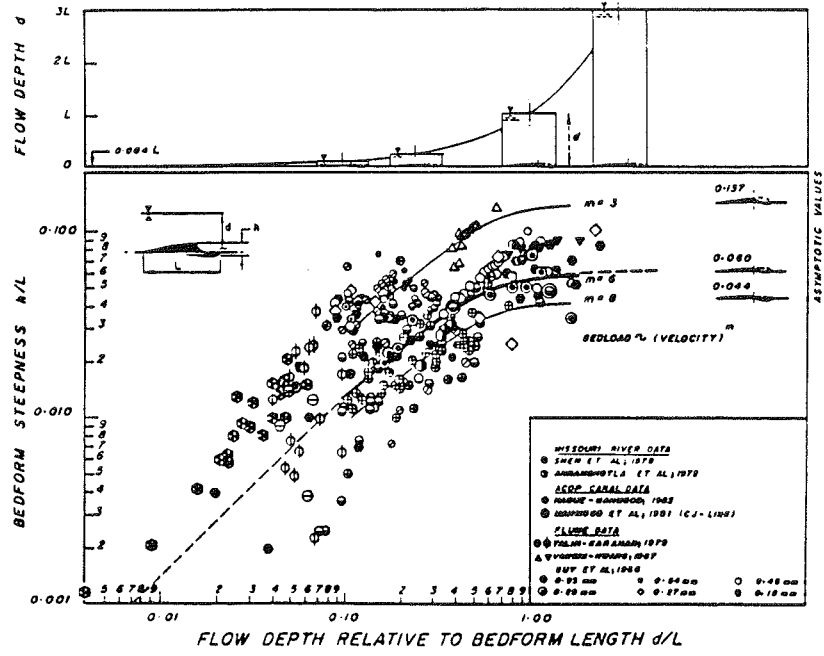


FIG. 11.—Comparison to Observed Data

Figure B.11.5.

## Notation

The author's full notation list is reproduced here.

- $a$  = height of the separation point from the stagnation point,
- $c$  = celerity of bedforms,
- $D$  = depth of flow at the crest,
- $d$  = average depth of flows,
- $E$  = error between functions  $V$  and  $N$ ,
- $h$  = bedform height,
- $k$  = dimensionless length of the upstream face,
- $L$  = bedform length,
- $L_e$  = eddy length,
- $m$  = a dimensionless index,
- $N$  = the bedform shape function,
- $q$  = volumetric sediment-transport rate per unit width,
- $q_c$  = sediment-transport rate at the crest,
- $t, t'$  = time in the fixed and the moving frame of reference,
- $u$  = magnitude of local velocity,
- $u_c$  = velocity tangential to bed at the crest,
- $u_\infty$  = undisturbed velocity at infinity,
- $V$  =  $(u/u_c)^m$ , normalized velocity function,
- $x, y$  = coordinates of a generic point in the fixed or moving frame of reference,
- $x', y'$  = coordinates of a generic point in the moving frame of reference, and;
- $\beta$  = a constant roughly equal to 0.8.

C. Empirical Methods. The complexity of river-flow phenomena, and the difficulties encountered in treating them via the formalism of mathematical fluid mechanics, have prompted resort to purely empirical methods of correlating the variables of interest and importance to river engineers. This line of attack was begun in the 19th century, by proponents of "regime theory" who sought reliable design guidelines for the irrigation canals of India, which transported flows with significant sediment concentrations, and often presented major maintenance problems arising from bed scour or deposition, or unstable channel alignment (bank erosion). It was only natural that dimensional analysis and related approaches be utilized also to predict and quantitatively describe riverine bed-forms.

Eight of the principal bed-form papers of this type are summarized in this section.

## C.1. Garde and Albertson (1959)

### Basis of theory

1. Dimensional analysis showing that dune steepness is a function of two dimensionless quantities:

$$\frac{h}{\lambda} = f \left[ \frac{\tau_o}{(\gamma_s - \gamma_f)d}, Fr \right] \quad (1)$$

### Principal results and observations

1. Functional relationship for (1) is obtained by curve fitting using laboratory and field data (Fig. C.1.1 for ripples; Fig. C.1.2 for dunes).
2. Criteria for different flow regimes are established (Fig. C.1.3).
3. No separate relations for dune height and dune length result from this analysis.

Figures

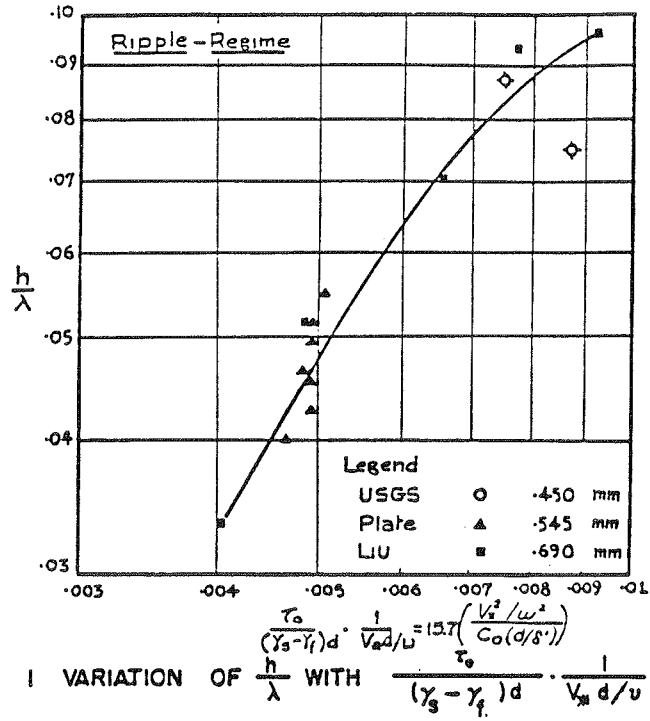


Figure C.1.1.

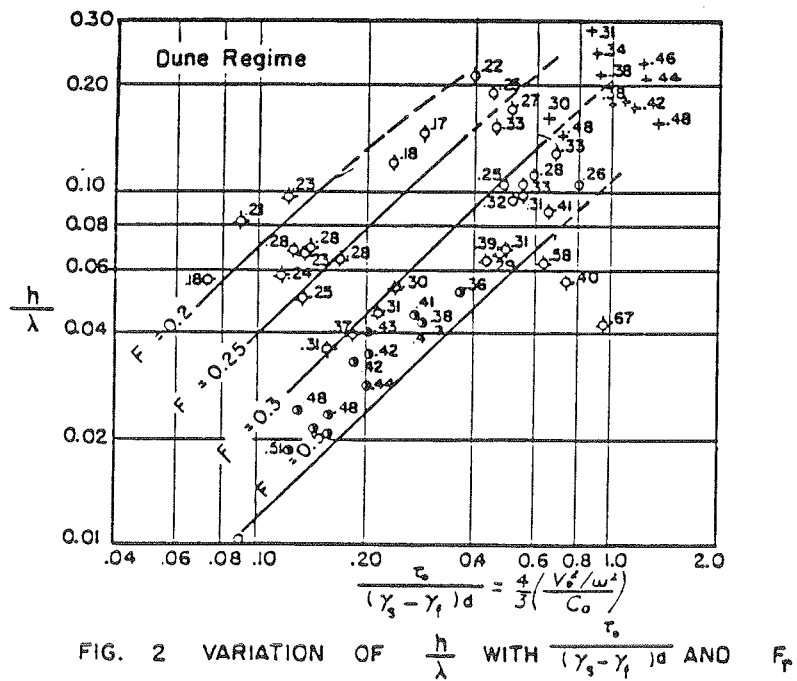


Figure C.1.2.

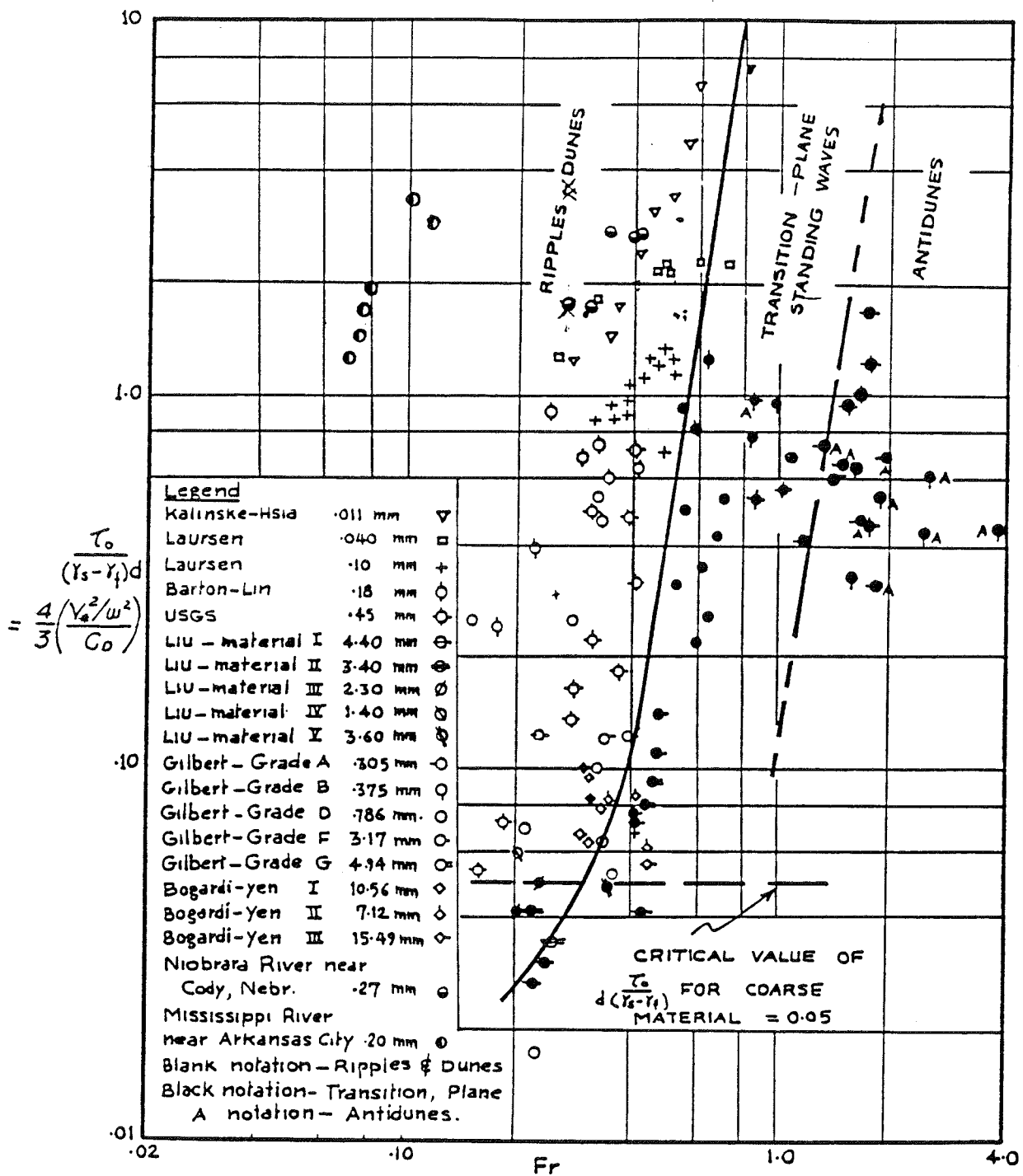


FIG. 3 CRITERIA FOR REGIMES OF FLOW

Figure C.1.3.

## Notation

$d$	=	size of bed material
$D$	=	depth of flow
$Fr$	=	Froude number ( $= V/\sqrt{gD}$ )
$h$	=	average height of ripples or dunes
$V$	=	mean velocity of flow
$\gamma_s, \gamma_f$	=	specific weights of sediment, water
$\lambda$	=	average length of dunes
$\tau_o$	=	average shear stress on the bed

## C.2. Yalin (1964)

### Basis of theory

1. Dune geometry as shown in Fig. C.2.1.
2. Assumption that

$$\tau_B = \tau_0 f_1\left(\frac{\Delta}{d}\right). \quad (1)$$

and

$$\tau_B \approx \tau_{cr} \quad (2)$$

3. Dimensional analysis yields

$$\frac{\Delta}{D} = \phi\left(\bar{X}, \frac{\bar{d}}{D}\right) \quad (3)$$

### Principal results and observations

1. Combining (1) and (2) yields

$$\frac{\Delta}{D} \approx \phi_1\left(\frac{\tau_0}{\tau_{cr}}\right) \quad (4)$$

If the variation in  $\tau_0/\tau_{cr}$  is a result of the variation of flow depth,  $d$ , only (i.e.,  $S = \text{const}$ ), then

$$\frac{\tau_0}{\tau_{cr}} = \frac{d}{d_{cr}} \quad (5)$$

2. Functional relationship for (4) is obtained by curve fitting using laboratory and field data (see Fig. C.2.2):

$$\frac{\Delta}{d} = \frac{1}{6} \left( 1 - \frac{d_{cr}}{d} \right) \quad (6)$$

3. For rough turbulent flow,  $X$  is unimportant, and (3) is reduced to

$$\frac{\Lambda}{D} = \phi_A \left( \frac{\bar{d}}{D} \right) \quad (7)$$

For hydraulically smooth flow,  $d/D$  is unimportant, and (3) is reduced to

$$\frac{\Lambda}{D} = \text{const} \quad (8)$$

4. Functional relationships for (7) and (8) are obtained by curve fitting using laboratory and field data (see Fig. C.2.3):

$$\phi_A \left( \frac{\bar{d}}{D} \right) \approx 5 \frac{\bar{d}}{D} \quad (X > \sim 20) \quad (9)$$

$$\text{const} \approx 1000 \quad (X < \sim 20) \quad (10)$$

Hence,  $\Lambda \approx 5d \quad (X > \sim 20) \quad (11)$

$$\Lambda \approx 1000 D. \quad (X < \sim 20) \quad (12)$$

5. (11) applies to dunes, and (12) to ripples

Figures

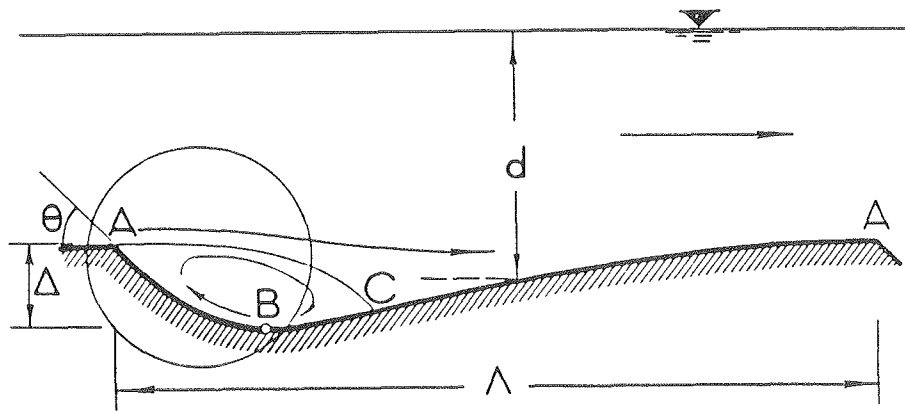
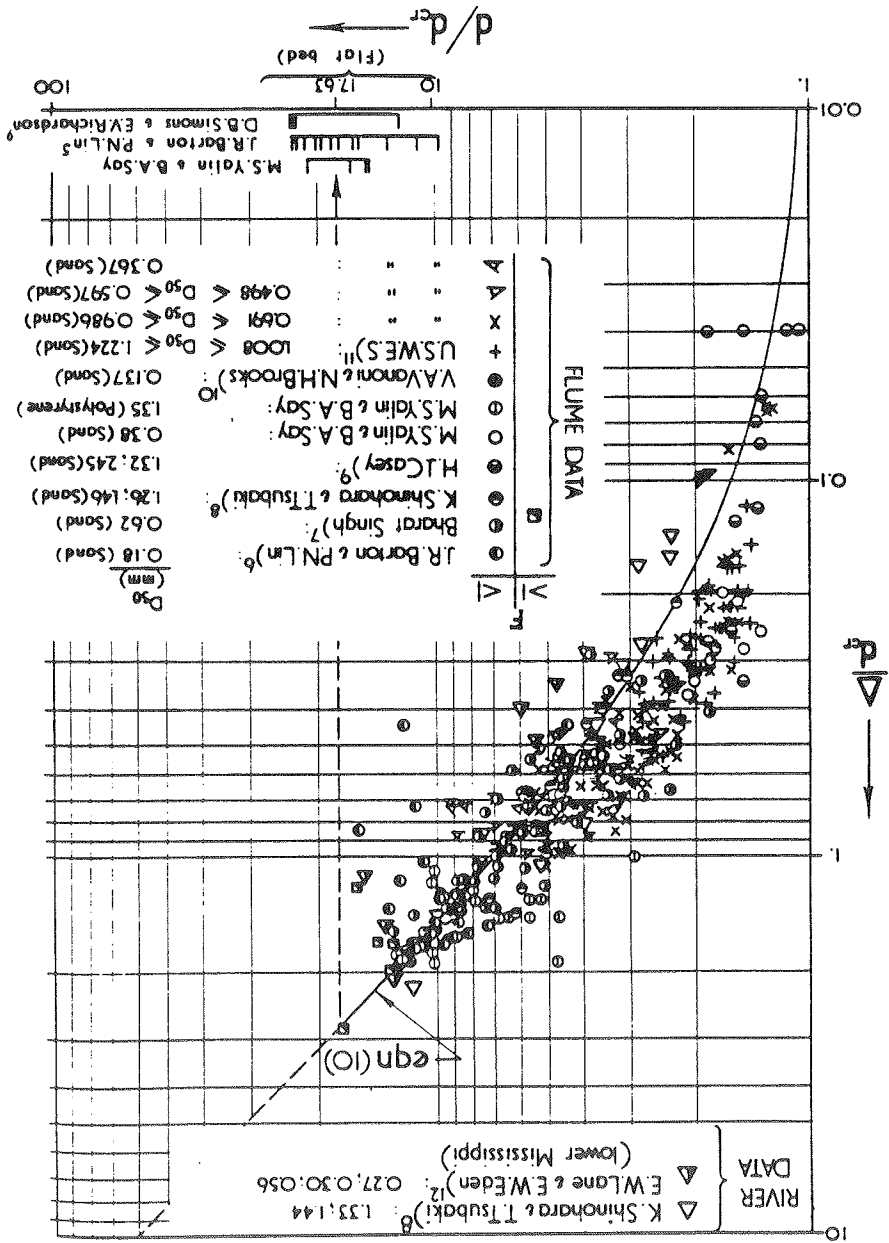


FIG. 1

Figure C.2.1.

Figure C.2.2.

FIG. 2



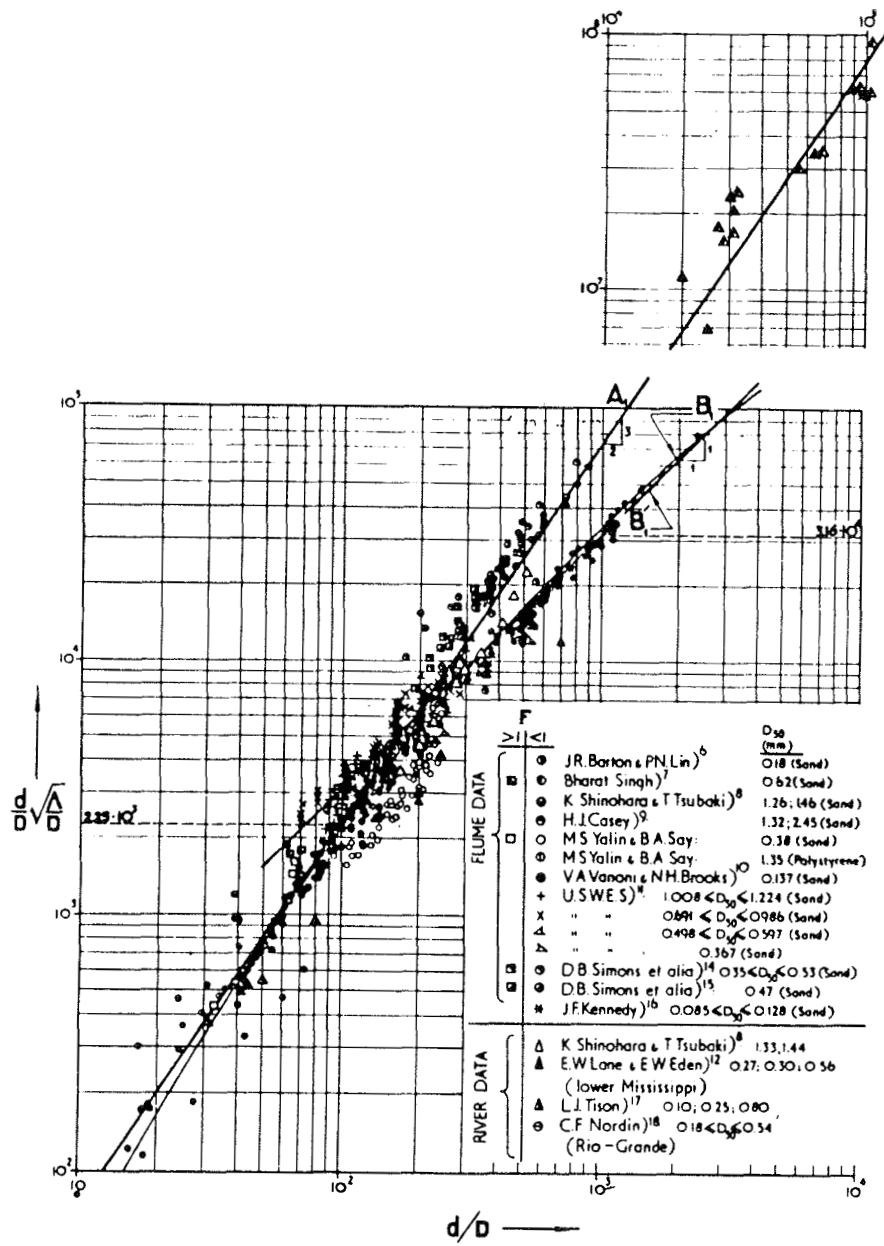


FIG. 4

Figure C.2.3.

## Notation

D	=	grain-size
d	=	depth of flow
F	=	Froude number
f()	=	function of
S	=	slope of uniform flow
v	=	average velocity of flow
$v_*$	=	$\sqrt{\tau_0/\rho}$ = shear velocity
X	=	$v_*D\rho/\mu$ = grain-size Reynolds number
$\gamma$	=	specific weight of fluid
$\Delta$	=	sand/waveheight
$\theta$	=	angle of repose
$\Lambda$	=	sand-wavelength
$\mu$	=	viscosity
$\rho$	=	density of fluid
$\tau_0$	=	shear stress on the surface of the bed = $\gamma Sd$
$\tau_B$	=	shear stress at point B(see Fig. C.2.1)
$\phi()$	=	function of

Subscript (cr) = critical value signifying beginning of particle movement.

The bar over the symbols signifying values corresponding to flow over a flat bed at  $t = 0$ .

C.3. Ranga Raju and Soni (1976).

Basis of theory

1. Assumption that all bed forms are two-dimensional and of identical, triangular form.
2. Dimensions (or scale) of bed forms are assumed to be directly related to rate of bed-load transport.
3. Equation for bed-load transport per unit width

$$q_B = \left(\frac{h}{2}\right) \cdot U_w \cdot (1-\lambda) \cdot \gamma_s \quad (1)$$

4. Empirical equation for migration speed of bedform

$$\frac{U_w}{\sqrt{gR_b}} = 0.021 \left(\frac{U}{\sqrt{gR_b}}\right)^4 \quad (2)$$

5. Empirical relation between bed-load transport and grain shear stress

$$\frac{q_B}{\gamma_s} \left(\frac{\gamma_f}{\gamma_s - \gamma_f}\right)^{1/2} \left(\frac{1}{gd^3}\right)^{1/2} = f_1(\tau'_O) \quad (3)$$

in which 
$$\tau'_O = \frac{\gamma_f R_b' S}{(\gamma_s - \gamma_f) d} \quad (4)$$

## Principal results and observations

1. Combining (1), (2) and (3) yields

$$\frac{h}{d} F_1^3 F_2 = f_2(\tau'_0) \quad (5)$$

$$\frac{L}{d} F_1^3 F_2 \frac{R_b}{d} = f_3(\tau'_0) \quad (6)$$

in which

$$F_1 = \frac{U}{\sqrt{gR_b}} \quad (7)$$

$$F_2 = \frac{U}{\sqrt{\frac{\gamma_s - \gamma_f}{\rho_f} d}} \quad (8)$$

2. Functional relationships for (5) and (6) are obtained by curve fitting using laboratory and field data (see Figs. C.3.1 and C.3.2, and Table C.3.1). Relation obtained from Fig. C.3.1 is

$$\frac{h}{d} F_1^3 \cdot F_2 = 6.5 \times 10^3 (\tau'_0)^{8/3} \quad (9)$$

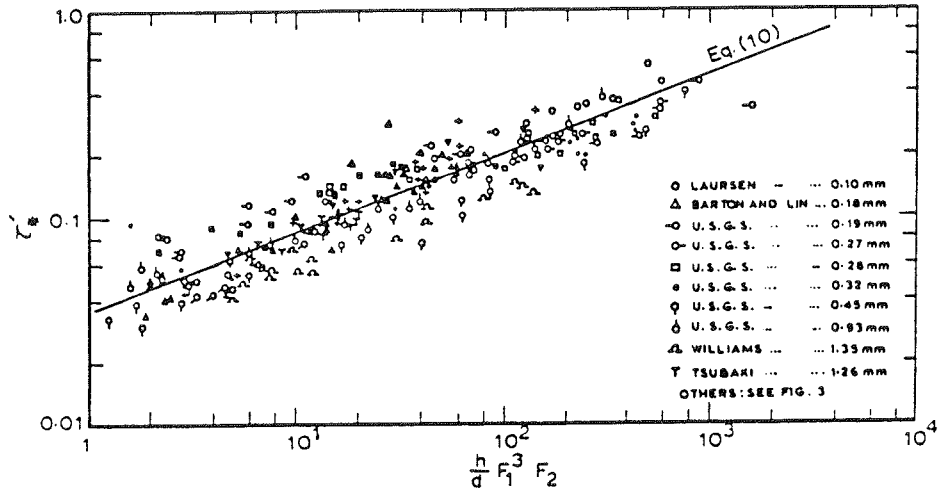
$R'_b$  is obtained from

$$U = \frac{1}{n_s} R'_b{}^{2/3} S^{1/2} \quad \text{and} \quad n_s = \frac{d^{1/6}}{24.0} \quad \text{in m.k.s. units}$$

3. The authors find that more than 75% of all the data fall within a  $\pm 50\%$  band around proposed curve. They also find that less than 50% of the data fall

within a  $\pm 50\%$  band around the curve proposed by Yalin (1964) (see Section C.2). Comparison is shown in Figs. C.3.3 and C.3.4.

Figures

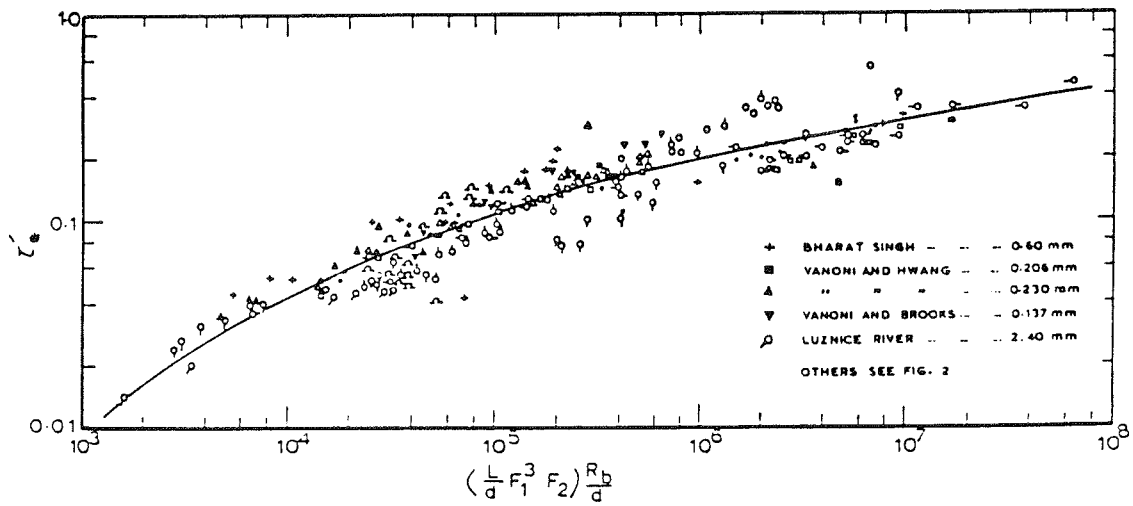


Variation de  $h/dF_1^3F_2$  with  $\tau'$ .

Fig. 2.

Variation de  $h/dF_1^3F_2$  avec  $\tau'$ .

Figure C.3.1.



Variation of  $(L/dF_1^3F_2)R_b/d$  with  $\tau'$ .

Fig. 3.

Variation de  $(L/dF_1^3F_2)R_b/d$  avec  $\tau'$ .

Figure C.3.2.

Table C.3.1

no. investigator	ref.	$d_{mm}$	$R_p$ ft	$S \times 10^3$	$U$ ft/s	$h$ ft	$L$ ft	overall range of parameters									
1. Guy et al.	[7]	0.19 - 0.93	0.290 - 1.070	0.15 - 6.50	0.70 - 3.43	0.005 - 0.650	0.29 - 17.7										
2. Vanoni and Wang	[14]	0.206 - 0.230	0.197 - 0.870	0.455 - 2.90	0.57 - 1.83	0.037 - 0.057	0.38 - 0.75										
3. Vanoni and Brooks	[15]	0.137	0.227 - 0.505	0.390 - 2.80	0.77 - 1.49	0.042 - 0.061	0.34 - 0.45										
4. Williams	[18]	1.35	0.223 - 0.376	1.33 - 10.88	1.50 - 2.65	0.042 - 0.167	1.30 - 8.90										
5. Laursen	[10]	0.10	0.180 - 0.797	0.43 - 1.86	1.07 - 3.36	0.063 - 0.110	0.45 - 0.56										
6. Barton and Lin	[2]	0.18	0.293 - 1.190	0.44 - 2.10	0.74 - 3.60	0.051 - 0.116	0.43 - 0.74										
7. Tsubaki	[13]	1.26	0.510 - 1.530	1.61 - 1.73	1.90 - 2.50	0.070 - 0.270	3.48 - 5.17										
8. Bharat Singh	[1]	0.60	0.120 - 0.412	1.00 - 7.00	0.84 - 2.66	0.009 - 0.066	0.48 - 1.92										
9. Martinec (Luznice River)	[11]	2.4	0.470 - 4.62	0.36 - 0.68	1.16 - 3.22	0.075 - 0.983	1.15 - 11.9										

Table I. Sources of data and Range of Variables

## Notation

The author's full notation list is reproduced here.

Notations			
$D$	Depth of flow	$u_*$	Shear velocity = $\sqrt{gR_bS}$
$d$	$d_{50}$ = median sediment size, for which 50% of the material, by weight, is finer	$U_w$	Velocity of bed wave
$F_1$	$U/\sqrt{gR_b}$	$\lambda$	Porosity of sand mass
$F_2$	$U/\sqrt{\frac{\gamma_s - \gamma_f}{\rho_f} d}$	$\phi_B$	Dimensionless transport parameter = $\frac{q_B}{\gamma_s} \left( \frac{\gamma_f}{\gamma_s - \gamma_f} \right)^{\frac{1}{3}} \left( \frac{1}{gd^3} \right)^{\frac{1}{3}}$
$g$	Acceleration due to gravity	$q_B$	Bed load transport in weight per unit time
$h$	Average height of undulations	$\gamma_f$	Specific weight of the fluid
$L$	Average length of undulations	$\gamma_s$	Specific weight of the sediment
$n_s$	Manning's roughness coefficient for plane bed	$\tau'_c$	Dimensionless shear stress corresponding to grains corresponding to grains = $\gamma_f R'_b S / (\gamma_s - \gamma_f) d$
$R_b$	Hydraulic radius of the bed	$\tau_c$	Critical shear stress
$R'_b$	Hydraulic radius of the bed corresponding to the grains	$\tau_0$	Average shear stress on the bed
$S$	Water surface slope	$\nu$	Kinematic viscosity of the fluid
$U$	Mean velocity of flow		

C.4. Yalin and Karahan (1979).

Basis of theory

1. Dimensional analysis showing that dune steepness  $\delta (= \Delta/\Lambda)$  is a function of  $\eta$ ,  $Z$ , and  $X$ :

$$\delta = f(\eta, Z, X) \quad (1)$$

where

$$\eta = \frac{\tau_o}{(\tau_o)_{cr}} \quad (2)$$

$$Z = \frac{h}{D} \quad (3)$$

$$X = \frac{v^*D}{v} \quad (4)$$

Principal results and observations

1. Analysis of data showing that when  $X > 25$  (dunes),  $\delta$  is independent of  $X$ :

$$\delta = \phi(\eta, Z) \quad (5)$$

2. Analysis of data showing that when  $Z > \approx 100$ ,  $\delta$  is independent of  $Z$ :

$$\delta = \phi(\eta) \quad (6)$$

3. Laboratory experiments are carried out to determine  $\delta$ 's dependence on  $Z$  for  $Z < \approx 100$ . Results are plotted in Figure 2.
4. Empirical relation is established:

$$\frac{\delta}{\delta_{\max}} = \xi \exp(1-\xi) \quad (7)$$

$$\delta_{\max} = (0.0127e^{-1})\bar{x} \quad (8)$$

in which  $\xi = x/\bar{x}$  and  $x = \eta - 1$ . Fit is shown in Figure 3.

Figures

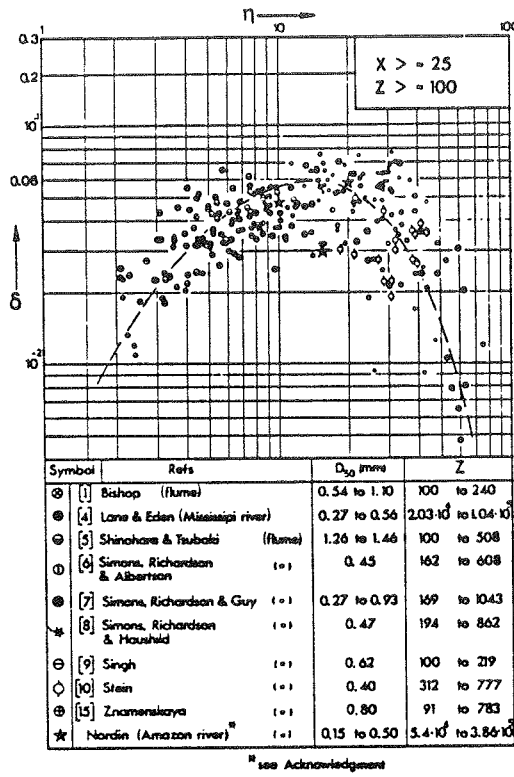


FIG. 1.—Variation of Dune Steepness with Relative Tractive Force for Large Values of Z

Figure C.4.1.

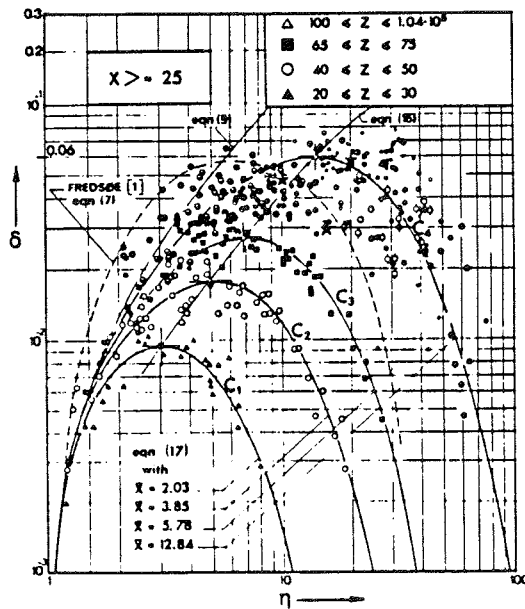


FIG. 2.—Variation of Dune Steepness with Relative Tractive Force for Various Ranges of Z

Figure C.4.2.

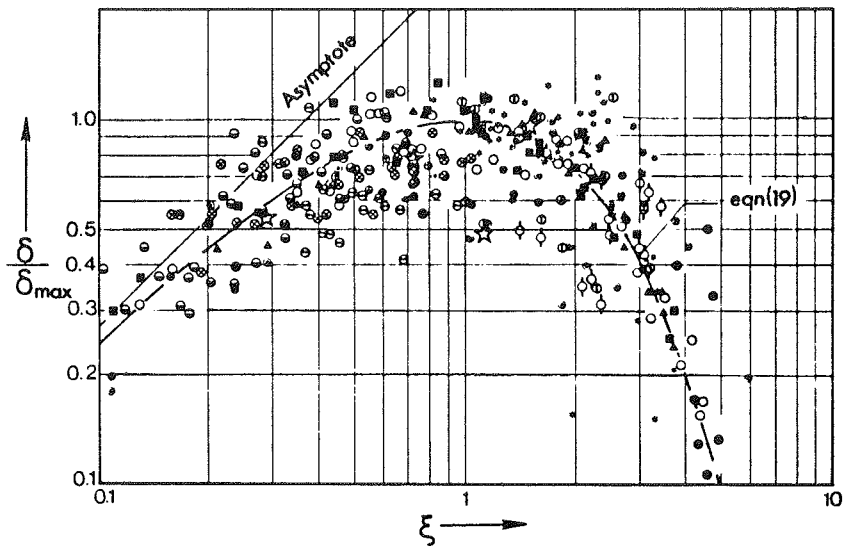


FIG. 3.—Relation between Normalized Dune Steepness and Tractive Force in Logarithmic System of Coordinates

Figure C.4.3.

## Notation

$cr$	=	subscript that signifies the beginning of sediment transport ("critical stage");
$D$	=	representative size of the bed material (usually selected as $D_{50}$ );
$e$	=	base of the natural logarithm;
$h$	=	flow depth;
$v^*$	=	shear velocity;
$X = v^*D/\nu$	=	grain size Reynolds number;
$x$	=	dimensionless excess of the tractive force;
$\bar{x}$	=	value of $x$ corresponding to $\delta_{max}$ ;
$Z = h/D$	=	dimensionless flow depth;
$\Delta$	=	dune height;
$\delta = \Delta/\Lambda$	=	dune steepness;
$\delta_{max}$	=	maximum value of $\delta$ corresponding to given (range of) $Z$ ;
$\eta = \tau_o/(\tau_o)_{cr}$	=	relative tractive force;
$\Lambda$	=	dune length;
$\nu$	=	kinematic viscosity;
$\xi = x/\bar{x}$	=	normalized value of $x$ ;
$\rho$	=	fluid density; and
$\tau_o$	=	shear stress acting on bed

C.5 Jaeggi (1984).

Basis of theory

1. Analysis of laboratory and field data.

Principal results and observations

1. Upper limit of alternate bar-formation

$$\eta = 2.93 \ln \eta_B = 3.13 Z_B^{0.15} \quad (1)$$

(see Fig. C.5.1).

2. Minimum slope of channel necessary for alternate-bar formation is

$$J > \frac{\exp \left[ 1.07 \left( \frac{B^{0.15}}{d_m} \right) + M \right]}{12.9 \frac{B}{d_m}} \quad (2)$$

where M varies from 0.34 for uniform bed material to 0.7 for widely graded material (see Fig. C.5.2).

3. Scour depth due to alternate bar formation is

$$S = 0.76 \Delta_{AB} = \frac{B}{6 Z_B^{0.15}} \quad (3)$$

Figures

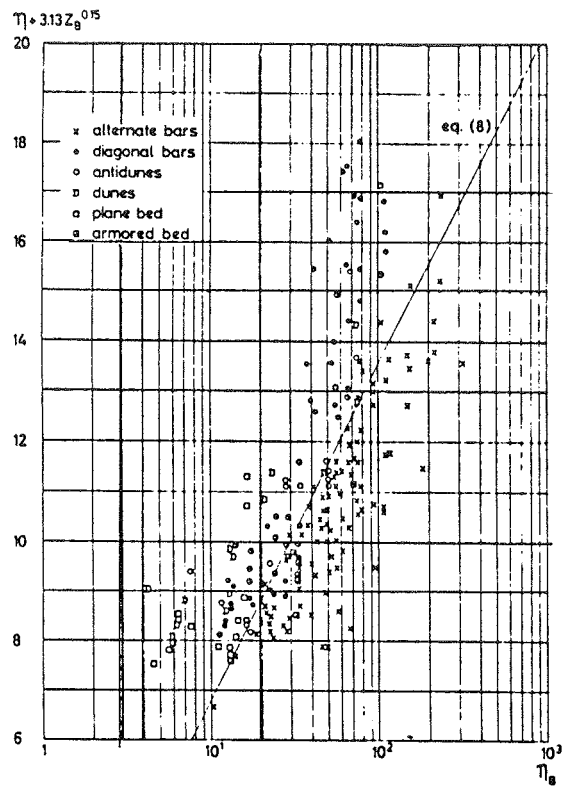


FIG. 3.—Criterion of Alternate Bar Formation (7), Compared with Test Results

Figure C.5.1.

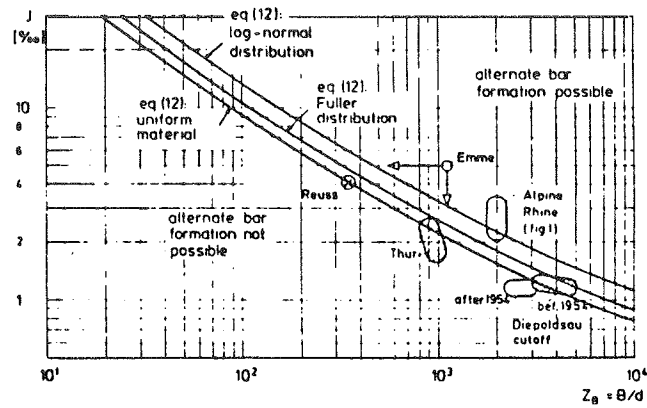


FIG. 5.—Diagram Giving Minimum Slope for Bar Formation for Channel Geometry and Bed Material (11). [Also Indicated are Areas which Characterize Some Swiss Rivers which All Fall in the Corresponding Region (with or without Bar Formation)]

Figure C.5.2.

## Notation

$B$	=	channel width;
$d_i$	=	grain size within the bed material mixture;
$d_m$	=	$\int d_i d_p$ ; mean grain size;
$M$	=	parameter which is function of sediment grading;
$p_i$	=	proportion of grain size;
$s$	=	relative density of bed material;
$S$	=	scour depth;
$\eta$	=	$\theta/\theta_{cr}$ , ratio of Shields factor to critical Shields factor;
$\eta_B$	=	$\theta_B/\theta_{cr}$ , ratio of Shields factor characterizing bar forming "horizontal movement" to critical Shields factor;
$\theta$	=	$hJ/(s - 1)d_m$ , Shields factor;
$\theta_{cr}$	=	critical Shields factor;
$\theta_B$	=	$BJ/(s - 1)d_m$ , Shields factor related to channel width
$v_m$	=	mean flow velocity;

C.6. Ikeda (1984).

### Basis of theory

1. Regime relation for meander wavelength

$$\lambda = \alpha B \beta = a \lambda_p \quad (1)$$

2. Linear stability analysis yields bar wave length of maximum instability

$$\lambda = \alpha 2 \sqrt{\pi} \sqrt{\frac{BD}{C_f}} \quad (2)$$

3. Dimensional analysis yields

$$\frac{\lambda}{B} = F \left( \frac{U}{\sqrt{gD}}, \frac{\rho g DS}{(\rho_s - \rho)gd}, \frac{\rho U D}{\mu}, \frac{B}{D}, \frac{D}{d} \right) \quad (3)$$

$$\frac{H_B}{D} = G \left( \frac{U}{\sqrt{gD}}, \frac{\rho g DS}{(\rho_s - \rho)gd}, \frac{\rho U D}{\mu}, \frac{B}{D}, \frac{D}{d} \right) \quad (4)$$

### Principal results and observations

1. Functional relationships are obtained by curve fitting using laboratory data:

$$\lambda = 5 \sqrt{\frac{BD}{C_f}} \text{ for } F < 0.8 \quad (5)$$

$$\frac{\lambda}{B} = 5.3 \left( \frac{B}{d} \right)^{-0.45} \frac{B}{D} \text{ for } F \geq 0.8 \quad (6)$$

or

$$\frac{\lambda}{B} = 5.3 \left(\frac{B}{D}\right)^{0.55} \left(\frac{D}{d}\right)^{-0.45} \quad (7)$$

and

$$\frac{H_B}{D} = 0.0442 \left(\frac{B}{d}\right)^{-0.45} \left(\frac{B}{D}\right)^{1.9} \quad (8)$$

Figs. C.6.1, C.6.2, and C.6.3 present verification of (1), (6), and (8), respectively.

Figures

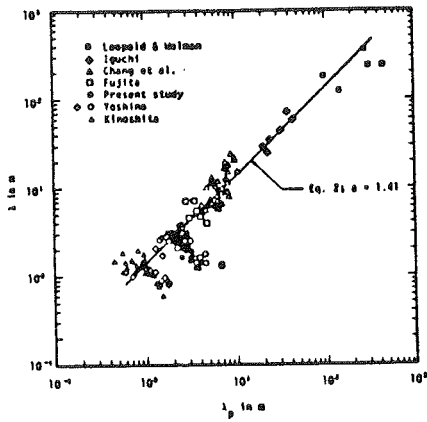


FIG. 4.—Test of Eq. 2

Figure C.6.1.

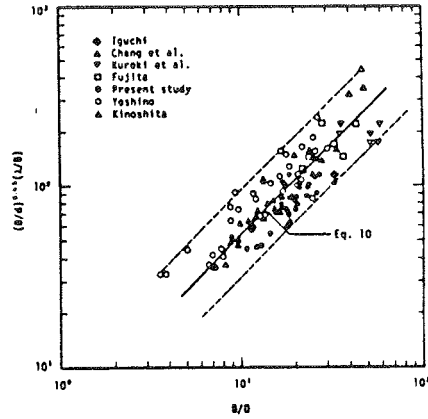


FIG. 8.— $(B/d)^{0.45} \lambda/B$  versus  $B/D$  for  $F \geq 0.8$ ; Broken Lines Indicate Possible Scatters; Data from Kuroki et al. Replotted from Ref. 20

Figure C.6.2.

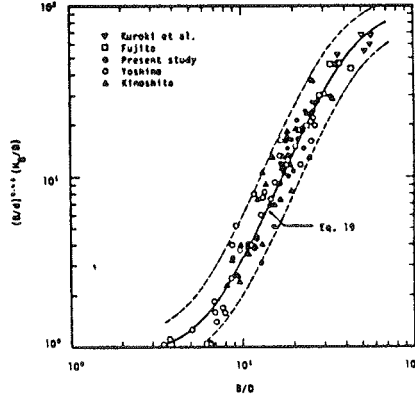


FIG. 12.— $(B/d)^{0.45} H_B/D$  versus  $B/D$ ; Broken Lines Indicate Possible Scatters

Figure C.6.3.

## Notation

$a$	=	numerical constant;
$B$	=	channel width;
$C_f$	=	resistance coefficient - $gDS/U^2$ ;
$D$	=	mean depth of flow;
$d$	=	sediment particle size;
$F$	=	functional relationship in Eq. 5;
$F$	=	Froude number - $U/\sqrt{gD}$ ;
$G$	=	functional relationship in Eq. 6;
$g$	=	gravitational acceleration;
$H_B$	=	bar height;
$S$	=	water surface slope;
$U$	=	mean fluid velocity
$\alpha$	=	numerical constant
$\beta$	=	numerical constant
$\rho_s, \rho$	=	mass density of sediment and fluid, respectively

C.7. van Rijn (1984).

### Basis of theory

1. Assumption that dimensions and migration speed of bed forms are determined by rate of bedload transport.
2. Assumption that bed-load transport is described by: (a) a dimensionless particle parameter  $D_*$ ; and (b) a transport-stage parameter  $T$

$$D_* = D_{50} \left[ \frac{(s-1)g}{v^2} \right]^{1/3} \quad (1)$$

$$T = \frac{(u_*')^2 - (u_{*,cr})^2}{(u_{*,cr})^2} \quad (2)$$

3. Two equations for rate of bedload transport per unit width:

$$q_b = \delta_b u_b c_b \quad (3)$$

$$q_b = (1 - p)\alpha\Delta u_d \quad (4)$$

### Principal results and observations

1. Combining (3) and (4) yields

$$\frac{\Delta}{d} = \frac{c_b}{(1 - p)\alpha} \frac{u_b}{u_d} \frac{\delta_b}{D_{50}} \frac{D_{50}}{d} \quad (5)$$

It is assumed that

$$c_b, \frac{\delta_b}{D_{50}}, \frac{u_b}{u_d} = F(D_*, T) \quad (6)$$

so that

$$\frac{\Delta}{d} = F\left(\frac{D_{50}}{d}, D_*, T\right) \quad (7)$$

and

$$\frac{\Delta}{\lambda} = F\left(\frac{D_{50}}{d}, D_*, T\right) \quad (8)$$

2. Functional relationships of (7) and (8) are obtained by curve fitting using laboratory and field data (see Figs. C.7.1 and C.7.2).

$$\frac{\Delta}{d} = 0.11 \left(\frac{D_{50}}{d}\right)^{0.3} (1 - e^{-0.5T})(25 - T) \quad (9)$$

and

$$\frac{\Delta}{\lambda} = 0.015 \left(\frac{D_{50}}{d}\right)^{0.3} (1 - e^{-0.5T})(25 - T) \quad (10)$$

Transport stage parameter  $T$  is calculated with  $u_*'$  given by

$$u_*' = \frac{g^{0.5} \bar{u}}{C'} \quad (11)$$

where

$$C' = 18 \log \left( \frac{12R_b}{3D_{90}} \right) \quad (12)$$

3. The author notes that (9) and (10) yield

$$\lambda = 7.3 d$$

which is in agreement with Yalin's result:  $\lambda = 2\pi d$ .

Figures

	source	flow velocity $\bar{u}$ (m/s)	flow depth $d$ (m)	particle size $D_{50}$ ( $\mu$ m)	temperature $T_e$ ( $^{\circ}$ C)
flume data	o <sup>-</sup> Guy et al	0.34-1.17	0.16-0.32	190	8-34
	x Guy et al	0.41-0.65	0.14-0.34	270	8-34
	$\Delta$ Guy et al	0.47-1.15	0.16-0.32	280	8-34
	b Guy et al	0.77-0.98	0.16	330	8-34
	$\square$ Guy et al	0.48-1.00	0.10-0.25	450	8-34
	$\phi$ Guy et al	0.53-1.15	0.12-0.34	930	8-34
	$\circ$ Williams	0.54-1.06	0.15-0.22	1350	25-28
	$\phi$ Delft Hydr. Lab.	0.45-0.87	0.28-0.49	790	12-18
	$\circ$ Stein	0.52-0.95	0.24-0.31	400	20-26
$\phi$ Znamenskaya	0.53-0.80	0.11-0.21	800	-	
field data	$\bullet$ Dutch Rivers	0.85-1.55	4.4-9.5	490-3600	5-20
	$\phi$ Rio Parana	1.0	12.7	400	-
	$\phi$ Japanese Channels	0.53-0.89	0.25-0.88	1100-2300	-
	$\blacksquare$ Mississippi River	1.35-1.45	6-16	350-550	-

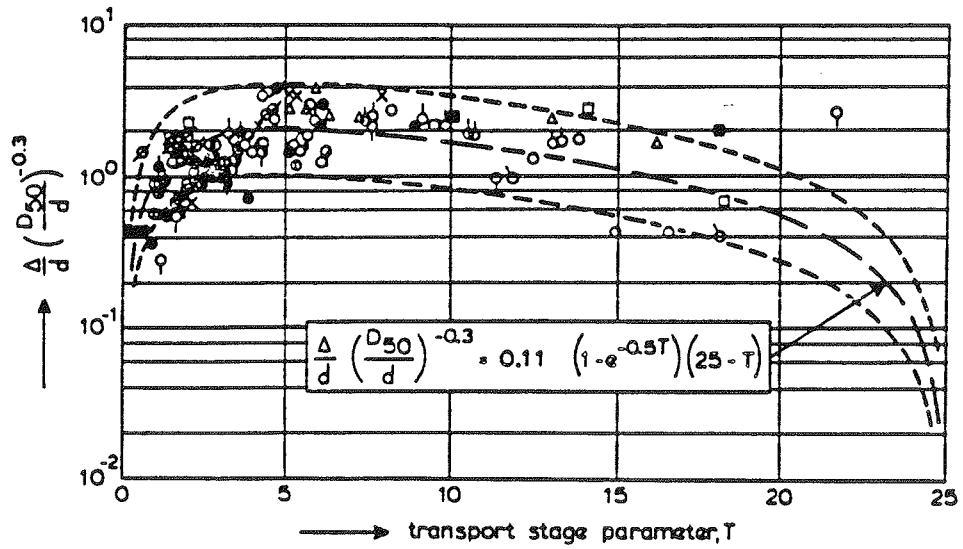
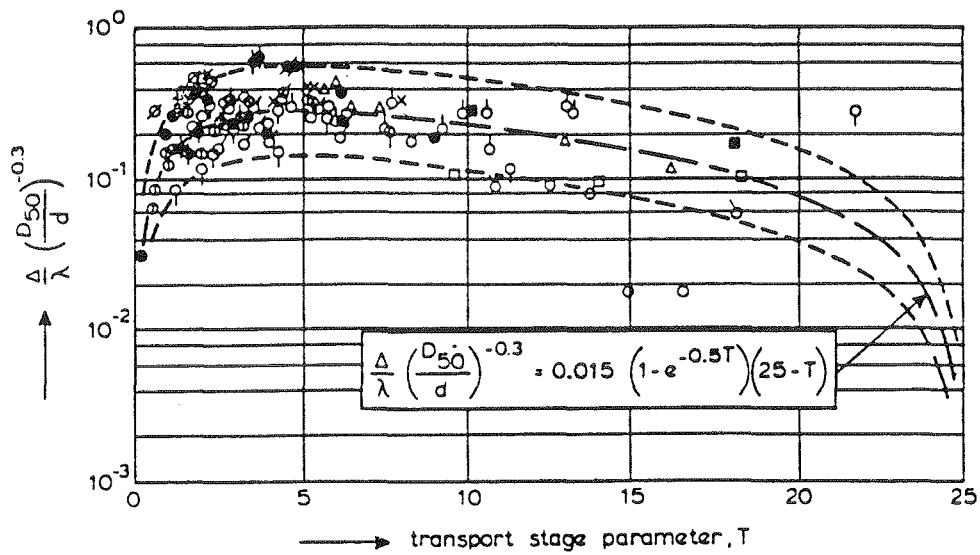


FIG. 2.—Bed-Form Height

Figure C.7.1.



**FIG. 3.—Bed-Form Steepness**

Figure C.7.2.

## Notation

$C'$	=	Chézy-coefficient related to grains;
$c_b$	=	bed-load concentration;
$D$	=	particle diameter;
$D_*$	=	particle parameter;
$d$	=	depth;
$g$	=	acceleration of gravity ( $LT^{-2}$ );
$p$	=	porosity;
$q_b$	=	bed-load transport per unit width ( $L^2T^{-1}$ );
$R_b$	=	hydraulic radius related to bed ( $L$ );
$s$	=	specific density = $\rho_s/\rho$ ;
$T$	=	transport stage parameter
$\bar{u}$	=	mean flow velocity;
$u_b$	=	velocity of bed-load particles
$u_d$	=	migration velocity of bed forms;
$u_*$	=	bed-shear velocity;
$u_*'$	=	bed-shear velocity related to grains;
$u_{*,cr}$	=	critical bed-shear velocity for initiation of motion;
$\alpha$	=	shape factor of bedform;
$\Delta$	=	bed-form height;
$\delta_b$	=	thickness of bed-load layer;
$\lambda$	=	bed-form length;
$\nu$	=	kinematic viscosity;
$\rho$	=	density of fluid;
$\rho_s$	=	density of sediment;

C.8. Menduni and Paris (1986).

Basis of theory

1. Flow over each dune is assumed to be unaffected by upstream dunes.
2. Momentum equation applied to control volume around dune (Fig. C.8.1), which yields

$$(\tau - \tau_B) L' = (p_1 - p_2) H \quad (1)$$

3. Dimensional analysis

Principal results and observations

1. By replacing the right-hand-side of (1) with drag force relation obtained from dimensional analysis, (1) reads

$$(\tau - \tau_B) L' = C_* H \rho \frac{u_*^2}{2} \quad (2)$$

By rearranging (2),

$$\frac{H}{L'} = \frac{2}{C_*} \left( 1 - \frac{\tau_B}{\tau} \right) \quad (3)$$

(Note that there are several typing errors in the authors' equations. These errors have been corrected herein.)

Total shear stress is calculated as

$$\tau = \rho g S h \quad (4)$$

Effective shear stress is calculated as

$$\tau_B = \rho \left( \frac{g}{h C'} \right)^2 \quad (5)$$

$$C' = 2.5 \log \left( \frac{11h}{2D} \right) \quad (6)$$

2. Laboratory and field data (see Table C.8.1) are used to determine  $C_*$  as a function of  $Re_*$ :

$$C_* = \frac{K_1}{Re_*} + K_2 10^{-K_3/Re_*}$$

$$K_1 = 10 (5.04 - 0.088B/h)$$

$$K_2 = 35$$

$$K_3 = 1000$$

		FLUME DATA	FIELD DATA
discharge	[m <sup>3</sup> /s]	0.017 - 0.357	0.121 - 1.751
slope		0.000075 - 0.0017	0.00037 - 0.0079
flow depth	[m]	0.05 - 0.47	0.2 - 2.5
grain size	[mm]	0.3 - 1.46	0.31 - 1.44
dune height	[m]	0.003 - 0.125	0.015 - 0.82
dune length	[m]	0.49 - 3.25	0.64 - 19.22
channel width	[m]	0.08 - 2.44	35.69 - 200.0

Table C.8.1. Experimental data ranges

3. Maximum dune steepness is calculated by setting  $\tau_B/\tau = 0$  (Fig. C.8.2). One curve is for "wide channel" ( $B = \infty$ ) and one for "narrow channel" ( $B = 0$ ).
4. A comparison of measured and computed dune steepness is presented (Fig. C.8.3).
5. The authors note that absolute maximum dune steepness is 0.07 (Fig. C.8.2).

Figures

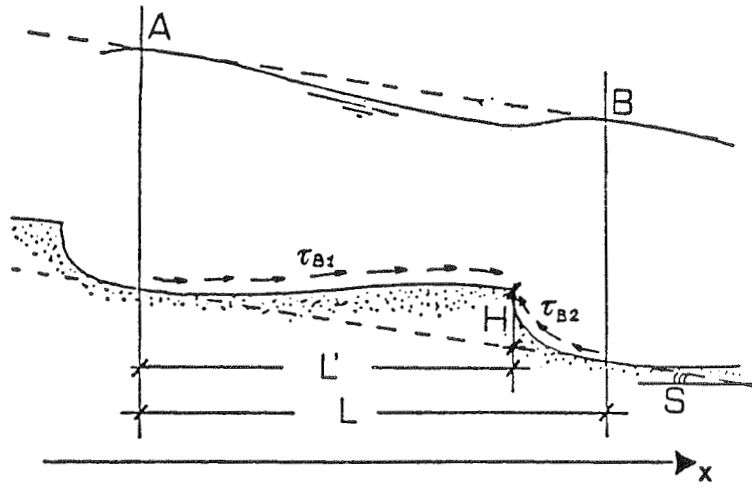


Figure 1. Sketch of control volume

Figure C.8.1.

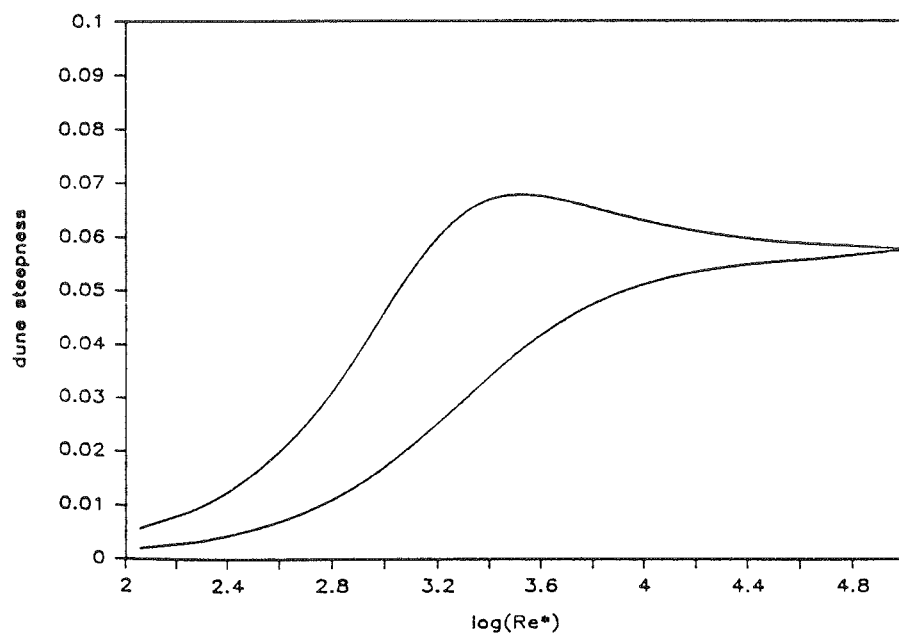


Figure 5. Maximum theoretical dune steepness

Figure C.8.2.

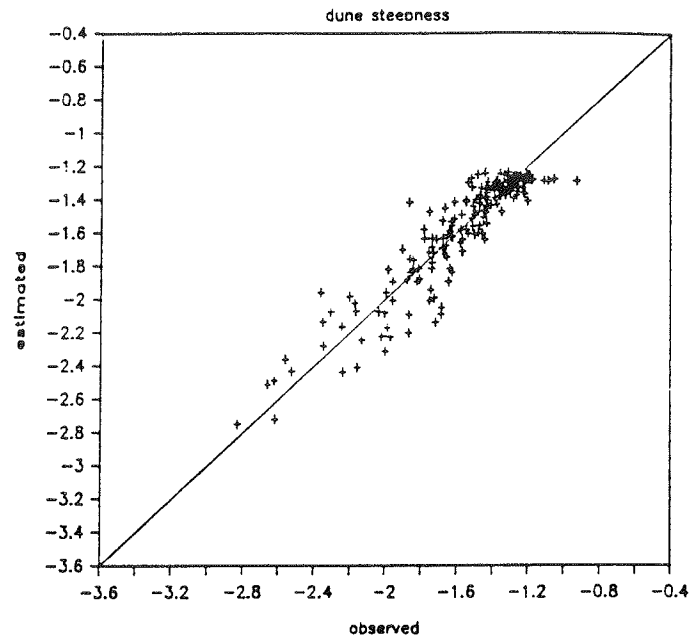


Figure C.8.3.

## Notation

$B$	=	channel width
$C_*$	=	form drag coefficient
$D$	=	mean grain diameter
$g$	=	acceleration due to gravity
$h$	=	flow depth
$H$	=	dune height
$L$	=	wavelength
$p$	=	pressure
$Re_*$	=	dune Reynolds number - $u_*H/\nu$
$S$	=	slope of water surface
$u_*$	=	shear velocity
$\rho$	=	density of fluid
$\tau$	=	total bed shear stress
$\tau_B$	=	effective bed shear stress
$\nu$	=	kinematic viscosity

D. Statistical Models. Following World War II, and especially during the 1950's and 1960's, wind waves (water waves generated by wind) received extensive research and engineering attention. Several problems, including planning for the wartime amphibious landings the construction of many off-shore structures, and the quest for better harbor design, prompted this wave research; review of these is beyond the scope of this report. Suffice it here to note that the differences between real wind waves, which include fairly wide spectra of wavelengths and periods, and monochromatic waves, which had been the subject of most of the classical wave studies, turned out to be quite important. At about the same time, the problems of describing, managing, and separating electromagnetic waves comprising many frequencies came to the fore, especially in radio communication and related fields. The techniques, notably time-series and spectral analysis, used in describing random and other multi-frequency electromagnetic waves found direct application in the study of wind waves. (A fascinating and comprehensive description of these developments is presented by Kinsman (1965) in his classical book Wind Waves.) In the 1960's the decidedly non-monochromatic character of riverine ripples and dunes gained increasing recognition, so it was only natural to apply the techniques of electromagnetic-wave wind-wave analysis to the description, and to some extent the analysis, of these bed forms.

Four of the numerous papers of this type are reviewed here, and others are cited.

### D.1. Nordin and Algert (1966).

This paper is the first to apply autocovariance and spectral-density analysis to bed forms, and as such was a major contribution to the subject. The study reported in this paper was the Masters thesis research of Algert (1965) carried out under the supervision of Nordin. The work was continued by Nordin as the subject of his Ph.D. thesis, which was also reported in a U.S.G.S. Professional Paper (Nordin 1971).

#### Basis of theory

1. The established mathematical techniques used in autocovariance and spectral-density analysis. These are outlined in the paper.
2. The estimate of the autocovariance function for discrete data given by

$$C_{\lambda} = \frac{1}{N - \lambda} \sum_{\ell = 1}^{N - \lambda} X(\ell) \cdot X(\ell + \lambda) \quad (1)$$

3. The estimate of the spectral density function for discrete data given by

$$G(f) \approx C_0 + 2 \sum_{\ell = 1}^{M - 1} \left(1 - \frac{\ell}{M}\right) C_{\ell} \cos \frac{2\pi \ell j}{M} \quad (2)$$

where the variance  $C_0$  is given by

$$C_0 = \frac{1}{N} \sum_{\ell = 1}^N X(\ell)^2 \quad (3)$$

Note: It might be useful to review briefly some of the characteristics of autocovariance and spectral density functions. First, it should be noted that one can speak indifferently of the autocorrelation and autocovariance functions because both exhibit precisely the same properties; the former is simply the autocovariance divided by the variance,  $C_0$ , so that the initial ordinate is unity. Second, the spectral-density function represents, in general terms, a method of assigning to any frequency or wave number a measure of its contribution to the "content" of the process or, more specifically,  $G(f) df$  represents the contribution to the variance from the frequency range  $f \pm \frac{df}{2}$ .

4. Bed profiles (bed elevations measured at discrete, regularly spaced points along the channels) from seven flows: 3 in a 4-foot-wide lab channel; 2 in an 8-foot-wide channel; and 2 in the Rio Grande conveyance channel. The data for these flows are summarized in Table D.1.1. Typical bed profiles are shown in Fig. D.1.1, and the autocovariance and spectral density functions for Run 2 (see Table D.1.1) are shown in Fig. D.1.2.
5. From inspection of covariance functions, the authors concluded that the dune process can be represented by a second-order autoregressive scheme, or a Markov second-order linear model:

$$X(\ell) = \alpha X(\ell - 1) - \beta X(\ell - 2) + \epsilon_\ell \quad (4)$$

Physical reasoning justifying this selection is presented by the authors.

### Principal results and observations

1. Typical observed and computed spectral density functions are shown in Fig. D.1.3.
2. The significant wave height (average amplitude of highest one-third of the waves) were found to be related to the variance by

$$H_{1/3} = 3C_0^{1/2} \quad (5)$$

(For ocean wind waves, the coefficient is 4.)

3.  $H_{1/3}$  was found to be a linear function of unit discharge,  $q$ , for all three channels.
4. The first three values of the covariance functions relate well to  $q$ , suggesting that the significant statistics to generate the models which approximate the process are functions of simple flow parameters.
5. The temporal autocorrelations (at a point) were similar to the spatial ones. Longer components were found to move more slowly.
6. Nordin's (1971) continuation of this work showed that the spatial-frequency spectra can be normalized as

$$G' = \frac{Gg}{V} = 0.0001 \left( \frac{fV^2}{g} \right)^{-3.2} \quad (6)$$

(see Fig. D.1.4). The equilibrium range of the spectrum is seen in this figure to end at about

$$\frac{fV^2}{g} \simeq 0.03 \quad (7)$$

which corresponds to a wave number,  $k = 2\pi f$ , given by

$$F^2 = \frac{0.19}{kd} \quad (8)$$

This wave number likely represents the longest, highest bed waves.

Figures and tables

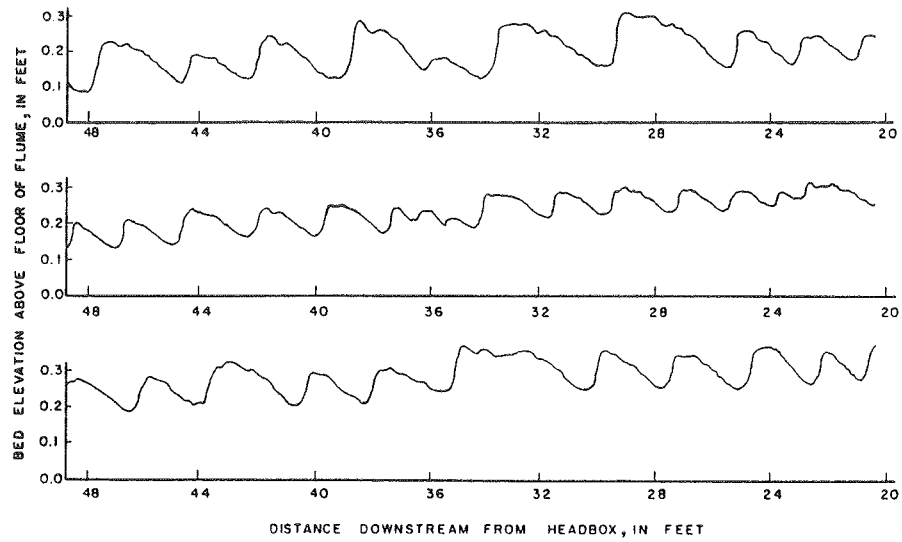


FIG. 2.—BED PROFILES FOR DUNES IN LABORATORY FLUME

**Figure D.1.1**

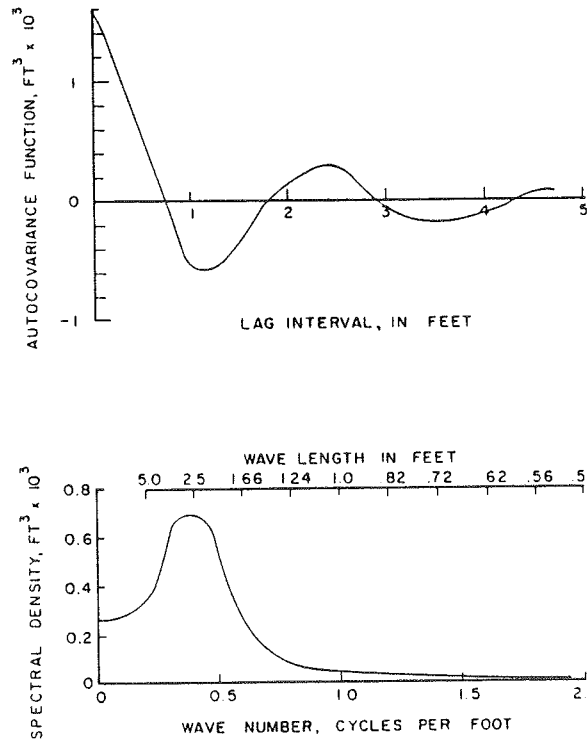


FIG. 4.—AUTOCOVARANCE AND SPECTRAL DENSITY FUNCTIONS FOR RUN NUMBER 2

**Figure D.1.2.**

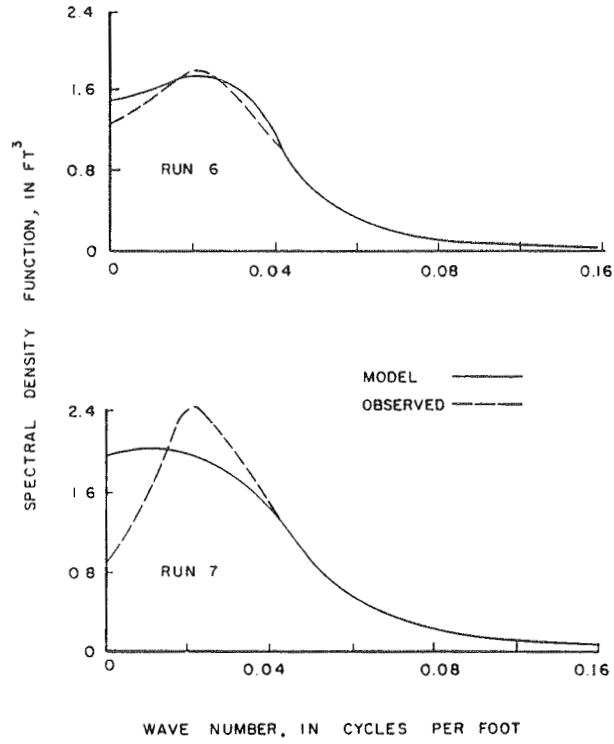


FIG. 8.—OBSERVED AND COMPUTED SPECTRAL DENSITY FUNCTIONS: RIO GRANDE CONVEYANCE CHANNEL NEAR BERNARDO

Figure D.1.3.

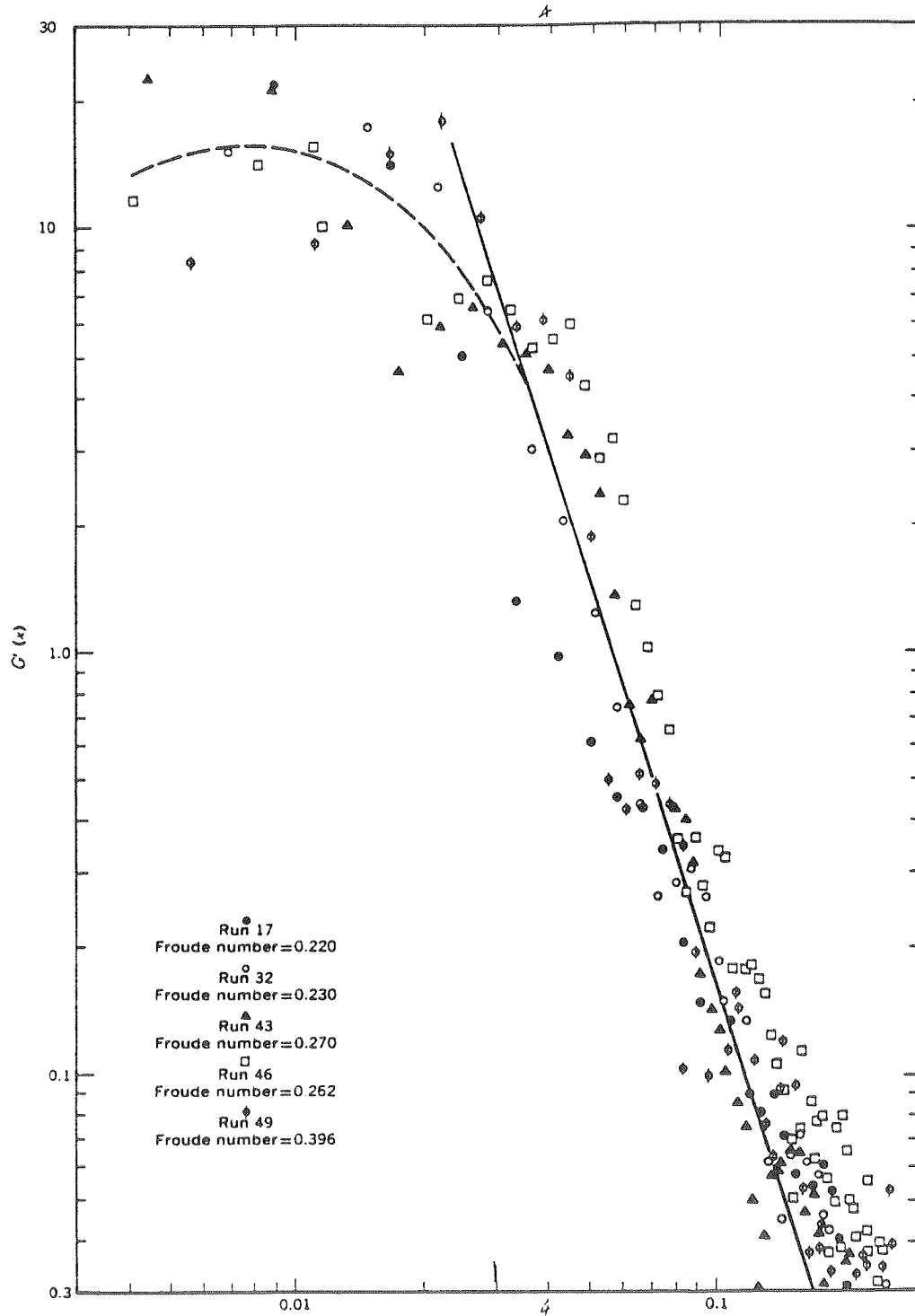


FIGURE 30. — Dimensionless spectra for the process  $y = y(x)$ .

Figure D.1.4.

TABLE 1.—SUMMARY OF HYDRAULIC DATA

Run number (1)	Unit discharge, in cfs per ft (2)	Depth, in feet (3)	Water surface slope (4)	Number of dunes used (5)	Average dune length, in feet (6)
1	0.697	0.400	0.0037	213	1.94
2	0.864	0.485	0.0038	235	2.26
3	1.05	0.580	0.0044	131	2.72
4	1.28	0.670	0.00136	20	4.73
5	2.22	1.05	0.00134	16	8.63
6	9.40	2.60	0.00058	13	24.6
7	10.3	4.15	0.00058	12	25.4

Table D.1.1

TABLE 2.—SUMMARY OF STATISTICS

Run number (1)	$C_o$ (2)	$\alpha$ (3)	$\beta$ (4)	$\sigma_\epsilon^2$ (5)	R (6)	Significant dune height, in feet (7)	Dune length of maximum variance, in feet (8)
1	0.000726	1.072	0.478	0.000264	0.797	0.081	2.56
2	0.00119	1.205	0.617	0.000326	0.852	0.104	2.70
3	0.00228	1.309	0.593	0.000483	0.893	0.144	3.34
4	0.01333	1.480	0.614	0.003062	0.856	0.346	8.4
5	0.03052	1.170	0.464	0.003782	0.936	0.525	13.4
6	0.419	1.270	0.518	0.0918	0.887	1.94	50
7	0.555	1.095	0.397	0.184	0.822	2.24	40

Table D.1.2.

## Notation

The author's full notation list is reproduced here.

- A = dune amplitude, in feet;
- $C_0$  = variance or  $\sigma_x^2$ , in square feet;
- $C_\lambda$  = autocovariance function, in square feet;
- $E(f)$  = expected value of  $f$ ;
- $f$  = wave number of frequency, in cycles per unit lag, cycles per foot, or cycles per second;
- $G(f)$  = observed spectral density function from data, in cubic feet;
- $g(f)$  = spectral density function model, in cubic feet;
- $H_{1/3}$  = average of one-third highest dunes, in feet;
- L = total distance interval considered, in feet;
- $\ell$  = distance along the bed profile, in feet;
- M = maximum lag used;
- N = number of data points in a profile;
- $R^2$  = multiple correlation between  $X(\ell)$ ,  $X(\ell - 1)$ ,  $X(\ell - 2)$ ;
- $r_k$  = correlation coefficient,  $C_k/C_0$ ;
- T = time period for a dune to pass a given point in minutes;
- $X(\ell)$  = the process of bed elevation X as a function of distance downstream,  $\ell$ , in feet;
- $X(t)$  = the process of bed elevation X as a function of time, t, in feet;
- $Z_x(f)$  = a random process with orthogonal increments;
  - $\alpha$  = autoregressive coefficient;
  - $\beta$  = autoregressive coefficient;
  - $\Gamma$  = dune length, in feet;
  - $\epsilon_\ell$  = random part of the process,  $X(\ell)$ , in feet;
  - $\theta$  = angle of repose of bed material, in degrees;
  - $\lambda$  = lag interval, in feet; and
  - $\sigma_\epsilon$  = variance of  $\epsilon_\ell$ , in square feet.
- V = mean velocity

D.2. Hino (1968).

Basis of theory

1. Observed from data of Nordin and Algert (1969) and Ashida and Tanaka (1967) that log-log plots of sand-wave spectra display an "equilibrium" range wherein

$$S(k) \sim k^{-3} \quad (1)$$

2. Corresponding power law (Kolmogorov) for turbulence is

$$E(k) \sim k^{-5/3} \quad (2)$$

3. Fourier transformations of autocorrelation functions for  $\eta$  and  $\eta'$  yield

$$S_{\eta\eta}(k) = \frac{S_{\eta'\eta'}(k)}{(2\pi k)^2} \quad (4)$$

4.  $S_{\eta'\eta'}$  has dimensions  $k^{-1}$ . Slope  $\eta'$  of sand waves cannot exceed angle of repose of bed material. Therefore

$$S_{\eta'\eta'}k = (2\pi)^2 \alpha(\phi)k^{-1} \quad (5)$$

5. (4) and (5) yield

$$S_{\eta\eta}(k) = \alpha(\phi)k^{-3} \quad (6)$$

## Principal results and observations

1. Fig. D.2.1. shows typical results.
2. The lower limit of the range of the "-3 power law" is given by (see Fig. D.2.2)

$$k_0 \approx 0.15/h \quad (7)$$

or

$$L \approx 7h \quad (8)$$

3. Ripples (as opposed to dunes) tend to conform to a "-2 power law".
4. Quantification of  $\alpha(\phi)$  from experimental data led to

$$S_{\eta\eta}(k) = 2.8 \times 10^{-4} k^{-3} \quad (9)$$

as relation for spectral density function in the equilibrium range.

Figures

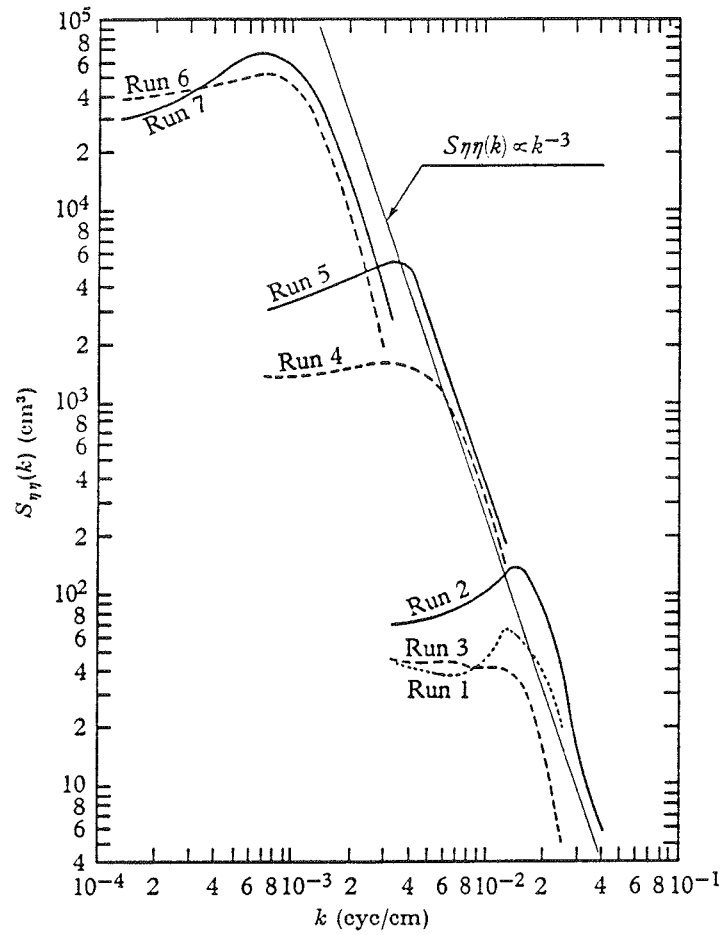


FIGURE 1. Wave-number spectra of sand waves compared with the  $k^{-3}$  power law, (10).  
(Curves are replotted from the graphs by Nordin & Algert (1966).)

Figure D.2.1.

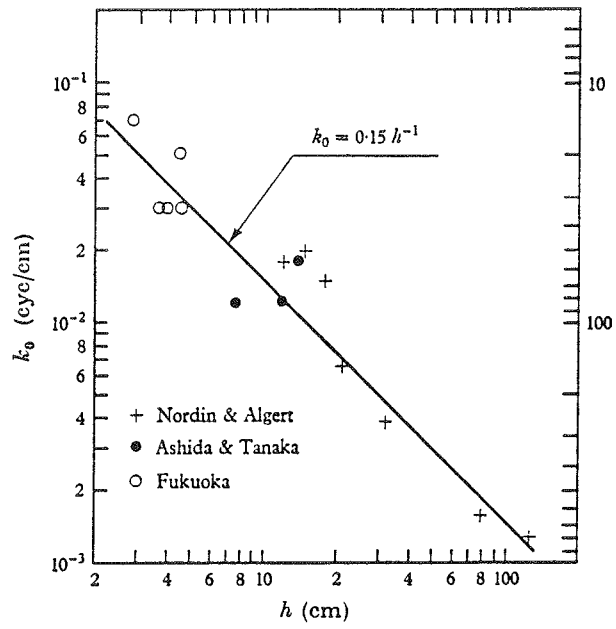


FIGURE 5. Relation between the lower limit wave-number  $k_0$  of the '-3 power law' and the depth of flow  $h$ .

Figure D.2.2

## Notation

$E(k)$	=	turbulence spectral density function
$h$	=	flow depth
$k$	=	wave number = $1/L$ (not $2\pi/L$ )
$L$	=	wavelength
$S_{\eta\eta}(k)$	=	bed-wave profile spectral density function
$S_{\eta'\eta'}(k)$	=	bed-wave slope spectral density function
$\alpha(\phi)$	=	same function of $\phi$
$\phi$	=	angle of repose of bed sediment
$\psi(k)$	=	wind-wave spectral density function

### D.3. Annambhotla, Sayre and Livesey (1972).

#### Basis of study

This study was, in many respects, a continuation and extension of the work of Algert and Nordin (see Section D.1) on the application of time-series or spectral analysis of bed forms. Its principal new contributions were:

1. Application of zero-crossing analysis to bed forms. This involves determination of a best-fit (according to whatever measure of fit is adopted) straight or monotonically curved line to the smoothed bed profile, and analysis of the distances between successive crossings of the best-fit line by the actual bed profile; see Fig. D.3.1.
2. Statistical analysis of detailed bed-form data from a moderately large river (the Missouri River).
3. Filtering of the raw bed-profile data to eliminate the very low-frequency (long wavelength) components due to meanders, spur dikes, etc. (see Fig. D.3.2). The autocorrelation and spectral analyses were based on the filtered data. Figure D.3.3 shows typical autocorrelation and spectral-density functions for the unfiltered and filtered data.
4. Frequency-distribution analysis of the: bed-elevation deviations from the mean (best-fit) line; wavelength; and amplitudes of the bed waves.

## Principal results and observations

1. The hydraulic data for the flows that produced the bed profiles analyzed are given in Table D.3.1.
2. The results obtained from the spectral analysis are summarized in Table D.3.2.
3. The results obtained from the zero-crossing analysis are summarized in Table D.3.3.
4. Weighted-average bed-wave characteristics are summarized in Table D.3.4. These were obtained by weighting the wave heights and lengths by: "the ratio of the product of the partial discharge assignable to a sailing line and the subreach length to the product of the total river discharge and the combined lengths of all sailing lines" (pp. 506-7).
5. An overview of the results of the study is presented in Fig. D.3.4.
6. The bed-form friction factor was found to correlate well with a modified relative roughness (see Fig. D.3.5).
7. The author's conclusions concisely state their principal findings, and are reproduced here (p. 508);
  1. The zero-crossing distances and amplitudes analysis method is better suited than the spectral analysis method for obtaining characteristic wave

heights and lengths from river data. This is mainly because the former method requires only stationarity of the mean, whereas the latter requires both mean and covariance stationarity. Bed profile data from rivers, even after filtering, are apt to be nonstationary in the covariance.

2. Bed elevations were found to be distributed approximately according to the normal probability law. The approximation was found to be better for the filtered than for the unfiltered data.

3. Wave lengths, amplitudes and heights, determined from the filtered data, were all found to be distributed in approximate accordance with the exponential probability law.

4. The bed form friction factor,  $f'$ , was found to decrease approximately exponentially with increasing values of the modified relative roughness,  $R/(eH)$ , asymptotically approaching zero as the contribution of the grain roughness to the total resistance becomes predominant. The parameter  $1/\sqrt{f'}$  was found to vary with  $R/(eH)$  in a manner that is roughly consistent with the von Karman-Prandtl logarithmic law for rough boundaries. Variations in the size distribution, shape and geometrical arrangement of bed forms, which are not adequately accounted for in the parameter,  $R/(eH)$ , are likely contributors to the scatter.

5. The roughness of the bed was observed to vary inversely with water temperature. However, changes in  $L_0$ ,  $H$ ,  $e$ ,  $RE/eH$ , and  $f'$  all tended to lead, sometimes by as much as 2 months to 3 months, rather than to lag the change in temperature. The reason for this is not understood, although it is suspected that unidentified factors such as seasonal variations in sediment size and supply may play a role.

Figures

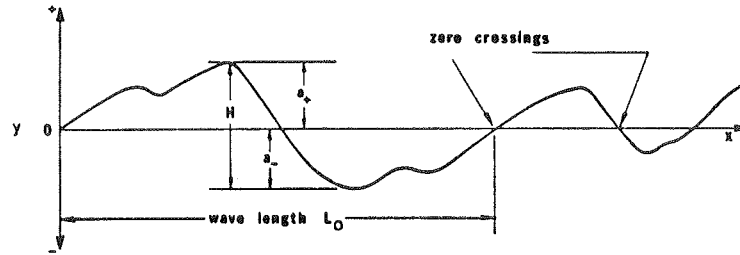


FIG. 1.—DEFINITION SKETCH OF CHANNEL BED PROFILE

Figure D.3.1.

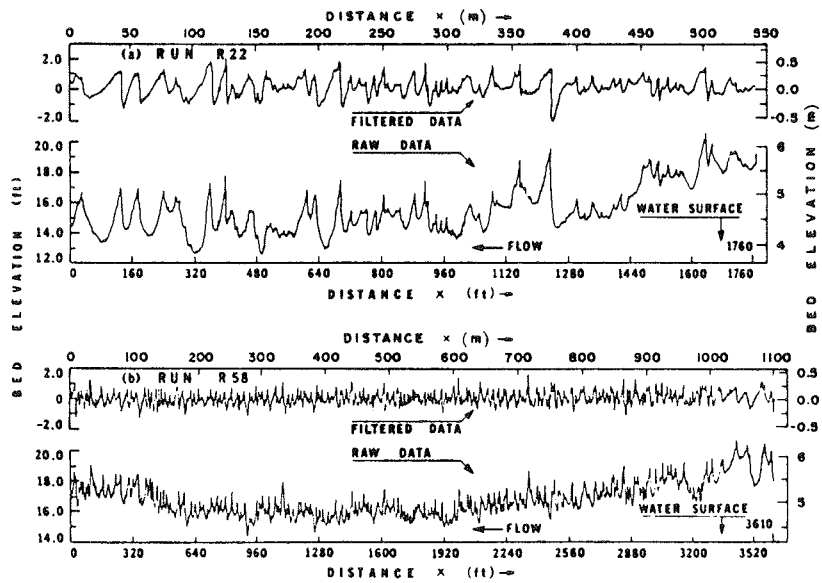


FIG. 2.—RAW AND FILTERED BED PROFILE DATA FOR: (a) RUN R22; AND (b) RUN R58

Figure D.3.2.

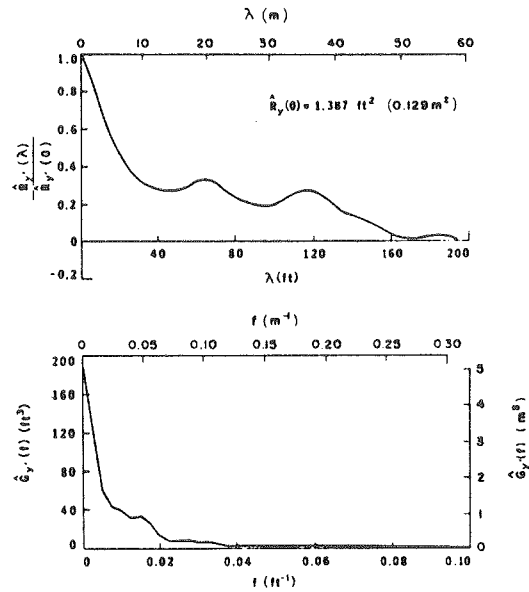


FIG. 4.—AUTOCORRELATION AND SPECTRAL DENSITY FUNCTIONS FOR UNFILTERED DATA FROM RUN R22

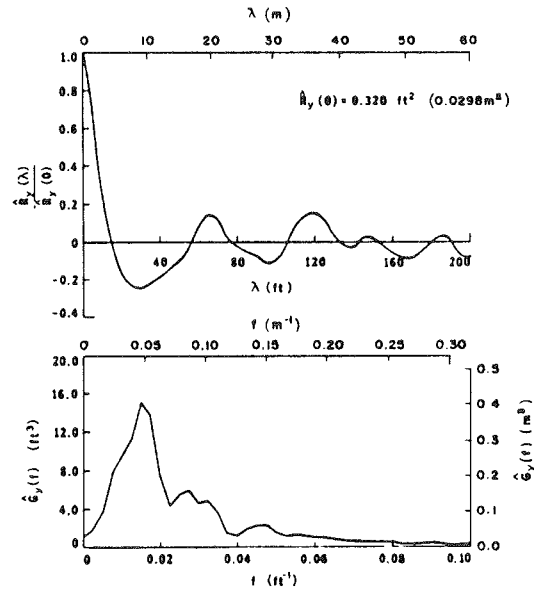


FIG. 5.—AUTOCORRELATION AND SPECTRAL DENSITY FUNCTIONS FOR FILTERED DATA FROM RUN R22

Figure D.3.3.

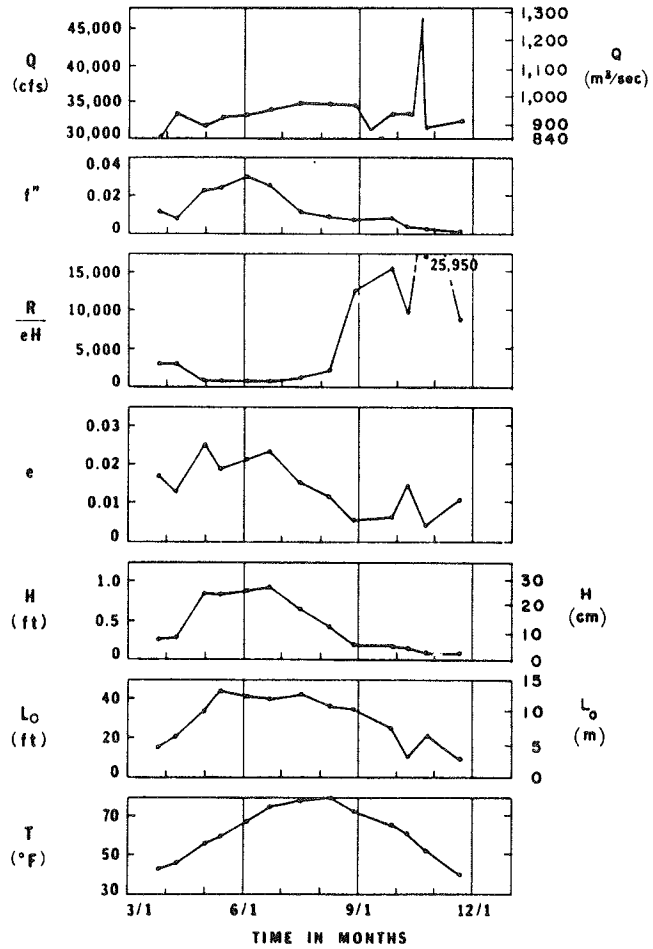


FIG. 9.—VARIATION OF WATER TEMPERATURE, ROUGHNESS CHARACTERISTICS, BED FORM FRICTION FACTOR, AND RIVER DISCHARGE WITH TIME OF YEAR, 1968, IN MISSOURI RIVER AT OMAHA

Figure D.3.4.

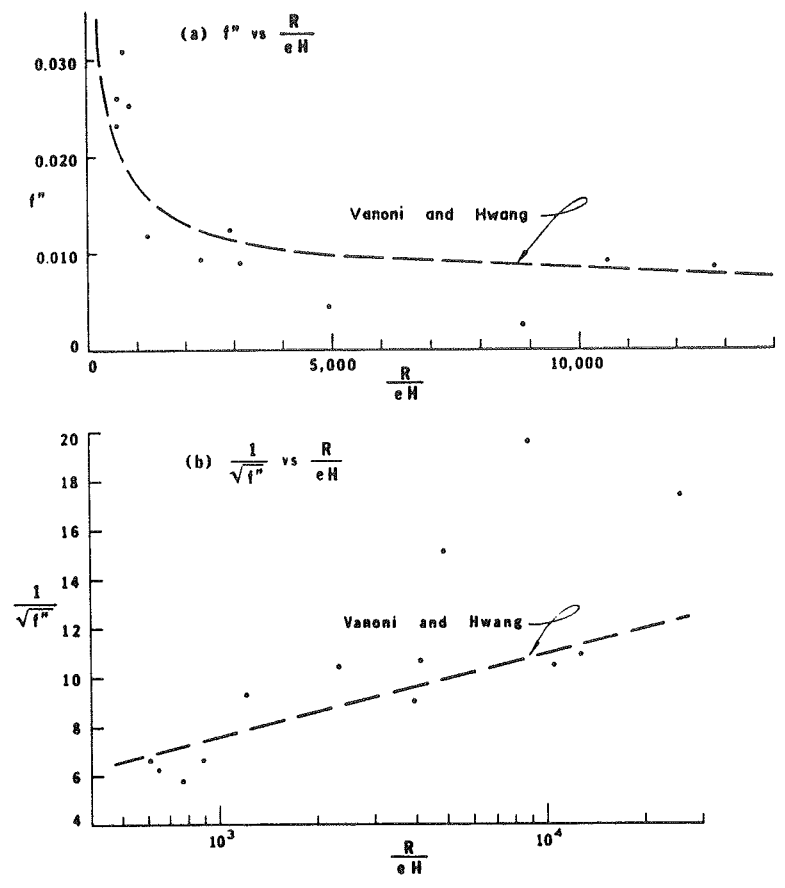


FIG. 8.—VARIATION OF BED FORM FRICTION FACTOR WITH MODIFIED RELATIVE ROUGHNESS

Figure D.3.5.

TABLE 1.—HYDRAULIC CONDITIONS FOR MISSOURI RIVER RUNS

Date (1)	Mile (2)	Water temperature, in degrees Fahrenheit (3)	Discharge, $Q$ , in cubic feet per second (cubic meters per second) (4)	Mean velocity, $U$ , in feet per second (meters per second) (5)	Hydraulic mean radius, $R$ , in feet (meters) (6)	Slope $S \times 10^4$ (7)	Darcy-Weisbach friction factor $f$ (8)	Grain roughness friction factor $f''$ (9)	Bed form friction factor $f'''$ (10)	Run numbers (11)
3/25/68	612.3	43	30,100 (844)	4.45 (1.36)	12.50 (3.81)	1.325	0.0212	0.0088	0.0124	R1-R5
4/8/68	612.3	46	33,000 (925)	5.10 (1.56)	10.32 (3.15)	1.740	0.0178	0.0090	0.0088	R6-R7
4/30/68	612.3	56	32,000 (896)	4.27 (1.30)	13.00 (3.96)	1.730	0.0320	0.0088	0.0232	R8-R10
5/13/68	612.3	59	32,400 (907)	3.98 (1.21)	13.82 (4.22)	1.510	0.0340	0.0087	0.0253	R11-R16
6/3/68	612.3	68	32,900 (921)	3.62 (1.11)	14.20 (4.33)	1.420	0.0395	0.0087	0.0308	R17-R19
6/20/68	612.3	75	34,300 (960)	3.74 (1.14)	14.00 (4.27)	1.350	0.0348	0.0087	0.0261	R20-R25
7/15/68	612.3	79	35,100 (983)	4.38 (1.34)	11.55 (3.52)	1.295	0.0205	0.0088	0.0117	R26-R30
8/8/68	612.3	80	35,000 (980)	4.65 (1.42)	11.15 (3.40)	1.360	0.0181	0.0088	0.0093	R31-R37
8/28/68	612.3	72	34,600 (969)	4.66 (1.42)	11.41 (3.49)	1.270	0.0173	0.0088	0.0085	R38-R40
9/27/68	612.3	66	33,300 (932)	4.52 (1.38)	11.21 (3.42)	1.270	0.0179	0.0088	0.0091	R41-R45
10/10/68	612.3	62	33,500 (938)	5.13 (1.57)	10.32 (3.15)	1.320	0.0133	0.0089	0.0044	R46-R49
10/24/68	612.3	52	31,500 (882)	4.99 (1.52)	10.20 (3.11)	1.173	0.0123	0.0090	0.0033	R50-R52
11/21/68	612.3	39	32,500 (910)	5.15 (1.57)	10.30 (3.14)	1.135	0.0117	0.0091	0.0026	R53-R55
3/12/68	612.3	—	17,700 (495)	3.46 (1.06)	9.20 (2.80)	1.540	0.0304	—	—	R56-R57
8/8/68	609.0	80	35,000 (980)	3.53 (1.08)	13.46 (4.10)	1.250	0.0347	0.0087	0.0260	R58

Table D.3.1.

TABLE 2.—STATISTICAL MEASURES OF BED ROUGHNESS OBTAINED BY SPECTRAL ANALYSIS

Run number (1)	Unfiltered Data				Filtered Data				Roughness concentration $e' = \frac{\sigma_y}{L_1}$ (10)
	$\sigma_y$ in feet (meters) (2)	$L_1 = \frac{\text{Mom}_0}{\text{Mom}_1}$ in feet (meters) (3)	$L_2 = \left[ \frac{\text{Mom}_0}{\text{Mom}_2} \right]^{1/2}$ in feet (meters) (4)	Spectral width, $\Delta^2$ (5)	$\sigma_y$ in feet (meters) (6)	$L_1 = \frac{\text{Mom}_0}{\text{Mom}_1}$ in feet (meters) (7)	$L_2 = \left[ \frac{\text{Mom}_0}{\text{Mom}_2} \right]^{1/2}$ in feet (meters) (8)	Spectral width, $\Delta^2$ (9)	
R17	1.750 (0.535)	233.00 (71.00)	108.50 (33.10)	0.988	0.531 (0.162)	56.00 (17.10)	34.60 (10.56)	0.945	0.0190
R18	1.650 (0.504)	175.80 (53.60)	75.80 (23.12)	0.988	0.627 (0.191)	43.20 (13.18)	28.60 (8.73)	0.929	0.0290
R19	1.510 (0.461)	152.00 (46.40)	70.20 (21.40)	0.982	0.623 (0.190)	41.40 (12.61)	29.70 (9.06)	0.910	0.0308
R20	1.208 (0.368)	137.30 (41.95)	50.60 (15.42)	0.982	0.466 (0.142)	31.20 (9.50)	19.35 (5.60)	0.885	0.0299
R21	1.160 (0.354)	91.00 (27.80)	45.70 (13.93)	0.972	0.576 (0.176)	34.75 (10.60)	23.05 (7.03)	0.900	0.0332
R22	1.170 (0.357)	106.50 (32.50)	50.80 (15.50)	0.970	0.565 (0.172)	34.55 (10.53)	24.20 (7.39)	0.890	0.0327
R23	1.670 (0.510)	88.20 (26.95)	53.10 (16.20)	0.974	0.868 (0.264)	45.80 (13.98)	30.05 (9.17)	0.930	0.0379
R24	1.373 (0.420)	96.50 (29.40)	40.00 (12.20)	0.972	0.635 (0.194)	26.55 (8.09)	17.90 (5.46)	0.875	0.0479
R25	1.600 (0.488)	102.00 (31.15)	59.00 (18.00)	0.979	0.735 (0.224)	48.10 (14.69)	29.00 (8.85)	0.934	0.0306
R56	0.710 (0.217)	28.00 (8.55)	23.20 (7.08)	0.677	0.670 (204)	25.40 (7.75)	21.80 (6.65)	0.632	0.0528
R57	0.410 (0.125)	25.00 (7.65)	21.70 (6.62)	0.546	0.384 (0.117)	22.40 (6.83)	20.20 (6.16)	0.500	0.0342
R58	0.917 (0.280)	72.50 (22.15)	30.90 (9.44)	0.945	0.475 (0.145)	17.71 (5.40)	14.38 (4.38)	0.750	0.0536

Table D.3.2.

TABLE 3.—WAVE LENGTHS AND AMPLITUDES FOR REPRESENTATIVE RUNS OBTAINED BY ZERO-CROSSING AND AMPLITUDES ANALYSIS

Run number	Wave Length		Positive Amplitude		Negative Amplitude		Wave Height, $\bar{H} = \bar{a}_+ +  \bar{a}_- $ , in feet (meters)	Roughness concentration $e = \bar{H}/\bar{L}_0$
	$\bar{L}_0$ , in feet (meters)	$C_v$	$\bar{a}_+$ , in feet (meters)	$C_v$	$-\bar{a}_-$ , in feet (meters)	$C_v$		
(1)	(2)	(3)	(4)	(5)	(6)	(7)	(8)	(9)
R17	36.65 (11.20)	1.690	0.287 (0.088)	1.280	0.251 (0.076)	1.574	0.538 (0.164)	0.0147
R18	43.99 (13.40)	0.929	0.473 (0.144)	0.765	0.582 (0.177)	1.325	1.015 (0.310)	0.0231
R19	43.66 (13.32)	0.739	0.662 (0.202)	0.741	0.525 (0.160)	0.873	1.130 (0.345)	0.0258
R20	21.60 (6.60)	1.335	0.300 (0.092)	1.031	0.305 (0.093)	1.578	0.605 (0.185)	0.0280
R21	44.67 (13.62)	0.794	0.396 (0.121)	1.131	0.344 (0.105)	1.373	0.740 (0.226)	0.0165
R22	32.57 (9.93)	0.800	0.557 (0.170)	0.870	0.418 (0.128)	0.953	0.976 (0.298)	0.0300
R23	60.42 (18.40)	0.712	0.722 (0.220)	0.692	0.589 (0.180)	2.150	1.186 (0.362)	0.0196

Table D.3.3.

TABLE 4.—AVERAGED PROPERTIES OF BED FORMS

Runs	Date	Description of river bed	Weighted Average Wave Characteristics			
			$\bar{L}_0$ , in feet (meters)	$\bar{H}$ , in feet (meters)	$c = \bar{H}/\bar{L}_0$	$R/\bar{H}$
(1)	(2)	(3)	(4)	(5)	(6)	(7)
R11-R15	3/25/68	Dunes, bars, plane	15.0 (4.58)	0.253 (0.077)	0.0169	2,940
R16-R17	4/8/68	Bars	20.8 (6.35)	0.262 (0.080)	0.0126	3,130
R18-R110	4/30/68	Dunes	33.6 (10.26)	0.845 (0.258)	0.0252	612
R11-R116	5/13/68	Dunes, bars	14.2 (4.35)	0.827 (0.252)	0.0187	894
R17-R119	6/3/68	Dunes, bars	41.3 (12.61)	0.872 (0.266)	0.0211	772
R20-R25	6/20/68	Dunes, bars	39.3 (12.00)	0.924 (0.282)	0.0235	645
R26-R30	7/15/68	Dunes, bars	42.5 (12.98)	0.636 (0.194)	0.0150	1,210
R31-R37	8/8/68	Transition, dunes, bars	36.0 (11.00)	0.415 (0.127)	0.0115	2,330
R38-R40	8/28/68	Transition, plane	31.2 (9.54)	0.175 (0.053)	0.00512	12,800
R40-R45	9/27/68	Transition, plane, dunes	25.1 (7.65)	0.163 (0.050)	0.00650	10,600
R46-R49	10/10/68	Plane, transition	10.1 (3.08)	0.144 (0.044)	0.0143	4,950
R50-R52	10/24/68	Plane, transition, long bars	21.3 (6.50)	0.092 (0.028)	0.00432	26,000
R53-R55	11/21/68	Plane	8.3 (2.53)	0.089 (0.027)	0.0108	8,830

Table D.3.4.

## Notation

The author's full notation list is reproduced here.

- $a_+$  = positive amplitude;
- $a_-$  = negative amplitude;
- $C_v$  = coefficient of variation;
- $e$  = roughness concentration, defined as  $H/L_0$ ;
- $f$  = Darcy-Weisbach friction factor; also frequency or wave number;
- $f'$  = component of friction factor associated with sand grain roughness;
- $f''$  = component of friction factor associated with form roughness;
- $G_y(f)$  = physically realizable one-sided spectral density function;
- $g$  = gravitational acceleration;
- $H$  = dune height defined as vertical distance between maximum and minimum elevation between successive zero-crossings;
- $H'$  = index of dune height (equal to  $2\sigma_y$ );
- $H(f)$  = frequency response function;
- $|H(f)|$  = gain of filter;
- $h$  = arbitrary wave height;
- $k_s$  = equivalent sand roughness;
- $L$  = wave length;
- $L_0$  = wave length obtained from zero-crossings analysis;
- $M$  = maximum number of lags in spectral estimation;
- $\text{Mom}_r$  =  $r$ th moment of spectral density function;
- $N$  = number of data in sample of bed profile;
- $n_0$  = number of zero-crossings in given length,  $X$ , of sample;
- $R_y(\lambda)$  = autocovariance function for  $y(x)$ ;
- $S$  = energy slope;
- $S'$  = component of energy slope associated with sand grain roughness;
- $S''$  = component of energy slope associated with form roughness;
- $U$  = mean flow velocity;
- $X$  = length of sample record; also a random variable;
- $x$  = distance along length of channel or sample record;
- $Y(f)$  = Fourier transform of  $y(x)$ ;
- $Y'(f)$  = Fourier transform of  $y'(x)$ ;
- $y(x)$  = bed elevation at distance  $x$ ;
- $y'(x)$  = bed elevation at distance  $x$  for raw data before filtering;
- $\{v(v)\}$  = stochastic process defining bed elevation;
- $z(\lambda)$  = standardized form of random variable  $y(x)$ ;
- $\alpha$  = parameter of filter;
- $\Delta^2$  = spectral width;
- $\Delta\lambda$  = sampling interval;
- $\kappa$  = von Karman's constant;
- $\lambda$  = lag distance;
- $\nu$  = kinematic viscosity;
- $\sigma_y$  = standard deviation of  $y$ ; and
- $\omega = 2\pi f$  = circular frequency.

D.4. Jain and Kennedy (1974).

Basis of theory

1. Bed profile is expressed in terms of its Fourier components.

$$\eta(x,t) = \int B(k,t) e^{ikx} dx \quad (1)$$

2. Velocity potential for flow shown in Fig. D.4.1 over wavy bed given by (1) is

$$\phi(x,y,t) = iU \int JB(k,t)e^{ikx} dx \quad (2)$$

where

$$J(k,y) = \frac{\cosh ky + F^2kd \sinh ky}{F^2kd \cosh kd - \sinh kd} \quad (3)$$

3. Sediment continuity

$$\eta_t + T_x = 0 \quad (4)$$

Note: subscripts denote partial differentiation.

4. Transport relation of Hayashi (1970)

$$T(x,t) = m[1 + \alpha\eta_x(x,t)][(U - U_c) + \phi_x(x - \beta, -d,t)]^n \quad (5)$$

5. (4) and (5) yield  $\eta_t(x,b)$ , which is Fourier transformed to yield

$$B_t(k,t) - \bar{T}k^2[\alpha - n_1 J_1 \exp(-ik\beta)]B(k,t) = 0 \quad (6)$$

after substitution of (5) and (6).

6. Solution of (6) is

$$B(k,t) = B(k,0)\exp[\bar{T}k^2\{\alpha - n_1 J_1 \exp(-ik\beta)\}] \quad (7)$$

7. Spectrum of bed profile is obtained by ensemble averaging the product of (7) and its complex conjugate

$$\Phi(k,t) = \Phi(k,0)\exp[2\bar{T}k^2(\alpha - n_1 J_1 \cos k\beta)t] \quad (8)$$

8. Speed  $c$  of contribution to  $\Phi$  with wave number  $k$  is found from Eqs. 1 and 7 to be

$$c = \bar{T}n_1 k J_1 \cos k\beta \quad (9)$$

9. Normalized growth rate of spectrum is

$$\frac{\Phi_t(k,0)}{\Phi(k,0)} \frac{d^2}{2T\alpha} = k^2 d^2 \left( 1 - \frac{n_1}{\alpha} J_1 \cos k\beta \right) = \Gamma \quad (10)$$

which has a singularity at the Airy celerity

$$F^2 = \tanh kd/kd \quad (11)$$

Component with wave number given by (6) develops linearly with time even on a flat bed:

$$\eta = \left[ n\bar{T} \frac{U}{(U - U_c)} \frac{Ak^2}{\sinh kd} \cos k(x - \beta) \right] t \quad (12)$$

10. Normalized growth rate given by (10) is shown in Fig. D.4.2.

11. A "conservation of variance" principle is formulated as (see Fig. D.4.3)

$$\frac{\partial}{\partial t} \Phi(k,t)dk = \Lambda(k,t)dk + \frac{1}{2\pi} \left\{ \int_k^\infty \Phi(k,t)kc(k,t)dk - \left[ \int_k^\infty \Phi(k,t)kc(k,t)dk - \frac{\partial}{\partial k} \left( \int_k^\infty \Phi(k,t)kc(k,t)dk \right) dk \right] \right\} \quad (13)$$

12. For sufficiently large  $kd$ ,  $J_1$  approaches infinity and Eq. (9) becomes

$$c \approx \bar{T} n_1 k \quad (14)$$

13. For steady-state conditions (equilibrium range), (13) becomes

$$\frac{d}{dk} \left( k \int_k^\infty \Phi c dk \right) = 0 \quad (15)$$

which, with (14), yields

$$\Phi \sim k^{-3} \quad (16)$$

### Principal results and observations

1. Spectra of bed forms developing on an initially flat bed exhibit two peaks, as predicted by (10) (see Fig. D.4.3). One peak is at the Airy celerity given by (11).
2. Author's explanation of evaluation of spectra is as follows:

At small times the spectra of bed forms developing on an initially flat bed are characterized by two peaks. One peak, generally that at the lower spatial frequency, traces its origin to the velocity-field perturbation and accompanying pattern of differential deposition and scour on the bed produced by a small amplitude, stationary surface wave; i.e. a wave train moving relative to the fluid with velocity just equal in magnitude but opposite in direction to the mean flow velocity. It is this equality that determines the frequency of one spectral peak. The second peak corresponds to bed waves resulting from the inherent instability of an interface between an erodible bed and a turbulent flow. Over wide ranges of flow conditions any small initial disturbance on an otherwise flat bed will produce a perturbation of the velocity field and hence also of the sediment-transport distribution, giving rise to a spatial pattern of scour and deposition that produces bed waves. This instability mechanism is not dependent on

the proximity of a free surface; it also produces, for example, ripples in very deep tidal flows and aeolian ripples on wind-swept sand deposits. The spatial frequency at which it is centered is a function of the flow and transport characteristics, reflected in  $n_1/\alpha$ ,  $J_1$  and  $\beta/d$ , and can be expected to occur at the value of  $kd$  where  $\Gamma$ , given by (10) and illustrated in figure 2, has a continuous maximum. Equation (9) indicates that the two different families of waves will move with different speeds, and this frequency dispersion probably accounts for the shift of the normalized spectra--- towards the lower frequencies as the bed configurations develop and mature.

This "variance-cascade" process, involving interaction between the water-surface (Airy) wave generated bed forms and the bed forms produced just by the bed-flow interaction was verified by the experiments of Nakagawa and Tsujimoto (1984).

3. Normalized (by  $d\sigma^2F^{5/3}$ ) spectra conform to (16) (see Fig. D.4.4).
4. Normalization by  $F^{5/3}$  suggests

$$L_{2/d} \equiv (M_0/M_2)^{1/2} \sim F^{5/3} \quad (17)$$

which is supported by Jain's data (see Fig. D.4.5). The data given in Fig. D.4.5 yield

$$F^{5/3} = \frac{0.51}{2\pi} \frac{L_2}{d} \equiv \frac{0.51}{k_2 d} \quad (18)$$

Nordin's data conform better to

$$L/d \sim F^2 \quad (19)$$

The field data of Annambhotla et al. (1972) do not conform to the relation suggested by Fig. D.4.5.

5. Examination of bed-wave spectra of several authors suggest  $F^{5/3}$  to be preferred in the spectrum normalization factor.

Figures

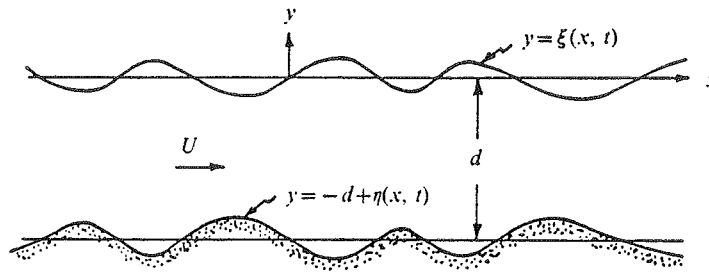


FIGURE 1. Definition sketch of free-surface flow over an irregular erodible bed.

Figure D.4.1.

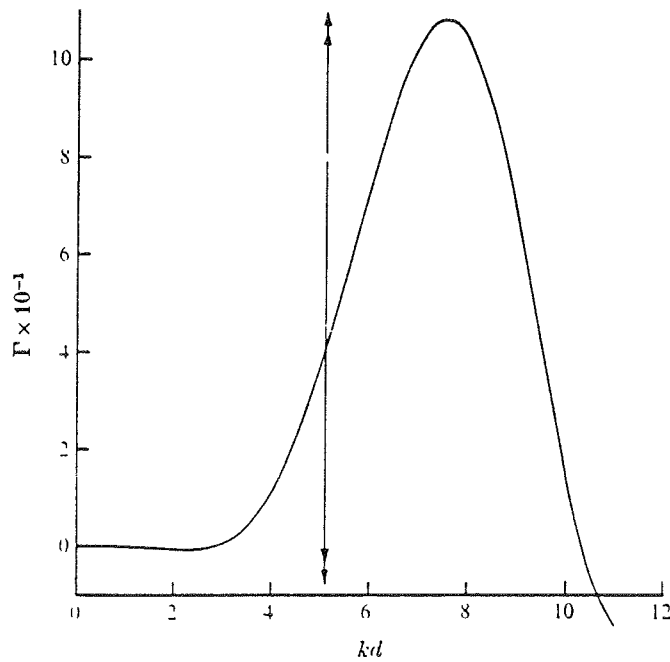


FIGURE 2. Variation of normalized growth rate  $\Gamma$  with  $kd$ , calculated from (15) for  $\eta_1/\alpha = 1.0$ ,  $\beta/d = 0.72$  and  $F = 0.44$ .

Figure D.4.2.

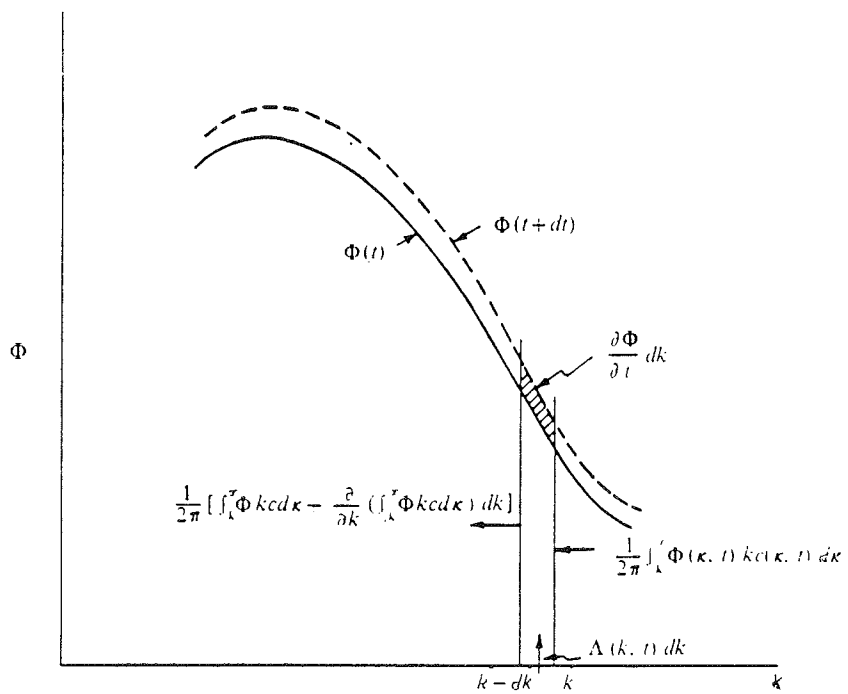


FIGURE 5. Schematic representation of differential relation for bed-wave variance, equation (19).

Figure D.4.3.

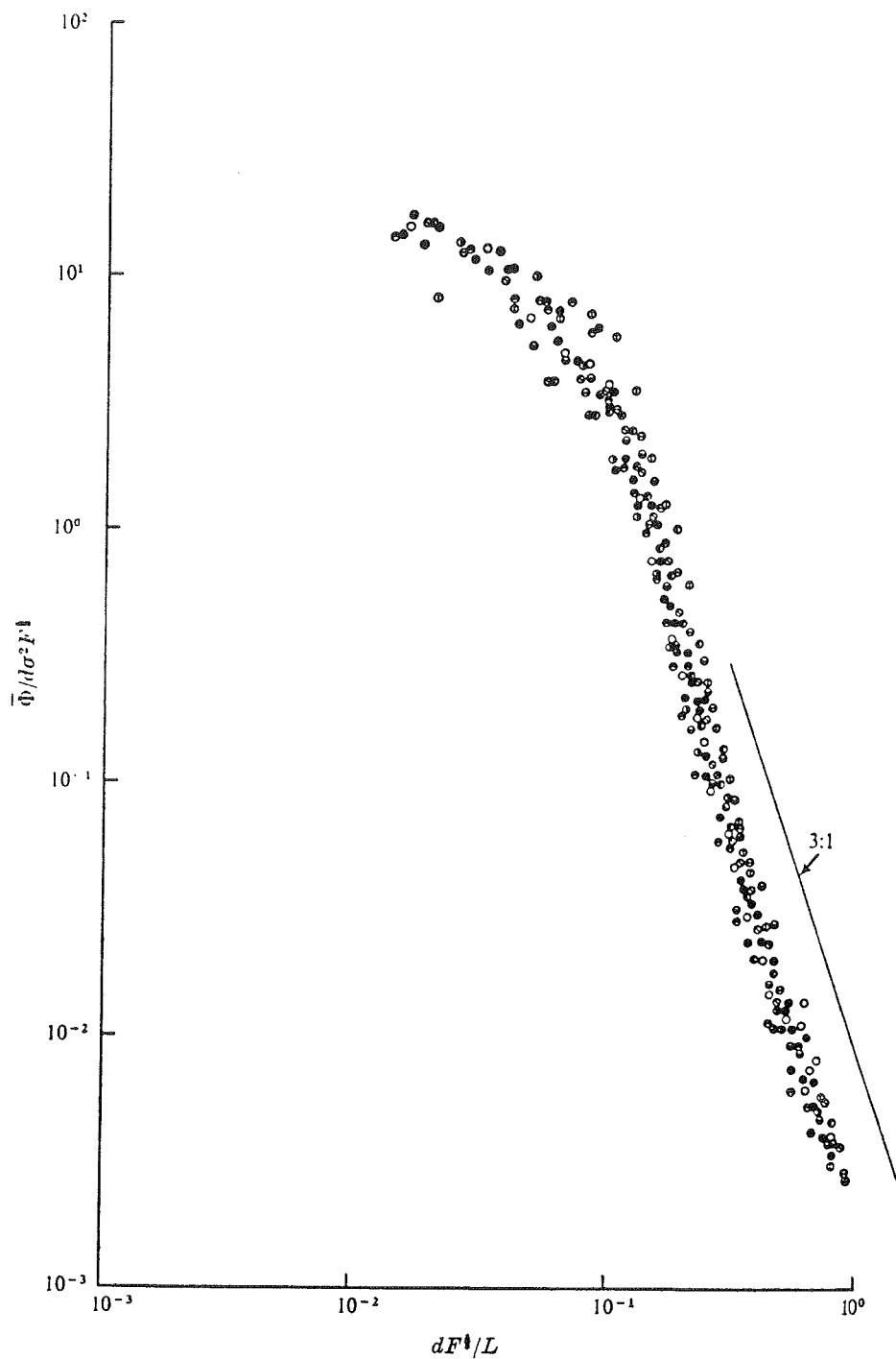


FIGURE 6. Non-dimensional plot of Jain's (1971) spectra data illustrating occurrence of minus-three-power law at higher frequencies.

	⊙	⊖	●	⊗	⊕	⦿	⦿	○	⊙	●	
$U$ (ft/s)	1.410	1.625	1.145	1.262	1.330	1.442	1.350	1.560	1.210	1.320	1.110
$d$ (ft)	0.329	0.331	0.248	0.253	0.267	0.246	0.437	0.402	0.335	0.353	0.417

Figure D.4.4.

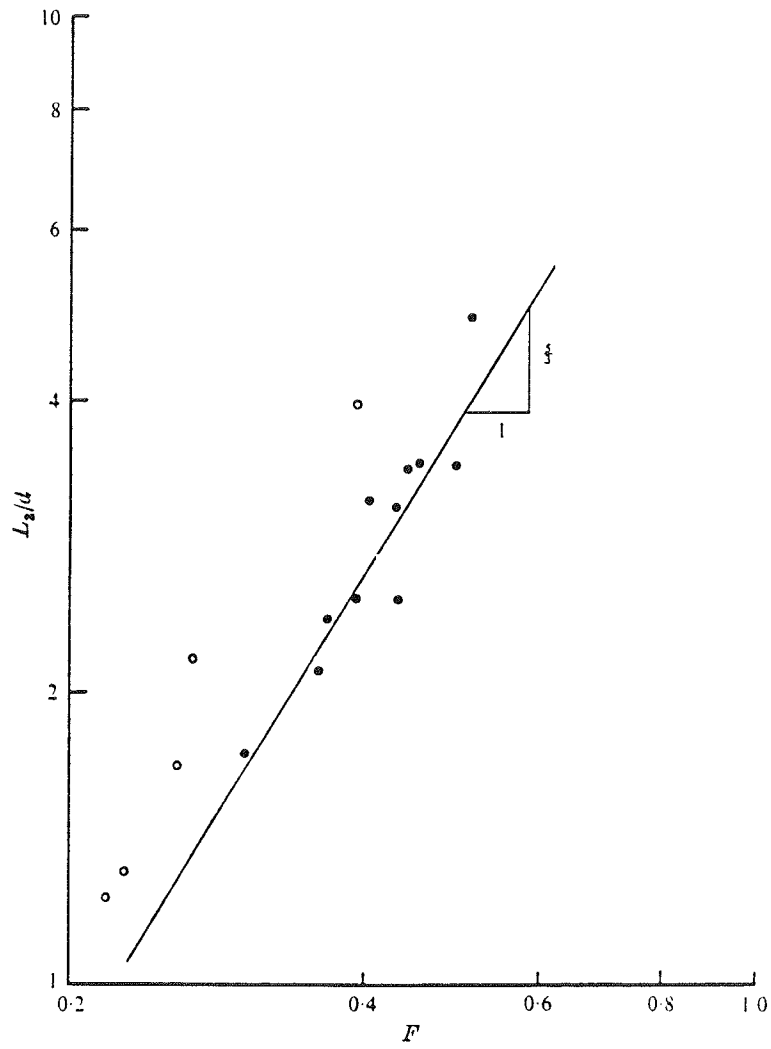


FIGURE 7. Relation between  $F$  and normalized wavelength for Jain's (1971) and Nordin's (1971) data. ●, Jain's data; ○, Nordin's data.

Figure D.4.5.

## Notation

Some of the notation is defined in Fig. D.4.1.

B	=	function defined by (1)
$c(k)$	=	celerity of bed-wave component with wave number k
F	=	Froude number = $U/\sqrt{gd}$
g	=	gravity constant
i	=	$\sqrt{-1}$
J	=	function defined by (3)
$J_1$	=	function defined in (6)
$J'_1$	=	$-J(k',-d)$
k	=	wave number = $2\pi/L$
L	=	wavelength
m,n	=	coefficient, exponent in sediment transport relation, (5)
$M_0, M_2$	=	zeroth, second moment of spectral density function
$n_1$	=	$nU/(U-U_c)$
t	=	time
T	=	local volumetric sediment discharge per unit width
$\bar{T}$	=	average volumetric sediment discharge per unit width
$u_c$	=	critical velocity for initiation of motion
$\alpha$	=	coefficient of bed-slope term in (5)
$\beta$	=	sediment-transport lag distance
$\Gamma$	=	normalized spectral growth rate; (10)
$\phi$	=	velocity potential
$\Phi$	=	spectral density function

### III. CURRENT STATUS AND PROSPECTS

A. Introduction. Section B of this chapter will précis what presently is known about the formation, behavior and characteristics of alluvial bed forms, and the principal deficiencies in our knowledge about them. Section C is given over to a (somewhat philosophical) discussion of the stumbling blocks that arise in formulating theories of bed-form behavior. The focus of this chapter is very long riverine dunes (so-called megadunes).

B. What Is Known. The following features of riverine bed forms and their behavior may be considered as fairly well to firmly established:

1. Bed forms are the result of an instability that is inherent, under most flow and sediment conditions, in the interaction between the primary shear flow and the bed, or between velocities induced by standing (stationary) surface waves and the bed (Exner 1925; Anderson 1953; Kennedy 1963, 1964, 1969; Reynolds 1965, Hayashi 1970; Engelund 1970; Fredsoe 1974, Richards 1980, and others). The underlying mechanisms of the instability are illustrated in Fig. B.4.1. Note that a free surface is not required for the formation of bed forms (except antidunes). The principal processes involved in this instability are as follow:
  - a. Something gives rise to a disturbance (small bump) on an otherwise initially flat sediment bed; or, in the case of free-surface flows, produces a standing water-surface wave.
  - b. The bed disturbance perturbs the flow field near the bed, and thereby perturbs the local sediment transport rate.

- c. If the distribution of local sediment-transport rate is perturbed so as to produce a pattern of scour and deposition that increases the amplitude of the bed disturbance, ripples, dunes, or antidunes result, depending on the flow and sediment characteristics.
  - d. If the distribution of local sediment-transport rate is perturbed so as to produce a pattern of scour and deposition that diminishes the amplitude of the initial bed disturbance, a flat bed results.
  - e. The bed forms migrate downstream (ripples and dunes) if scour occurs on their upstream (stoss) slopes and deposition on their downstream (lee) slopes. Upstream migration (antidunes) results in the opposite case.
2. Over a fairly wide range of flow and sediment conditions, intermediate to those that produce ripples/dunes and antidunes, the flow-bed interface is stable, and remains flat. Any induced bed disturbance diminishes in amplitude and disappears.
  3. The bed configuration has a dramatic effect on riverine friction factors. The Darcy-Weisbach friction factor often changes by a factor of ten or greater between flat-bed and ripple/dune conditions (Vanoni 1975, pp. 114-118).
  4. There are no generally accepted definitions or criteria for distinguishing between ripples and dunes. Their behaviors are quite similar. Dunes are longer and higher than ripples, typically by a factor of five and greater.

Ripples often occur in the stoss slopes of dunes. There does not appear to be a continuous spectrum of wavelengths between ripples and dunes; on plots involving bed-form wavelength, dunes appear as an isolated group of points (e.g., the points in the lower-left of Fig. B.4.3).

5. There is no readily discernable difference between the spectral density functions of ripples and dunes, except perhaps for their equilibrium - range slopes (see item 13, below).
  
6. A phase shift between the local bed-wave displacement and the local sediment discharge is essential to the initiation and growth of bed forms (see references cited in item 1. above). The factors that have been identified as contributing to this shift, and their relative importances, are (Kennedy 1978) (note: 1 = very important → 4 = not important):
  - a. Phase shift between bed shear stress and bed waves (i.e., bed displacement and/or slope), due to effects of nonuniform streamwise pressure gradient on the velocity distribution. (1 for ripples, 2 for dunes, 3 for antidunes).
  
  - b. Phase shift between bed waves and suspended-load transport rate, caused by time required for sediment to be entrained into an accelerating flow and to settle out of a decelerating flow. (1 for antidunes, 2 for dunes, 3 for ripples).

- c. Gravitational force, which impedes particle motion up stoss slopes and aids it down lee slopes. (1 for ripples, 2 for dunes, 3 for antidunes).
  - d. Flow separation from downstream slopes. (1 for fully developed ripples and dunes, 4 for antidunes).
  - e. Particle inertia. (3 for antidunes; 4 for others).
  - f. Phase shift between local flow shear and local turbulence characteristics; i.e., the "history" effect on turbulence. (2 for antidunes, 3 for dunes, 4 for ripples).
  - g. Phase shift between bed and water-surface waves, and hence also between bed waves and local mean depth and velocity. (2 for antidunes, 3 for dunes, unimportant for ripples).
7. Practically all of the successful analytical models developed to date for bed forms are based on small-perturbation theory. This involves:
- a. Deformation (mathematically) of the sediment bed into a small-amplitude, slowly moving wave (usually a sinusoid).
  - b. Calculation of the flow field over the deformed bed.

- c. Calculation of the local sediment discharge, along the deformed bed, produced by the perturbed flow field.
  - d. Application of the sediment-continuity equation (Exner relation) to calculate the subsequent deformation of the bed.
  - e. Interpretation of the calculated bed profile to explain the occurrence and behavior of different types of bed forms.
8. The analyses outlined in item 3, above, are limited to small-amplitude bed forms, and cannot explain several important features of fully developed bed forms. In particular, they cannot predict the behavior and properties of mature, fully developed bed forms which are dominated by nonlinear effects.
9. Three principal items are forthcoming from most of these small-perturbation analyses:
- a. The dominant wavelength, calculated as the wavelength with the fastest amplitude growth rate.
  - b. Bed-wave celerity as a function of wavelength, the flow characteristics, and the sediment and sediment-transport properties of the flow.
  - c. Conditions for occurrence of the different types of bed forms (see, e.g., Fig. B.4.2). These predictions invariably involve parameters

involved with the bed-elevation--transport-rate phase shift, and are difficult to apply to predict occurrence of different types of bed forms.

10. Most small-perturbation theories predict ranges of flow and transport relations under which the bed-wave amplitude diminishes with time. This is interpreted as a flat bed.
11. Riverine bed waves produced over a fairly wide range of wavelengths, and the resulting bed forms are the superposition of waves of many lengths (Jain 1971, Jain and Kennedy 1974, Nakagawa and Tsujimoto 1984). Free-surface flows are observed to produce two spectral peaks in the bed waves that first develop on the initially flattened bed; one of these is at the wavelength of the Airy wave, and corresponds to the bed forms produced by standing water-surface waves. Its wavelength is given by the Airy relation,

$$U^2 = g/k \tanh kd \quad (\text{III.1})$$

The second spectral-peak is produced by the interaction between the primary shear flow and the bed. The two sets of bed-waves interact, by the shorter, faster-moving ones overtaking and merging with the slower, longer ones. This "variance-cascade" process was described by Jain and Kennedy (1974) (see Section II.D.4 for quotation of their explanation).

12. The spectral peak corresponding to the Airy celerity is not present in bed forms produced by closed-conduit flows, and evolving bed forms in closed-

conduit flows do not exhibit the progressive lengthening described by Raichlen and Kennedy (1965) and analyzed by Jain and Kennedy (1974). This has been demonstrated by the experiments of Nakagawa and Tsujimoto (1984).

13. Fully developed dune spectra exhibit an "equilibrium range" in which the spectral density function,  $\Phi$ , varies as

$$\Phi \sim k^{-3} \quad (\text{III.2})$$

where  $k = 2\pi/L$ ; and  $L =$  wavelength (Hino 1968, Jain and Kennedy 1974).

For ripple spectra, Hino (1968) suggests

$$\Phi \sim k^{-2} \quad (\text{III.3})$$

The first of these relations has been well corroborated experimentally.

14. Some data compilations indicate that very long bed forms--megadunes--are a distinctive class of bed waves. This is suggested by, for example, the grouping of the cluster of points for megadunes in the lower-left corner of Fig. B.4.3. However, spectral density functions for these bed forms do not indicate that they are statistically different from other bed forms.
15. Megadunes have maximum wavelengths of about six- to eight-times the flow depth (Jackson, 1976). This is consistent with the wavelength of the lower end of the equilibrium-spectrum ( $\Phi \sim k^{-3}$ ) range (see Section II.D.2,

Eqs. 7 and 8), as has been shown by Hino (1968). This corresponds to a vertical line in Fig. B.4.3, which is seen to be a crude estimate of dune wavelength.

16. A better approximation to the wavelengths of dunes can be obtained from the spectral analyses of Nordin (1971; cited in Sec. II.D.1) and Jain and Kennedy (1974; see Sec. II.D.4) indicating that better estimates of the wavelength are

$$F^2 = \frac{0.19}{kd} \quad (\text{III.4})$$

((18) in Sec. II.D.1); and

$$F^{5/3} = \frac{0.51}{2\pi} \frac{L_2}{d} \quad (\text{III.5})$$

((19) in Sec. II.D.4), respectively.

17. Raudkivi's (1963) detailed subcritical-flow measurements of flow over a mobile-sand and a rigid, two-dimensional model of a ripple (actually, likely a dune), 15-inches long and 1.1-inches high, revealed several interesting aspects of this flow, as follow (refer to Fig. III.B.1):
- a. Entrainment and bed-load transport take place on the stoss slopes of ripples and dunes at values of the temporal mean bed stress well below Shields' critical stress, which is reached more than half-way up the stoss slope of the bed form.

- b. The temporal mean shear stress is a maximum on the crest of the bed form, and there is very nearly equal to the mean shear stress for the same flow over same sand bed in its initial flat condition. This flat-bed value of shear stress appears to govern the amount of sediment transport.
  - c. The streamlines of the main flow are approximately sinusoidal, rising over the wakes and falling over the crests of ripples.
  - d. The flow over the wake in the lee of a ripple reattaches to the bed about five to eight (average of about six) ripple-heights downstream of the ripple crest. At the reattachment point, the bed shear stress is practically zero. These observations are consistent with those made in boundary layers downstream from impervious "fences" perpendicular to walls; and downstream from negative steps on conduit boundaries.
  - e. In the region where boundary shear stress is less than the critical value, the sediment entrainment and transport are due primarily to the agitation (intense turbulence) in the wakes of the bed forms.
18. There is presently no completely reliable predictor for the conditions of occurrence of the different bed configurations (ripples, dunes/megadunes, flat bed, antidunes). The principal stumbling block is an inadequate understanding and formulation of the transport-rate phase shift (see Fig.

B.4.2). Vanoni's (1974) bed-form charts (Fig. III.B.2 and Table III.1) remain the best practical tool for bed-configuration prediction.

19. The Nobel Prize for a riverine-bed-form theory is still waiting to be won.

Figures

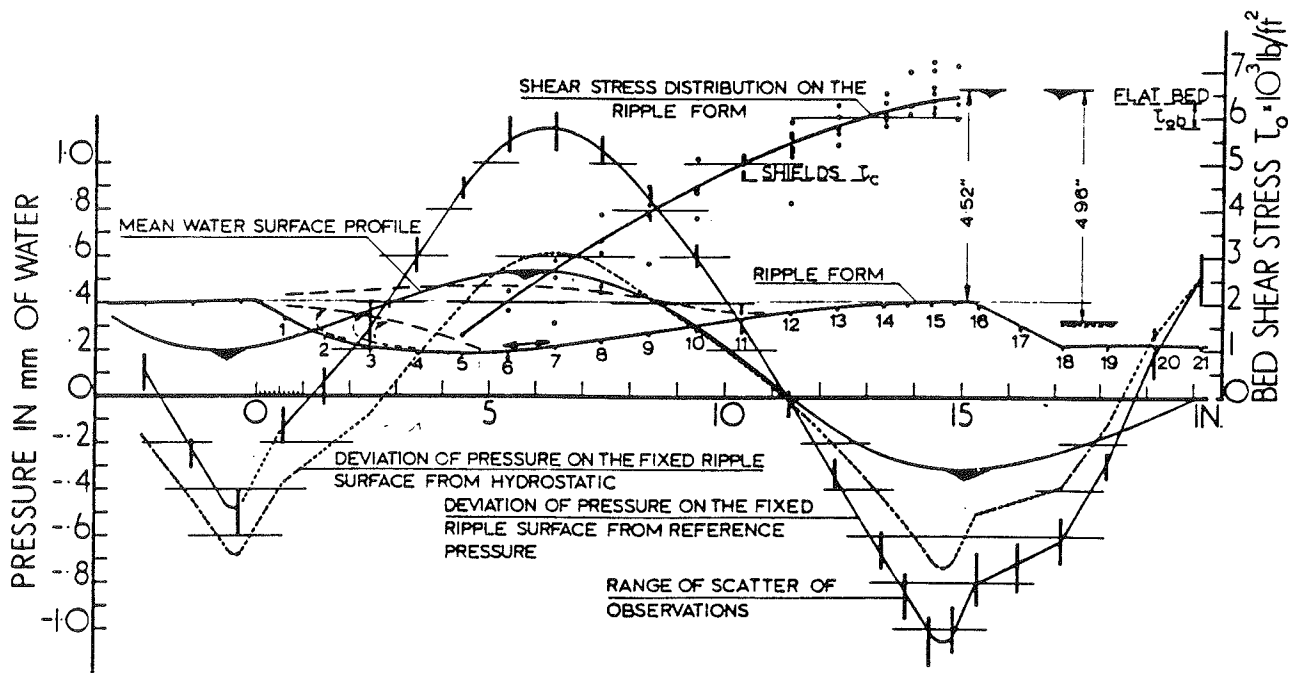


FIG. 4.—RIPPLE FORMATION, WATER SURFACE PROFILE, AND DISTRIBUTION OF PRESSURE DEVIATIONS AND BED SHEAR STRESS

III.B.1.

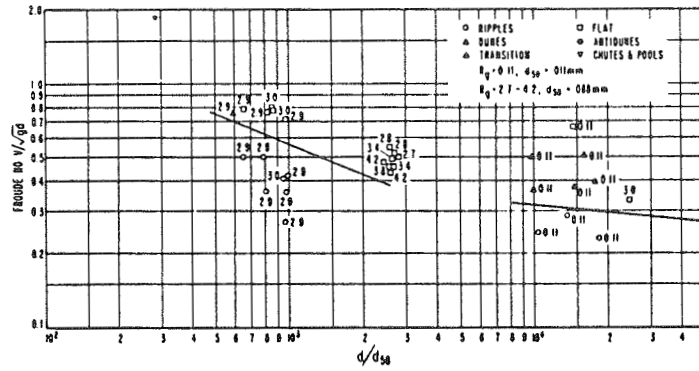


FIG. 1.—Bed-Form Chart for  $R_g = 0.11$  and  $2.7-4.2$  ( $d_{50} = 0.011$  mm and  $0.088$  mm)

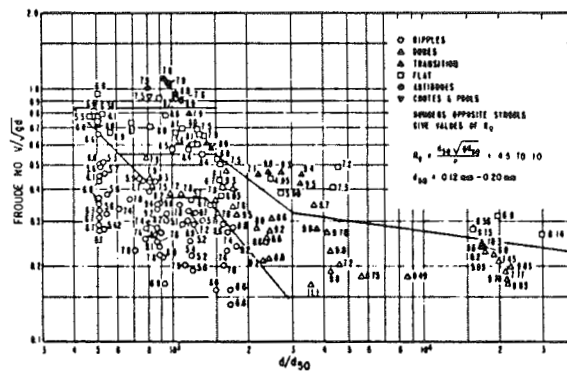


FIG. 2.—Bed-Form Chart for  $R_g = 4.5-10$  ( $d_{50} = 0.12$  mm– $0.200$  mm)

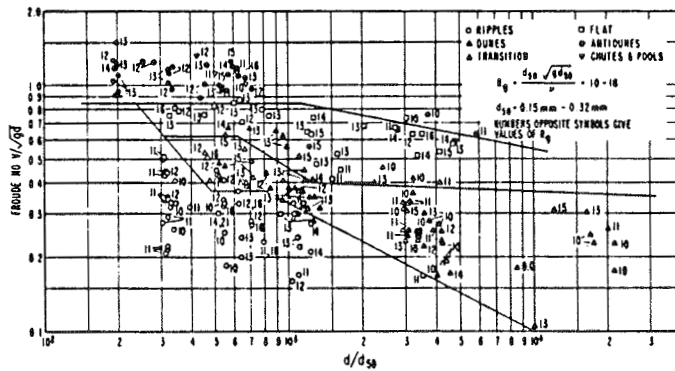


FIG. 3.—Bed-Form Chart for  $R_g = 10-16$  ( $d_{50} = 0.15$  mm– $0.32$  mm)

### III.B.2

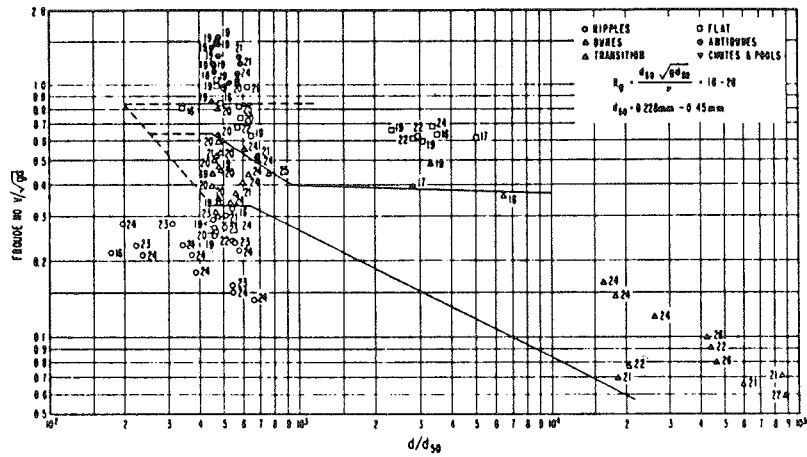


FIG. 4.—Bed-Form Chart for  $R_s = 16-26$  ( $d_{50} = 0.228 \text{ mm}-0.45 \text{ mm}$ )

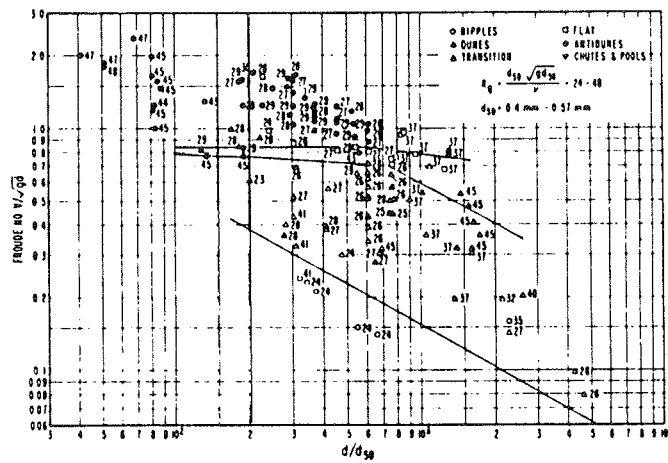


FIG. 5.—Bed-Form Chart for  $R_s = 24-48$  ( $d_{50} = 0.4 \text{ mm}-0.57 \text{ mm}$ )

Figure III.B.2. (continued)

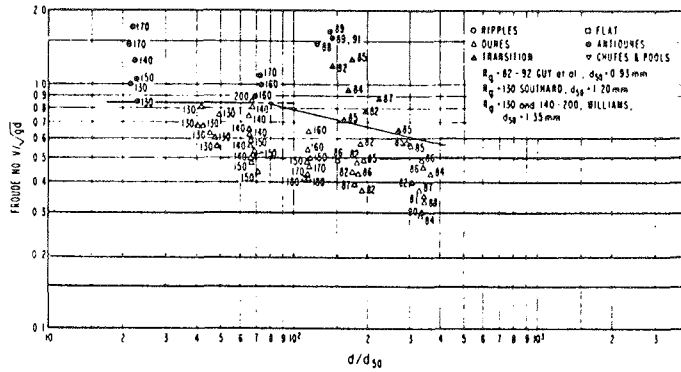


FIG. 6.—Bed-Form Chart for  $R_g = 82-92, 130, \text{ and } 140 \text{ to } 200$  ( $d_{50} = 0.93 \text{ mm}, 1.20 \text{ mm}, \text{ and } 1.35 \text{ mm}$ )

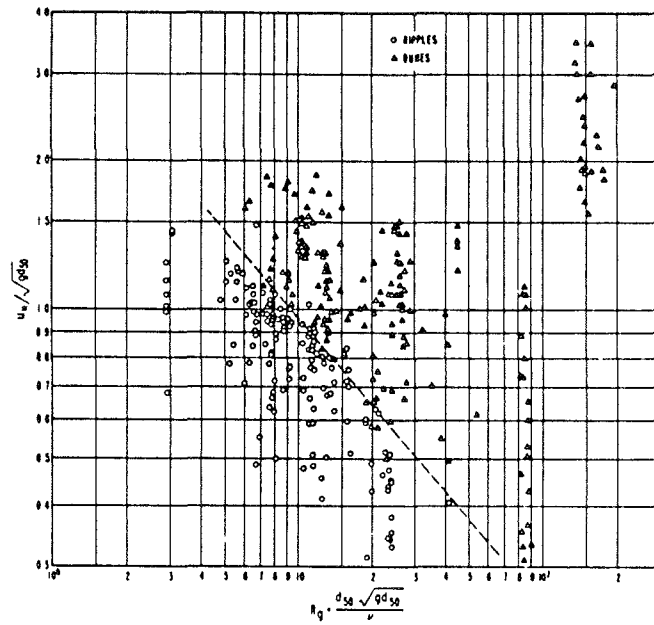


FIG. 7.—Plot of  $R_g$  against  $u_* / \sqrt{g d_{50}}$  for Flows with Ripple and Dune Beds

Figure III.B.2. (continued)

Table

**TABLE 1.—Ranges of  $R_g$  and  $d_{50}$  for Data Plotted on each of Bed-Form Charts Figs. 2-7**

Figure number (1)	Ranges of $R_g$ $= (d_{50} \sqrt{gd_{50}})/v$ (2)	Ranges of median sediment size, $d_{50}$ , in millimeters (3)
1	0.11 and 2.7-4.2	0.011 and 0.088-0.15
2	4.5-10	0.12-0.20
3	10-16	0.15-0.32
4	16-26	0.23-0.45
5	24-50	0.4-0.6
6	82-92 and 126-197	0.93, 1.20, 1.35

Table III.1.

C. Why is the "Dune Problem" so Intractable? The foregoing outline of "what is known", and the selected-literature survey of the preceding chapter, suggest, accurately, that the mechanisms responsible for the initiation and small-amplitude behavior (the linearized problem) of riverine bed forms are quite well understood and fairly well formulated. The principal remaining stumbling blocks involve the usual problems attendant to the analysis of strongly nonuniform turbulent shear flows, and further elucidation and formulation of the phase shift between local bed displacement and local sediment-transport rate. The perceptive reader will have noted, however, that relatively little has been reported herein concerning analytical description of the properties and behavior of fully developed bed forms. That is because there is not much to report, either analytical or experimental, on this problem. The notable exceptions are:

1. Fredsoe's (1982) analysis of the shape of fully developed ripples and dunes) (see Section II.B.10).
2. Haque and Mahmood's (1985) series of publications reporting analytical treatment and finite-element simulation of flow past mature ripples and dunes (see Section II.B.11).
3. Several dimensional-analysis treatments of the geometry of mature bed forms and Vanoni's (1974) bed-form charts.
4. Some success in determining "universal" nondimensional spectral density functions of ripples and dunes (see Chapter II, Section D).
5. Kennedy's (1963) finding that antidune height is limited by the stability of the accompanying surface waves (see Section II.B.3).

6. The relationship between the geometry and kinematics of ripples and dunes, and sediment discharge, as analyzed by Simons, Richardson and Nordin (1965), Kennedy (1969), and Willis and Kennedy (1978).

In an attempt to answer the question posed in the heading of this section, let us consider what a complete analysis of finite-amplitude ripples and dunes must include, and the stumbling blocks encountered in its development. We will consider periodic, fully developed ripples or dunes moving with celerity  $c$  without changing their form, as shown in Fig. III.C.1. These waves are described by

$$\eta(x,t) = h f(x - ct) \quad (\text{III.C.1})$$

where, in addition to the nomenclature defined in Fig. III.C.1,  $f$  = function of  $(x-ct)$  defined by the bed profile and Eq. III.C.1, and  $t$  = time. The equation of sediment continuity is

$$\frac{\partial \eta}{\partial t} + \frac{\partial q_s}{\partial t} = 0 \quad (\text{III.C.2})$$

where  $q_s$  = volumetric sediment discharge (which includes the porosity). Substitution of Eq. III.C.1 into Eq. III.C.2, and integrating the resulting equation over  $x$  yields

$$q_s(x,t) = c\eta(x,t) + C(t) \quad (\text{III.C.3})$$

where  $C$  = constant or function of time, and represents sediment discharge that does not participate in the bed-form-migration process.

In Eq. III.C.3,  $\eta$  is seen to vary linearly with  $q_s$ . Thus for equilibrium bed forms,  $\eta$  must evolve such that it produces a flow field, and associated turbulence and shear field, that at every point along the bed produces a  $q_s$  that satisfies Eq. III.C.3. This relation must be satisfied in the strongly separated flow in the wakes of the bed forms; in the reattachment zone, where the separation streamline from a bed-form crest approaches the stoss slope of the adjacent downstream bed form; and in the nonuniform internal boundary layer along the stoss slope downstream of the reattachment point. In short,  $q_s$  must be proportional to  $\eta$  throughout the complex flow above ripples and dunes. The transport relation must also take into account the effects of bed-form slope on transport rate, including the gravity flow of sediment down the lee slopes. It must also consider the strong interchange between bed-load and suspended-load discharges that occurs along the bed profile, including the wake zone. The spectral properties of the bed profile would have to be included, especially the "production of bed profile" at the larger wave numbers, and the "decay of bed profile" at smaller wave numbers. Calculation of  $\eta(x,t)$  and the corresponding flow and stress fields and resulting  $q_s(x)$  that satisfy these relations, as calculation of equilibrium bed forms would require, is indeed a tall order. To appreciate the difficulty of the problem, it should be recalled that the problem of calculating the total sediment discharge of streams, even over flat beds, cannot be considered as satisfactorily solved.

#### IV. A NEW THEORY FOR DUNE HEIGHTS.

This model is concerned primarily with megadunes, of the type described by Carry and Keller (1957), among others. It is these bed forms that pose the greatest problem to navigation, water-diversion structures, etc.

The model is based on the following concepts and assumptions:

1. The grain-roughness shear stress,  $\tau'$ , varies linearly along the stoss face of each dune (see Fig. III.C.1), from zero a distance  $\alpha h$  downstream from the dune crest to the flat-bed value (based on the mean depth  $d$ )  $\tau'_0$ , at the dune crest. This assumption is well supported by the detailed measurements of Raudkivi (1963) of velocity and stress distributions in flows over dunes. Based on his experiments, and the work of others cited by him,  $\alpha \approx 5$ . The negative  $\tau'$  upstream from this point to the dune crest will be neglected. Thus, the average energy slope due to the grain roughness,  $S'$ , is expressed by

$$\rho g d S' = \frac{1}{2} \lambda \tau'_0 \frac{L - \alpha h}{L}$$

or

$$S' = 1.2 \frac{1}{16} \lambda f_0 F^2 \left(1 - \alpha \frac{h}{L}\right) \quad (\text{IV.1})$$

where, in addition to the terms defined in Fig. III.C.1,  $\lambda$  = coefficient ( $\approx 1$ );  $f_0$  = rigid-flat-bed Darcy-Weisbach friction factor; and  $F$  = Froude number. The factor 1.2 is introduced to take into account Karim and Kennedy's

(1989) finding that the friction factors of flows over mobile flat beds are about 20 percent greater than those of flows over rigid beds with equal roughness size.

2. The energy slope produced by form drag on the dunes will be estimated from Carnot's formula for the head loss across an abrupt expansion in a conduit, as was done by Engelund (1966). The average energy slope,  $S''$ , produced by this expansion loss is (refer to Fig. IV.1)

$$\begin{aligned}
 S'' &= C_D \frac{1}{L} \frac{q^2}{2g} \left[ \frac{1}{(d-\frac{h}{2})} - \frac{1}{(d+\frac{h}{2}) - S_d \beta h} \right]^2 \\
 &= \frac{C_D}{2} F^2 \frac{h^2}{Ld} \left[ \frac{1-S_d\beta}{1 - \frac{h^2}{d^2} \left( \frac{1}{4} - \frac{S_d\beta}{2} \right) - S_d\beta \frac{h}{d}} \right]^2 \\
 &\approx \frac{C_D}{2} F^2 \frac{h^2}{Ld} \tag{IV.2}
 \end{aligned}$$

where  $C_D$  = loss coefficient ( $\approx 1$ );  $S_d$  = average slope of stoss face of dune ( $\approx \frac{h}{L}$ ); and  $\beta h$  = distance from dune-profile nadir to point of free-streamline bed reattachment, as shown in Fig. IV.1. Note that  $S_d\beta \ll 1$ , as are products involving  $S_d\beta$ .

3. The total energy slope is then

$$S = \frac{fF^2}{8} = S' + S'' = 1.2 \frac{1}{16} \lambda f_o F^2 (1 - \alpha \frac{h}{L}) + \frac{1}{2} C_D F^2 \frac{h^2}{Ld} \tag{IV.3}$$

where  $f$  = Darcy-Weisbach friction factor and  $F$  = Froude number. (IV.3)  
yields

$$\frac{f}{f_0} = \frac{1.2}{2} \lambda \left( 1 - \alpha \frac{h}{L} \right) + \frac{4C_D}{f_0} \left( \frac{h}{d} \right)^2 \frac{d}{L} \quad (\text{IV.4})$$

4. The ratio  $\frac{d}{L}$  will be estimated from the results of the spectral analyses of Nordin (1971) and Jain and Kennedy (1974) (see item 16 of Sec. III.B). Specifically,

$$F^2 = \frac{C_1}{dk} = \frac{C_1 L}{2\pi d} \quad (\text{IV.5})$$

will be adopted. It is expected that  $C_1 \approx 0.25$  for megadunes. (VI.5) is a reasonable approximation to the "megadune" points in the lower left of Fig. B.3.2.

5. Karim and Kennedy's (1989; their Eq. 17) regression relation will be utilized for the friction-factor ratio  $f/f_0$ :

$$\frac{U}{\sqrt{g(s-1)D_{50}}} = 6.683 \left( \frac{d}{D_{50}} \right)^{.626} (S)^{.503} \left( \frac{f}{f_0} \right)^{-.465} \quad (\text{IV.6})$$

where  $s$  = specific gravity of bed material; and  $D_{50}$  = median bed-particle size.

6. The rigid-flat-bed friction factor,  $f_0$ , is taken from Karim and Kennedy (1989) to be

$$f_0 = \frac{8}{\left\{6.25 + 2.5 \lambda \ln \frac{d}{2.5 D_{50}}\right\}^2} \quad (\text{IV.7})$$

7. (IV.4) and (IV.5) yield

$$\frac{h}{d} = \frac{1}{2} \left\{ \frac{1.2 \lambda \alpha f_0}{8 C_D} + \left[ \left( \frac{1.2 \lambda \alpha f_0}{8 C_D} \right)^2 + \frac{2 \pi F^2 f_0}{C_D C_1} \left( \frac{f}{f_0} - \frac{1.2 \lambda}{2} \right) \right]^{1/2} \right\} \quad (\text{IV.8})$$

where  $f_0$  is given by (IV.7);  $C_1 \simeq 0.25$ ;  $\lambda \simeq 1$ ;  $C_D \simeq 1$ ; and  $\frac{f}{f_0}$  is given by (IV.6).

8. (IV.8) can be simplified (by neglecting the terms in  $\frac{1.2 \lambda \alpha f_0}{8 C_D}$  and  $\frac{1.2}{2} \lambda$ , which are small for all but flows over nearly flat beds) to

$$\frac{h}{d} = \frac{F}{2} \sqrt{\frac{2 \pi f}{C_D C_1}} \quad (\text{IV.9})$$

Several comments concerning the prospective usefulness of (IV.9) and (IV.10) are in order:

1. They valid only for flows that produce ripples and/or dunes. Karim and Kennedy (1989) suggest that this flow regime occurs over the range

$$0.06 < \frac{\tau_0}{\rho g (s-1) D_{50}} < 1.3 \quad (\text{IV.10})$$

where 0.06 corresponds to the Shields dimensionless shear stress for incipient motion. The limits given in (IV.10) are tentative and approximate.

Additionally, dunes can be expected only if the Froude number is less than about 0.6 to 0.7. Vanoni's (1974) bed-form charts (see item 18 of Sec. III.B, and Fig. III.B.2) also should be consulted to determine if dunes can be expected.

2. Because ripples and dunes are composed of spectra of wavelengths and amplitudes, any prediction for these quantities, or their ratio, should be regarded as yielding representative values.
3. (IV.9) can be expected to be valid only for fairly large values of  $\frac{h}{d}$ .



## V. VERIFICATION

The relative dune-height,  $\frac{h}{d}$ , predictions of six of the empirically based relations were compared with data reported by Guy et al. (1966). Only their runs conducted in the eight-foot-wide flume which had dunes as the reported bed configuration were used in this comparison. Regretably, no field data collection suitable for verification were found.

The ranges of variables covered by these experiments utilized in the comparison are:

- d = flow depth (ft): 0.30 - 1.33
- D<sub>50</sub> = grain size (mm): 0.19 - 0.93
- F = Froude number: 0.25 - 0.65
- S = Slope:  $0.37 \times 10^{-3}$  -  $4.37 \times 10^{-3}$
- V = velocity (ft/s): 1.30 - 3.32

The following relations were used in the verifications:

(1) Yalin (1964)

$$\frac{h}{d} = \frac{1}{6} \left( 1 - \frac{\tau_c}{\tau} \right)$$

$$\frac{\tau_c}{\tau} = \frac{\theta_c(\rho_s - \rho)gD}{\rho g S d} = \frac{\Delta D \theta_c}{S d} \quad (\theta_c = 0.06)$$

(2) Gill (1971)

$$\frac{h}{d} = \frac{1 - F^2}{2n\alpha} \left( 1 - \frac{\tau_c}{\tau} \right) \quad (\text{assume } f \text{ is independent of } U)$$

$$\alpha = 0.5 \text{ (triangular dunes)}$$

$$n = 3/2 \text{ (corresponds to Meyer-Peter and Mueller equation).}$$

(3) Ranga Raju and Soni (1976)

$$\frac{h}{d} = 6.5 \times 10^3 \frac{D/d}{F_1^3 F_2} (\tau_*')^{8/3}$$

$$F_1 = \frac{U}{\sqrt{gR_b}} \quad F_2 = \frac{U}{\sqrt{\frac{\Delta\rho}{\rho} gD}}$$

$$n_s = \frac{D^{1/6}}{24} \text{ (m}^{1/6}\text{)}$$

$$(R_b')^{2/3} = \frac{n_s U}{S^{1/2}}; \quad U \text{ in m/s}; \quad \tau_*' = \frac{R_b' S}{\Delta D}$$

(4) Fredsoe (1982)

$$\frac{h}{d} = \frac{\Phi_b}{2\theta \left( \frac{d\Phi_b}{d\theta} + \frac{d\Phi_s}{d\theta} \right)}$$

Fig. B.104 portrays this relation after  $\theta$ ,  $\Phi_b$ ,  $\Phi_s$  are expressed as functions of  $\theta$ :

(5) Van Rijn (1984)

$$\frac{h}{d} = 0.11 \left( \frac{D}{d} \right)^{0.3} (1 - e^{-0.5T}) (25 - T)$$

$$T = \frac{u_*'^2 - u_{*c}^2}{u_{*c}^2} \quad u_*'^2 = \frac{gu^2}{C'^2}$$

$$C' = 18 \text{ Log} \left( \frac{12R_b}{3D_{90}} \right) \quad u_{*c}^2 = \theta_c \Delta g D$$

$$\theta_c = 0.06$$

The results of this verification are presented in Figs. V.1 to V.5. These figures suggest that none of the relations evaluated is fully satisfactory. The model developed herein appears to give the best results, and could be improved by calibration to adjust the constants it contains.

(6) Present paper (Chapter IV).

$$\frac{h}{d} = \frac{1}{2} \left\{ \frac{1.2\lambda\alpha f_0}{8C_D} + \left[ \left( \frac{1.2\lambda\alpha f_0}{8C_D} \right)^2 + \frac{2\pi F^2 f_0}{C_D C_1} \left( \frac{f}{f_0} - \frac{1.2\lambda}{2} \right) \right]^{1/2} \right\}$$

where

$$f_o = \frac{8}{\left\{6.25 + 2.5 \lambda \ln \frac{d}{2.5 D_{50}}\right\}^2}$$

$$\alpha \approx 5$$

$$\lambda \approx 1$$

$$C_1 \approx 0.25$$

$$C_D \approx 1$$

Figures

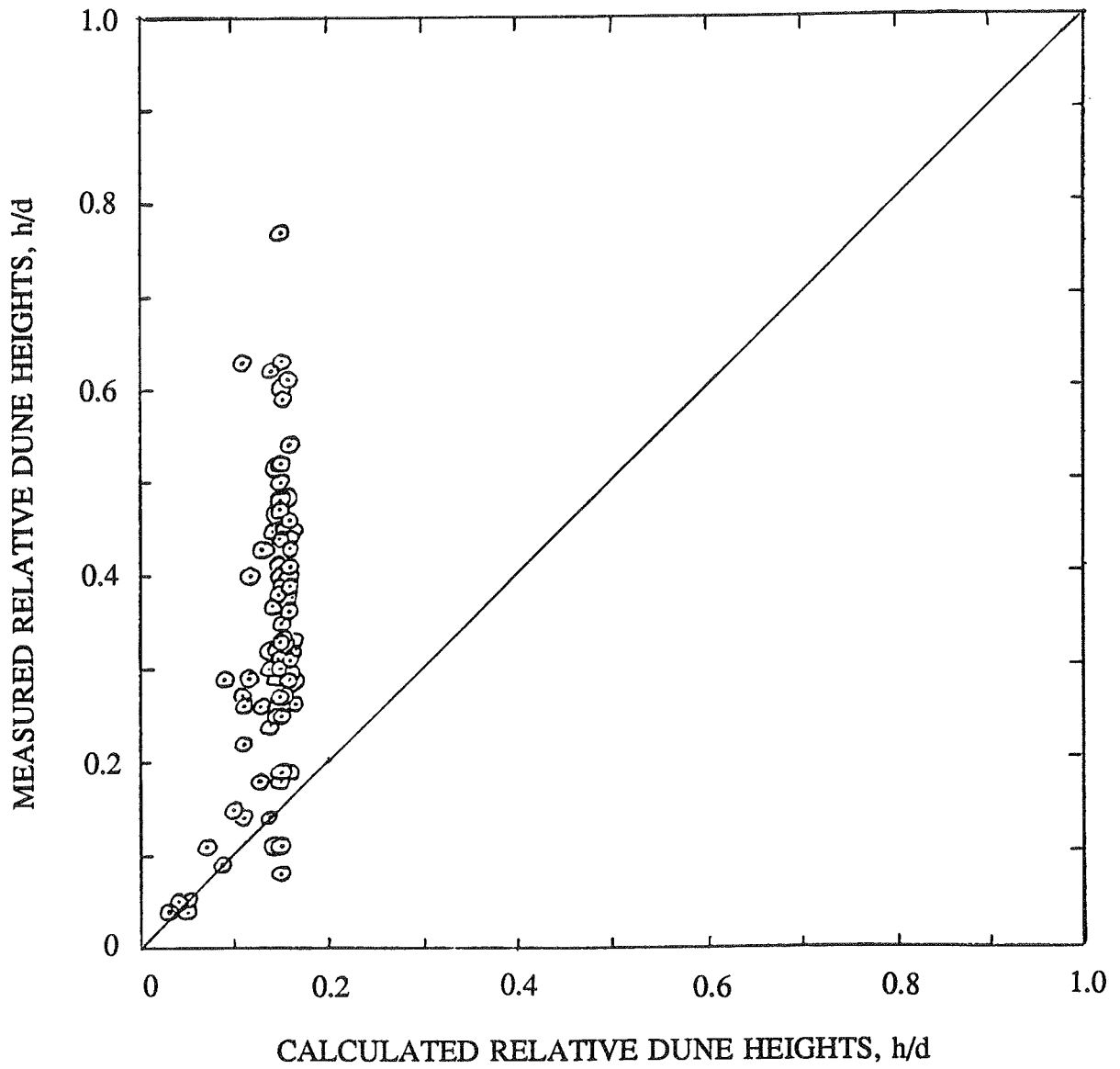


Figure V.1. Verification of the dune-height predictor of Yalin (1964).

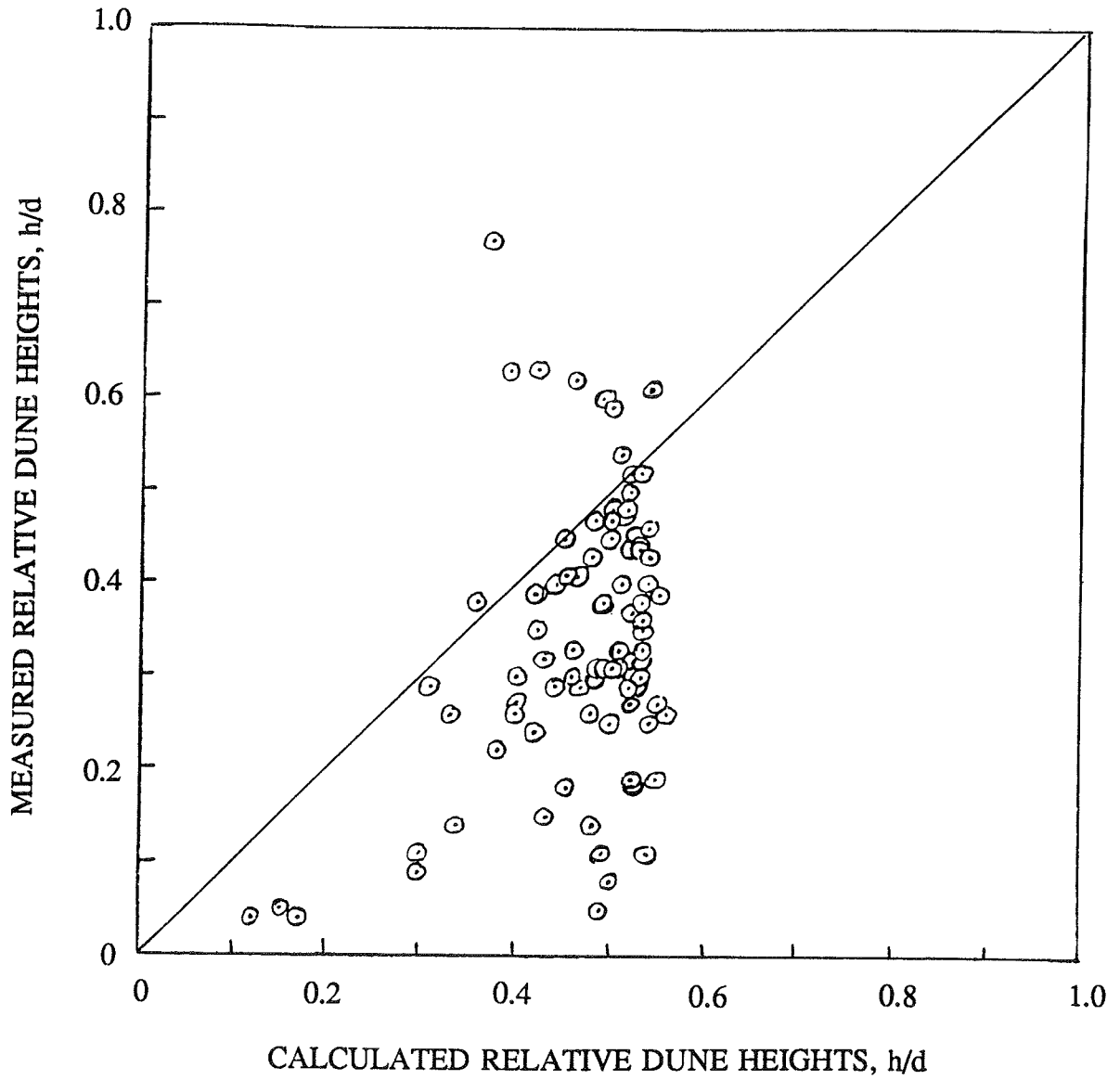


Figure V.2. Verification of the dune-height predictor of Gill (1971).

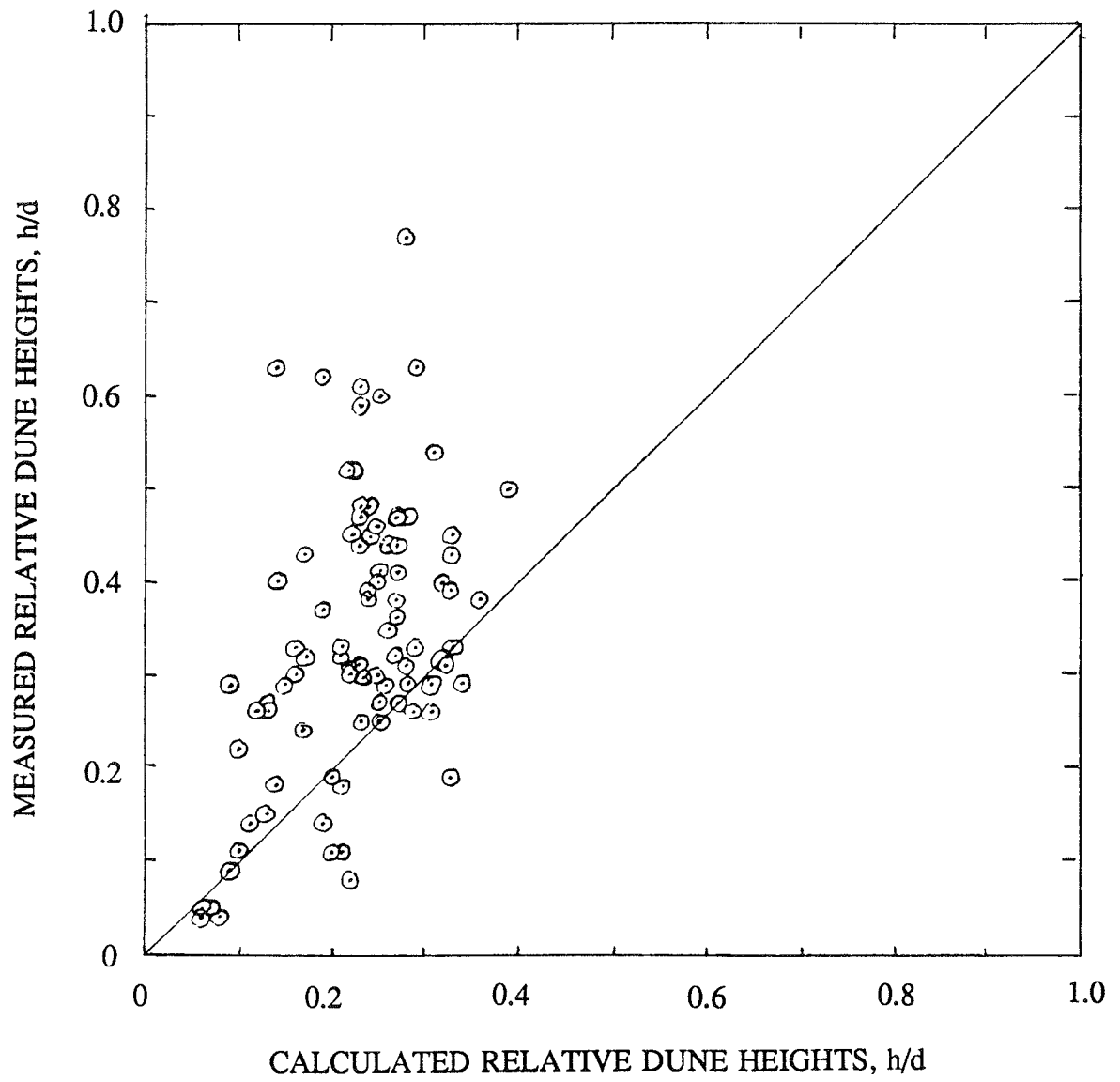


Figure V.3. Verification of the dune-height prediction of Ranga-Raju and Soni (1971).

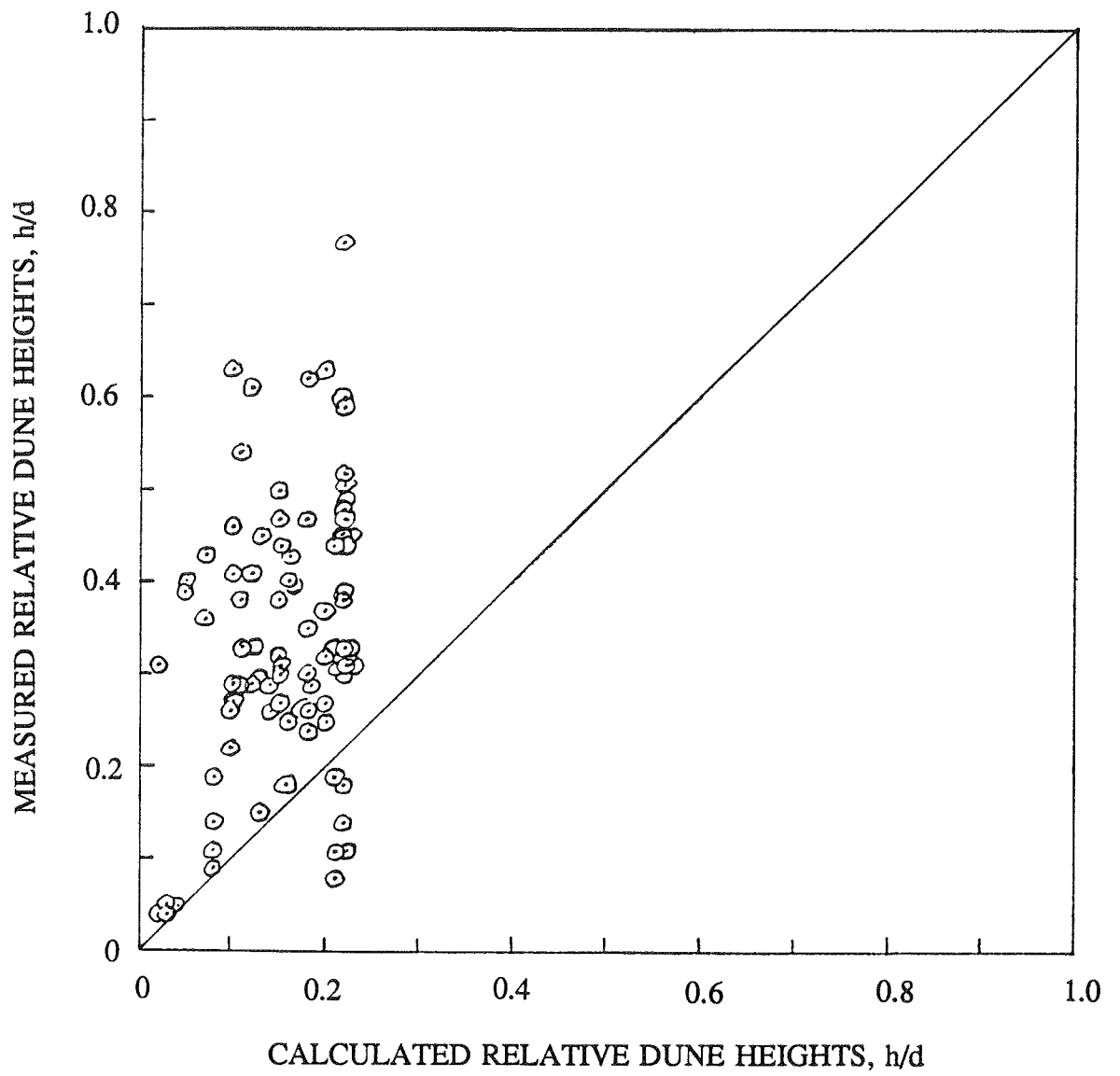


Figure V.4. Verification of the dune-height prediction of Fredsoe (1982).

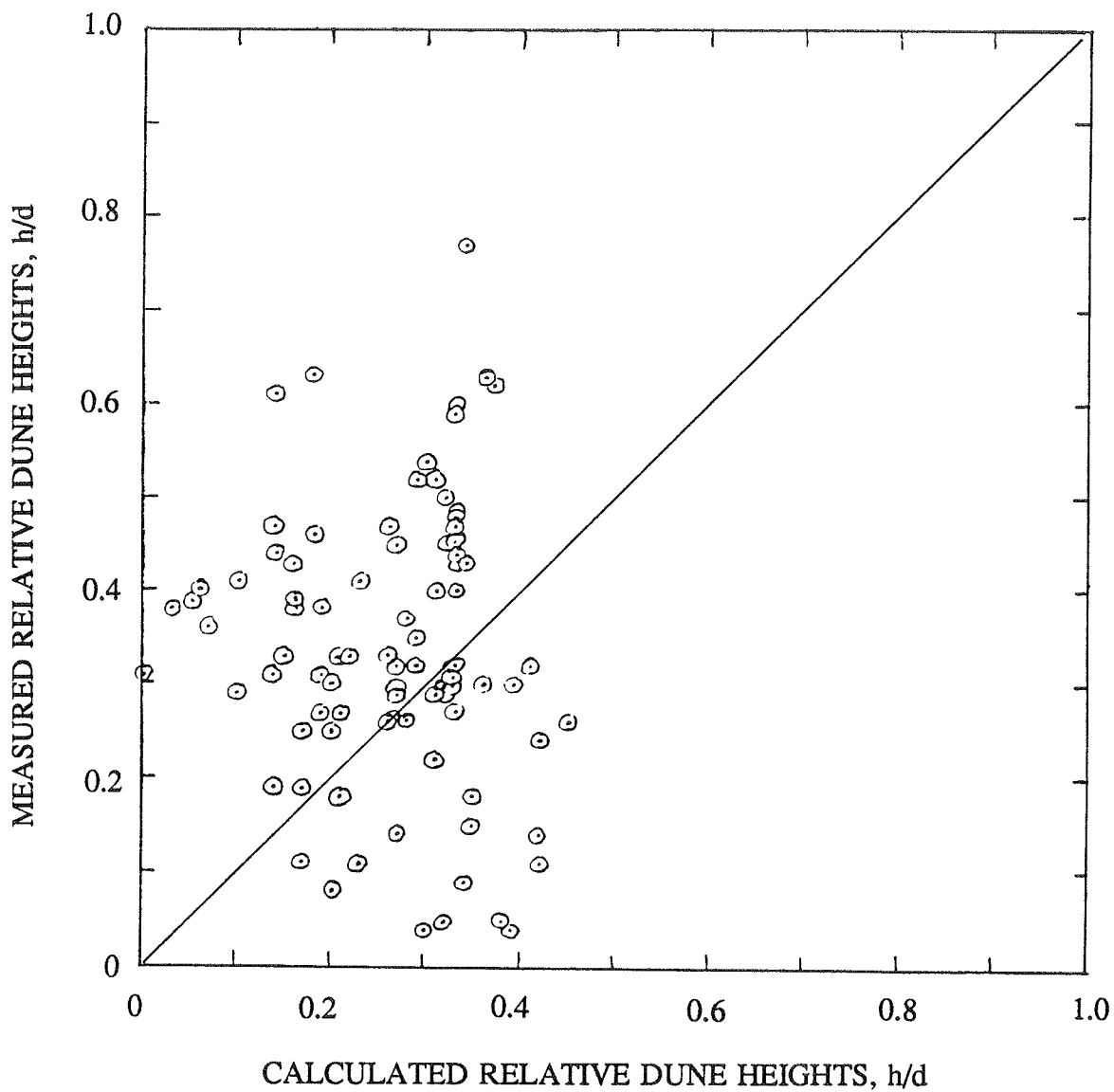


Figure V.5. Verification of the dune-height predictor of van Rijn (1984).

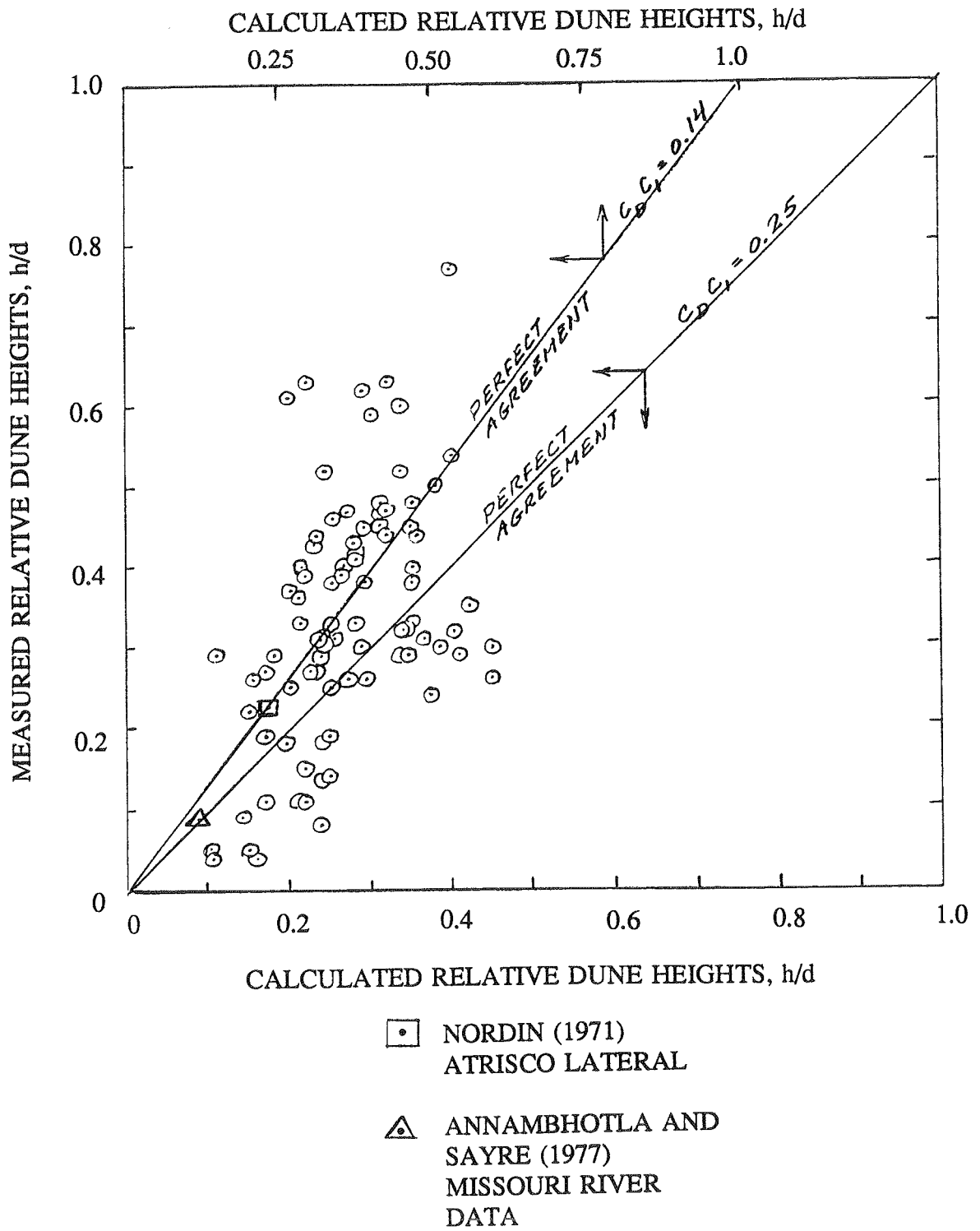


Figure V.6. Verification of the dune-height predictor developed herein (Chapter IV).

## VI. DUNE-CONTROL METHODS

In the extensive literature search carried out in the course of this study, no innovative means of dune control were found. Dredging to obtain short-term relief of local problems seems presently to be the common practice.

A technique whose potentials as a control measure have not been fully explored is the submerged vanes technique. Both laboratory and field tests (Odgaard and Kennedy 1983, Odgaard and Spoljaric 1986, Odgaard and Mosconi 1987, Wang 1989, Fukuoka 1989, Fukuoka and Watanabe 1989) suggest that this technique has a broad range of applications including dune control. The vanes are small flow-training structures (foils) designed to modify the near-bed flow pattern and redistribute flow and sediment transport within the channel cross section. The structures are installed at an angle of attack of 15-25° with the flow, and their initial height is 0.2-0.4 times local water depth at design stage. The vanes function by generating secondary circulation in the flow. The circulation alters magnitude and direction of the bed shear stress and causes a reduction in velocity and sediment transport in the vane controlled area. As a result, the bed configurations change. The river bed aggrades in the vane controlled area and degrades outside.

The technique was originally developed to stop or reduce bank erosion in river curves. In this application the vanes are laid out so that the vane generated secondary current eliminates the centrifugally induced secondary current, which is the root cause of bank undermining. The first field test with this application was in a bend of East Nishnabotna River, Iowa (Odgaard and Mosconi 1987). The results from this test are very satisfactory. Other successful field tests are reported by Fukuoka and Watanabe (1989) and Kunzig (1989).

Recent laboratory and field tests suggest that the vane technique is also effective in ameliorating shoaling problems in rivers (Odgaard and Wang 1990). Figures VI.1 and VI.2 show results of a laboratory experiment in which vanes were installed along the right side of a straight laboratory channel. The objective was to generate an increase in flow depth in the left portion of the channel. The vanes were 0.8 mm thick sheet metal plates, 7.4 cm high and 15.2 cm long, installed in arrays with four vanes in each array and angled 20° toward the bank. Average flow depth was about 17 cm and velocities were of the order of 0.4 m/s. It is evident that this vane system caused a considerable redistribution of sediment. The vanes reduced the depth near the right bank by about 50%. This caused the depth near the left bank to increase by 20-30%.

One of the most important observations made in these tests was that the vane induced changes in cross-sectional profile occurred without causing measurable changes of the area of the cross sections and of the longitudinal slope of the water surface. This observation is important because it implies that the vanes will not cause any changes of the stream's sediment transport capacity upstream or downstream from the vane field and therefore should not alter the overall characteristics of the stream.

Another important observation was that the bedforms in the deepened part of the channel did not appear to be larger than before vanes were installed. It appeared that the vanes lowered the bed level outside the vane field without causing the height of the bedforms there to be increased. This observation suggests that vanes may be an effective means of controlling not only the depth but also the size of the bedforms. However, more experimentation is needed to quantify the performance of the vanes in this regard.

It is recommended that the use of submerged vanes for control of bedforms be investigated further. A logical approach would be to use the theoretical basis obtained

herein (the relationships between bedform geometry and flow and sediment characteristics) for designing and conducting a series of experiments in a straight, movable-bed hydraulic model. The main objective would be to develop relationships between vane-system characteristics (design and layout), flow and sediment conditions, and dune dimensions within and outside the vane controlled region of the model. The experiments should be designed so that the feasibility of the technique in typical prototype situations can be determined. The model could, for example, be a representation of a prototype problem reach. Other techniques may also emerge from such experiments.

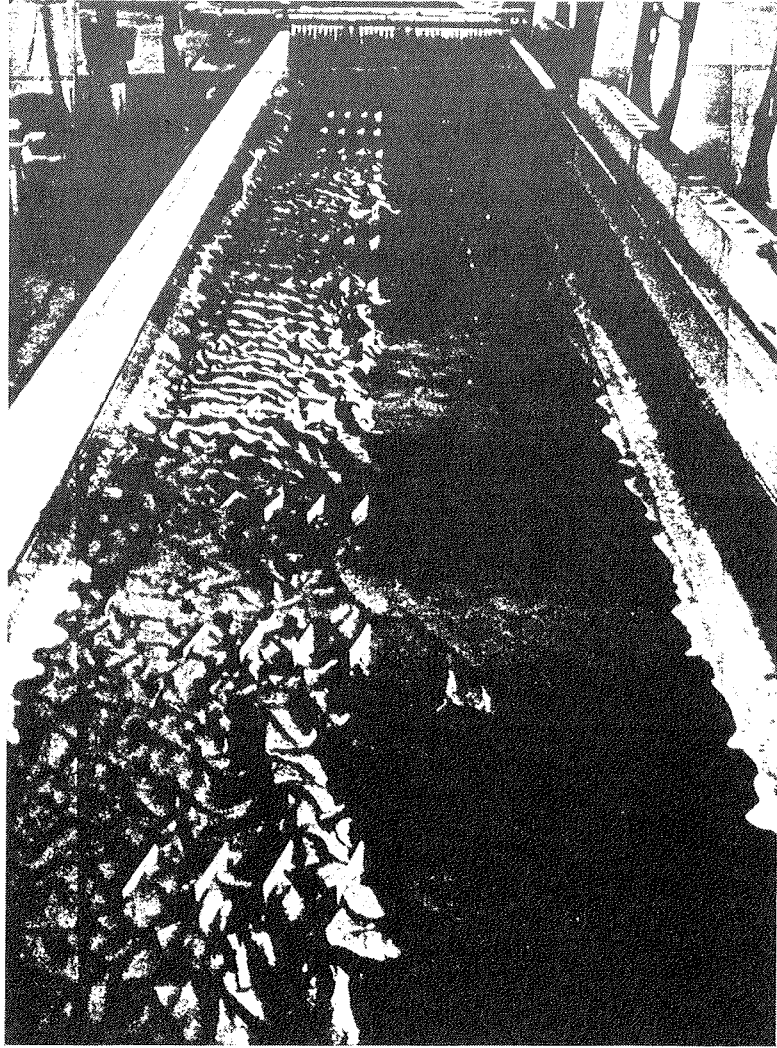


Figure VI.1. Submerged vanes for sediment management: test in straight, alluvial channel. Upstream view of nearly drained channel.

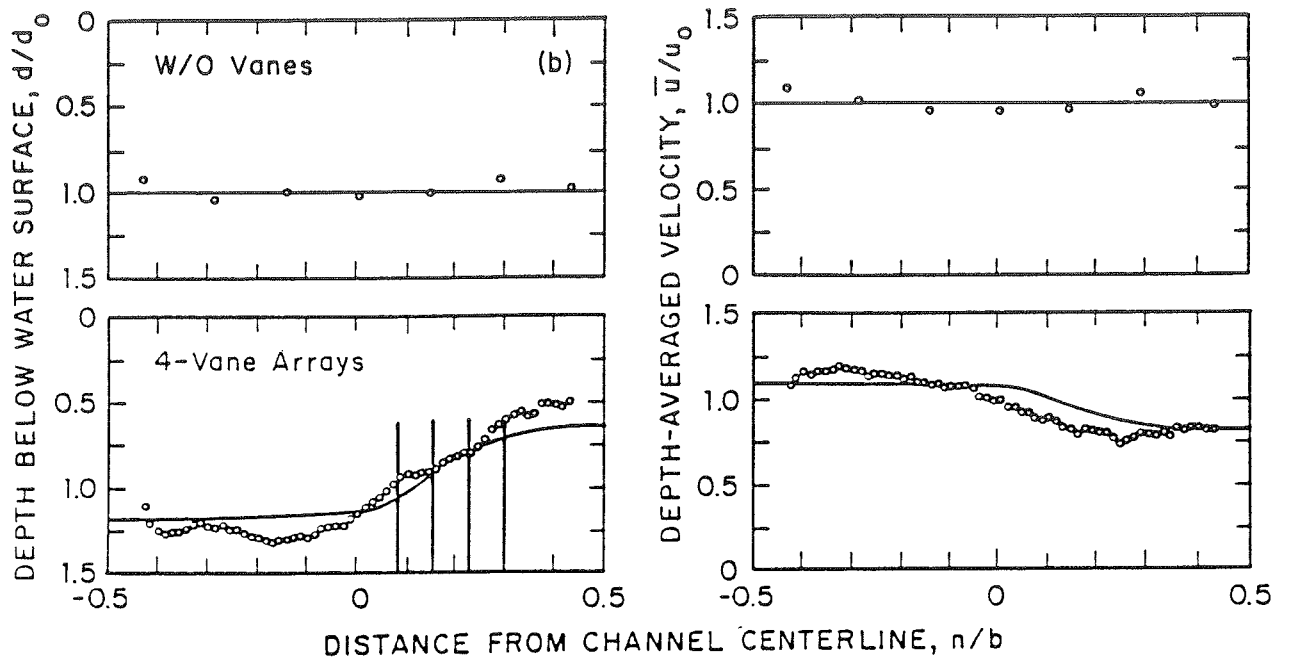


Figure VI.2. Submerged vanes for sediment management: test in straight alluvial channel. Velocity and depth distributions with and without vanes.

## VII. SUMMARY AND CONCLUSIONS

The principal findings forthcoming from the literature survey are presented in Section III.B, which should be considered a part of the summary and conclusions of this study.

Five of the published, empirically based predictors for relative dune height,  $h/d$ , were evaluated (Chapter V). None of them was found to be satisfactory. A new dune-height predictor was derived (Chapter IV), using in "inverse approach", in which the dune height was estimated from a verified predictor for alluvial-river friction factors. This relation was found to give more accurate predictions of  $h/d$  than the previously published ones. Its accuracy no doubt could be improved by calibration against other data to refine the constants it contains; and by omitting some of the assumptions made in its formulation, although this would be done at the expense of greater computational complexity.

The most promising, innovative means of dune control is judged to be use of submerged vanes, as described by Odgaard and Wang (1990). As a matter of fact, no other innovative means was discovered. There is a growing body of field experience which demonstrates that submerged vanes, suitably deployed, are very effective sediment management and control devices. It is recommended that their use for control of objectionable shoaling resulting from dunes be further explored.

## REFERENCES\*

- \* 1. Not all references listed here are cited in the text.
- 2. The listed references are classified according to the following key:
  - A. Analytical (theoretical) models and studies
  - B. Empirical or dimensional-analysis models and studies
  - C. Statistical (generally spectral) models and studies
  - D. Field observations
  - E. Bed forms in curved channels
  - F. Bed forms in unsteady flows
  - G. Control methods
  - H. Reviews
  - I. General references

- 
- H ASCE, "Nomenclature for Bed Forms in Alluvial Channels," Report of the Task Force on Bed Forms in Alluvial Channels of the Committee on Sedimentation, Journal of the Hydraulics Division, ASCE, Vol. 92, No. HY3, pp. 51-64, May 1966.
  - C Algert, J.H., "A Statistical Study of Bed Forms in Alluvial Channels," Colorado State University Report CER65JHA26, 1965.
  - I Allen, J.R.L., Physical Processes of Sedimentation, Elsevier, New York, 1970.
  - A Anderson, A.G., "The Characteristics of Sediment Waves Formed by Flow in Open Channels," Proceedings of the Third Midwestern Conference on Fluid Mechanics, University of Minnesota, Minneapolis, Minnesota, March 1953.
  - C,D Annambhotla, V.S., Sayre, W.W., and Livesey, R.H., "Statistical Properties of Missouri River Bed Forms," Journal of the Waterways, Harbors and Coastal Engineering Division, ASCE, Vol. 98, No. WW4, pp. 489-510, November 1972.
  - C Ashida, K., and Tanaka, Y., "A Statistical Study of Sand Waves," Proceedings of the 12th Congress of International Association for Hydraulic Research, Fort Collins, Colorado, Vol. 2, pap. B12, pp. 103-110, 1967.
  - D Carey, W.C., and Keller, M.D., "Systematic Changes in the Beds of Alluvial Rivers," Journal of the Hydraulics Division, ASCE, Vol. 83, No. HY4, Proc. Paper 1331, August 1957.
  - A,B,C Crickmore, M.J., "Effect of Flume Width on Bed-Form Characteristics," Journal of the Hydraulic Division, ASCE, Vol. 96, No. HY2, pp. 473-496, February 1970.
  - C,D Dinehart, R.L., "Dune Migration in a Steep, Coarse-Bedded Stream," Water Resources Research, AGU, Vol. 25, No. 5, pp. 911-923, May 1989.

- I Engelund, F., and Hansen, E., A Monograph on Sediment Transport in Alluvial Streams, Teknisk Forlag, Copenhagen, 1967.
- A Engelund, F., "Instability of Erodible Beds," Journal of Fluid Mechanics, Vol. 42, Part 2, pp. 225-244, 1970.
- H Engelund, F. and Fredsoe, J., "Sediment Ripples and Dunes," Annual Review of Fluid Mechanics, Vol. 14, pp. 13-37, 1982.
- A Exner, F.M., "Über die Wechselwirkung Zwischen Wasser und Geschiebe in Flüssen", Sitzenberichte der Academie der Wissenschaften, Wien, Osterreich, Section IIA, Vol. 134, p. 199, 1925.
- A Fredsoe, J., "On the Development of Dunes in Erodible Channels," Journal of Fluid Mechanics, Vol. 64, Part 1, pp. 1-16, 1974.
- A,F Fredsoe, J., "Unsteady Flow in Straight Alluvial Streams: Modification of Individual Dunes," Journal of Fluid Mechanics, Vol. 91, Part 3, pp. 497-512, 1979.
- B Fredsoe, J., discussion of "Steepness of Sedimentary Dunes," by Yalin, M.S. and Karahan, E., (Proc. Paper 14502), Journal of the Hydraulics Division, ASCE, Vol. 106, No. HY4, p. 623, April 1980.
- A Fredsoe, J., "Shape and Dimensions of Stationary Dunes in Rivers," Journal of the Hydraulics Division, ASCE, Vol. 108, No. HY8, pp. 932-947, August 1982.
- G Fukuoka, S. and Watanabe, A., "New Bank Protection Methods Against Erosion in the River," Proceedings of the Japan-China Joint Seminar on Natural Hazard Mitigation, Kyoto, Japan, pp. 439-448, July 16-20, 1989.
- G Fukuoka, S., "Groins and Vanes Developed Basing Upon a New Concept of Bank Protection," Proceedings of the ASCE National Conference on Hydraulic Engineering, New Orleans, pp. 224-229, August 1989.
- B Garde, R.J. and Albertson, M.L., "Sand Waves and Regimes of Flow in Alluvial Channels," Proceedings of the 8th International Association for Hydraulic Research Congress, Montreal, Canada, Vol. IV, Paper 28, 1959.
- A,B Gill, M.A., "Height of Sand Dunes in Open Channel Flows," Journal of the Hydraulics Division, Vol. 97, No. HY12, pp. 2067-2074, Dec. 1971.
- B Gill, M.A., discussion of "Steepness of Sedimentary Dunes," by Yalin, M.S., and Karahan, E., (Proc. Paper 14502), Journal of the Hydraulics Division, ASCE, Vol. 106, No. HY1, pp. 233-234, January 1980.
- A Gradowczyk, M.H., "Wave Propagation and Boundary Instability in Erodible-Bed Channels," Journal of Fluid Mechanics, Vol. 33, Part 1, pp. 93-112, 1968.
- I Graf, W.H., Hydraulics of Sediment Transport, McGraw-Hill, New York, 1971.

- H Guy, H.P., Simons, D.B., and Richardson, E.V., "Summary of Alluvial Channel Data from Flume Experiments, 1956-61," U.S. Geological Survey Professional Paper 462-I, 1966.
- A Haque, M.I., "Analytically Determined Ripple Shapes," M.S. Thesis submitted to Colorado State University, Ft. Collins, 1970.
- A Haque, M.I., and Mahmood, K., "Geometry of Ripples and Dunes," Journal of Hydraulic Engineering, ASCE, Vol. 111, No. 1, pp. 48-63, January 1985.
- A Haque, M.I., Mahmood, K., and Choudri, A.M., "Mechanics of Sedimentary Ripples and Dunes," Mechanics of Alluvial Channels, Water Resources Publications, Proc. of the 3rd U.S.-Pakistan Binational Symposium on the Mechanics of Alluvial Channels, pp. 136-150, 1985.
- A Haque, M.I., and Mahmood, K., "Analytical Study on Stepness of Ripples and Dunes," Journal of Hydraulic Engineering, ASCE, Vol. 112, No. 3, pp. 220-236, March 1986.
- G Hartman, G.L. and Beeman, O., "Bedload Transport and Sand Wave Dredging Concepts," Proceedings of the Twentieth Dredging Seminar, Toronto, Canada, pp. 214-228, September 1987.
- A Hayashi, T., "Formation of Dunes and Antidunes in Open Channels," Journal of the Hydraulics Division, ASCE, Vol. 96, No. HY2, pp. 357-367, February 1970.
- C Hino, M., "Equilibrium-Range Spectra of Sand Waves Formed by Flowing Water," Journal of Fluid Mechanics, Vol. 34, Part 3, pp. 565-573, 1968.
- B Ikeda, S., "Prediction of Alternate Bar Wavelength and Height," Journal of Hydraulic Engineering, ASCE, Vol. 110, No. 4, pp. 371-386, April 1984.
- A Iwasa, Y., and Kennedy, J.F., "Free Surface Shear Flow over a Wavy Bed," Journal of the Hydraulics Division, ASCE, Vol. 94, No. HY2, pp. 431-454, March 1968.
- A Jackson, R.G., "Sedimentological and Fluid-dynamic Implications of the Turbulent Bursting Phenomenon in Geophysical Flows," Journal of Fluid Mechanics, Vol. 77, pp. 531-560, 1976.
- B Jaeggi, M.N.R., discussion of "Stepness of Sedimentary Dunes," by Yalin, M.S., and Karahan, E., (Proc. Paper 14502), Journal of the Hydraulics Division, ASCE, Vol. 106, No. HY1, pp. 230-233, January 1980.
- A,B Jaeggi, M.N.R., "Formation and Effects of Alternate Bars," Journal of Hydraulic Engineering, ASCE, Vol. 110, No. 2, pp. 142-156, February 1984.
- C Jain, S.C., "Evaluation of Sand Wave Spectra," Ph.D. Thesis, Department of Mechanical and Hydraulic Engineering, The University of Iowa, Iowa City, January 1971.

- C Jain, S.C., and Kennedy, J.F., "The Growth of Sand Waves," Proceedings of International Symposium on Stochastic Hydraulics, Pittsburgh, pp. 449-471, May 31-June 2, 1971.
- A,C Jain, S.C., and Kennedy, J.F., "The Spectral Evolution of Sedimentary Bed Forms," Journal of Fluid Mechanics, Vol. 63, Part 2, pp. 301-314, 1974.
- I Karim, M.F. and Kennedy, J.F., "A Menu of Coupled Velocity and Sediment-Discharge Relations for Rivers," Journal of Hydraulic Engineering, ASCE, accepted for publication, 1990.
- A Kennedy, J.F., "The Mechanics of Dunes and Antidunes in Erodible-Bed Channels," Journal of Fluid Mechanics, Vo. 16, pp. 521-544, 1963.
- A Kennedy, J.F., "The Formation of Sediment Ripples in Closed Rectangular Conduits and in the Desert," Journal of Geophysical Research, AGU, Vol. 69, No. 8, pp. 1517-1524, April 1964.
- A Kennedy, J.F., "The Formation of Sediment Ripples, Dunes, and Antidunes," Annual Review of Fluid Mechanics, Vol. 1, pp. 147-167, 1969.
- H Kennedy, J.F., "Bed Forms in Alluvial Streams: Some Views on Current Understanding and Identification of Unresolved Problems," U.S.-Japan Seminar on Erosion and Sedimentation, Honolulu, HA, 20-24 March 1978.
- I Kinsman, B., Wind Waves, Prentice-Hall, Englewood Cliffs, New Jersey, 1965.
- H Klaassen, G.J., Ogink, H.J.M., and van Rijn, L.C. , "DHL-Research on Bed Forms, Resistance to Flow and Sediment Transport," Proceedings of the 3rd International Symposium on River Sedimentation, Jackson, Mississippi, pp. 58-82, March 31-April 4, 1986.
- D Klaassen, G.J., Vermeer, K., and Uddin, N., "Sedimentological Processes in Jamuna (Lower Brahmaputra) River, Bangladesh," Supplementary Volume to the Proceedings of the International Conference on Fluvial Hydraulics, Budapest, Hungary, pp. 381-394, May 30-June 3, 1988.
- H Kunzig, R., "Wandering rivers," Discover, 10(11), pp. 69-71, 1989.
- I Leliavsky, S., An Introduction to Fluvial Hydraulics, Constable & Company LTD., London, 1955.
- D,H Lillycrop, W.J., Rosati, J.D., and McGehee, D.D., "A Study of Sand Waves in the Panama City, Florida, Entrance Channel," Technical Report CERC-89-7, Department of the Army, Waterways Experiment Station, Corps of Engineers, July 1989.
- A Mahmood, K., and Haque, M.I., "Bedforms -Their Genesis and Implications," Proceedings of the 3rd International Symposium on River Sedimentation, Jackson, Mississippi, pp. 655-664, March 31-April 4, 1986.

- D McKee, E.D., "Sedimentary Structures and Textures of Rio Orinoco Channel Sands, Venezuela and Colombia," Chapter B, U.S. Geological Survey Water-Supply Paper No. 2326, 1989.
- A McLean, S.R., and Smith, J.D., "A Model for Flow over Two-Dimensional Bed Forms," Journal of Hydraulic Engineering, ASCE, Vol. 112, No. 4, pp. 300-317, April 1986.
- A,B Menduni, G., and Paris, E., "On the Prediction of Geometric Characteristics of Dunes," Proceedings of the 3rd International Symposium on River Sedimentation, Jackson, Mississippi, pp. 665-674, March 31-April 4, 1986.
- A Mercer, A.G., "Analytically Determined Bed-Form Shape," technical note, Journal of the Engineering Mechanics, ASCE, Vol. 97, No. EM1, pp. 175-180, February 1971.
- A Mercer, A.G., and Haque, M.I., "Ripple Profiles Modeled Mathematically," Journal of the Hydraulics Division, ASCE, Vol. 99, No. HY3, pp. 441-459, March 1973.
- C Nakagawa, H., and Tsujimoto, T., "Spectral Analysis of Sand Bed Instability," Journal of Hydraulic Engineering, ASCE, Vol. 110, No. 4, pp. 467-483, April 1984.
- C Nakagawa, H., and Tsujimoto, T., "Study of Formation of Sand Wave Spectrum," Transactions of the J.S.C.E., Hydraulic and Sanitary Engineering Division, Vol. 15, pp. 269-271, 1985.
- C Nordin, C.F. Jr., and Algert, J.H., "Spectral Analysis of Sand Waves," Journal of the Hydraulics Division, ASCE, Vol. 92, No. HY5, pp. 95-114, September 1966.
- C Nordin, C.F. Jr., "Statistical Properties of Dune Profiles," Sediment Transport in Alluvial Channels, U.S. Geological Survey Professional Paper, No. 562-F, 1971.
- D Nordin, C.F. Jr., and Perez-Hernandez, D., "Sand Waves, Bars, and Wind-Blown Sands of the Rio Orinoco, Venezuela and Colombia," Chapter A, U.S. Geological Survey Water-Supply Paper, No. 2326, 1989.
- C,E O'Loughlin, E.M., and Squarer, D., "Areal Variations of Bed-Form Characteristics in Meandering Streams," Proceedings of the 12th Congress of International Association for Hydraulic Research, Fort Collins, Colorado, Vol. 2, pp. 118-127, 1967.
- G Odgaard, A.J. and Kennedy, J.F., "River-Bend Bank Protection by Submerged Vanes," Journal of Hydraulic Engineering, ASCE, Vol. 109, No. HY8, pp. 1161-1173, August 1983.
- G Odgaard, A.J. and Spoljaric, A. "Sediment Control by Submerged Vanes," Journal of Hydraulic Engineering, ASCE, Vol. 112, No. HY12, pp. 1164-1181, December 1986.

- G Odgaard, A.J. and Mosconi, C.E., "Streambank Protection by Submerged Vanes," IIHR Report No. 306, Iowa Institute of Hydraulic Research, Iowa City, January 1987.
- G Odgaard, A.J. and Wang, Y., "Sediment Control in Bridge Waterways," IIHR Report No. 336, Iowa Institute of Hydraulic Research, Iowa City, February 1990.
- B Paris, E., "Considerations on Bed Form Effects in Subcritical Flows," Proceedings of the 23rd International Association for Hydraulic Research Congress, Lausanne, pp. 351-356, 1987.
- A Parker, G., "Sediment Inertia as Cause of River Antidunes," Journal of the Hydraulics Division, ASCE, Vol. 101, No. HY2, pp. 211-221, February 1975.
- A,B Raichlen, F., and Kennedy, J.F., "The Growth of Sediment Bed Forms from an Initially Flattened Bed," Proceedings of the 11th Congress of International Association for Hydraulic Research, Leningrad, Vol. 3, paper 3.7., 1965.
- B Ranga Raju, K.G., and Soni, J.P., "Geometry of Ripples and Dunes in Alluvial Channels," Journal of Hydraulic Research, IAHR, Vol. 14, No. 3, 1976.
- A,B Raudkivi, A.J., "Study of Sediment Ripple Formation," Journal of the Hydraulics Division, ASCE, Vol. 89, No. HY6, pp. 15-33, November 1963.
- A,B Raudkivi, A.J., "Bed Forms in Alluvial Channels," Journal of Fluid Mechanics, Vol. 26, Part 3, pp. 507-514, 1966.
- A Reynolds, A.J., "Waves on the Erodible Bed of an Open Channel," Journal of Fluid Mechanics, Vol. 22, Part 1, pp. 113-133, 1965.
- H Reynolds, A.J., "A Decade's Investigation of the Stability of Erodible Stream Beds," Nordic Hydrology, No. 7, pp. 161-180, 1976.
- A Richards, K.J., "The Formation of Ripples and Dunes on an Erodible Bed," Journal of Fluid Mechanics, Vol. 99, Part 3, pp. 597-618, 1980.
- F Sawai, K., "Transformation of Sand Waves due to the Time Change of Flow Conditions," Journal of Hydroscience and Hydraulic Engineering, JSCE, Vol. 5, No. 2, pp. 1-14, February 1988.
- C Shen, H.W., and Cheong, H.F., "Statistical Properties of Sediment Bed Profiles," Journal of the Hydraulics Division, ASCE, Vol. 103, No. HY11, pp. 1303-1321, November 1977.
- B Simons, D.B., and Richardson, E.V., "Resistance to Flow in Alluvial Channels," Journal of the Hydraulics Division, ASCE, Vol. 86, No. HY3, May 1960.
- B Simons, D.B., and Richardson, E.V., "Forms of Bed Roughness in Alluvial Channels," Journal of the Hydraulics Division, ASCE, Vol. 87, No. HY3, pp. 87-105, May 1961.

- A Song, C.S., "Modified Kinematic Model: Application to Bed Forms," Journal of Hydraulic Engineering, ASCE, Vol. 109, No. 8, pp. 1133-1151, August 1983.
- C,E Squarer, D., "Friction Factors and Bed Forms in Fluvial Channels," Journal of the Hydraulics Division, ASCE, Vol. 96, No. HY4, pp. 995-1017, April 1970.
- B van Rijn, L.C., "Equivalent Roughness of Alluvial Bed," technical note, Journal of the Hydraulics Division, ASCE, Vol. 108, No. HY10, 1982.
- B van Rijn, L.C., "Sediment Transport, Part III: Bed Forms and Alluvial Roughness," Journal of Hydraulic Engineering, ASCE, Vol. 110, No. 12, pp. 1733-1754, December 1984.
- B Vanoni, V.A., and Hwang, L.S., "Relation Between Bed Forms and Friction in Streams," Journal of the Hydraulics Division, ASCE, Vol. 93, No. HY3, 1967.
- B Vanoni, V.A., "Factors Determining Bed Forms of Alluvial Streams," Journal of the Hydraulics Division, ASCE, Vol. 100, No. HY3, pp. 363-377, March 1974.
- H Vanoni, V.A. (ed), Sedimentation Engineering, ASCE Manuals and Reports on Engineering Practice No. 54, American Society of Civil Engineers, New York, 1975.
- G Wang, Y., "Bank Protection with Submerged Vanes," Proceedings of the XXIII Congress of International Association for Hydraulic Research, Vol. S, pp. 17-23, 1989.
- A Watanabe, K., and Hirano, M., "Effects of Suspended Sediment on Formation of Sand Waves," Journal of Hydroscience and Hydraulic Engineering, JSCE, Vol. 6, No. 2, pp. 29-43, December 1988.
- F Wijnbenga, J.H.A., and Klaassen, G.J., "Changes in Bed Form Dimensions under Unsteady Flow Conditions in a Straight Flume," Publication No. 260, Delft Hydraulics Laboratory, The Netherlands, 1981.
- C Willis, J.C., "A Lag-Deviation Method for Analyzing Channel Bed Forms," Water Resources Research, AGU, Vol. 4, No. 6, pp. 1329-1334, December 1968.
- C Willis, J.C. and Kennedy, J.F., "Sediment Transport in Migrating Bed Forms", Proceedings of the ASCE Hydraulics Division Specialty Conference, College Park, Maryland, August 1978.
- B Yalin, M.S., "Geometrical Properties of Sand Waves," Journal of the Hydraulics Division, ASCE, Vol. 90, No. HY5, pp. 105-119, September 1964.
- H Yalin, M.S., Mechanics of Sediment Transport, Pergamon, Braunschweig, 1972.

- B Yalin, M.S., and Karahan, E., "Steepness of Sedimentary Dunes," Journal of the Hydraulics Division, ASCE, Vol. 105, No. HY4, pp. 381-392, April 1979.
- A,B Yalin, M.S., "On the Formation Mechanism of Dunes and Ripples," Vortrag gehalten anlässlich EUROMECH 215, Mechanics of Sediment Transport in Fluvial and Marine Environments, Genoa, September 1987.
- E Zimmermann, C., Sohlausbildung. Reibungsfaktoren und Sediment transport in gleichförmig gekrümmten und Geraden Gerinnen, Ph.D. Thesis, University of Karlsruhe, 1974.